Winter 1998

Placement of Piezoelectric Actuators for Active Control of Vibration Using Modal Parameters

Xuegeng Zhu
Old Dominion University

PLACEMENT OF PIEZOELECTRIC ACTUATORS FOR ACTIVE CONTROL OF VIBRATION USING MODAL PARAMETERS

by

Xuegeng Zhu
B.S. July 1983, Shanghai Jiao Tong University, Shanghai, China
M.S. January 1989, Shanghai Jiao Tong University, Shanghai, China

A Dissertation Submitted to the Faculty of
Old Dominion University in Partial Fulfillment of the
Requirement for the Degree of

DOCTOR OF PHILOSOPHY

AEROSPACE ENGINEERING

OLD DOMINION UNIVERSITY
December 1998

Approved by:

Thomas E. Alberts (Director)

Chuh Mei (Member)

Jeng-Jong Ro (Member)

Jen-Kuang Huang (Member)

ABSTRACT

PLACEMENT OF PIEZOELECTRIC ACTUATORS FOR ACTIVE CONTROL OF VIBRATION USING MODAL PARAMETERS

Xuegeng Zhu
Old Dominion University, 1998
Director: Dr. Thomas E. Alberts

An equation is derived to model the piezoelectric actuators incorporation with flexible structures. This equation permits the comparison of the performance indices over the entire structure for a piezoelectric actuator with constant area, which is unachievable if the Finite Element Method is used for complicated structures.

An index has been developed for placement of piezoelectric actuator for control of vibration of a flexible structure. This index is derived from the definition of H_2 norm. Computation of the proposed index requires only the natural frequencies and corresponding mode shapes of the structures of interest. The method is well suited to large structure application because of the simplicity of the calculation. The proposed index is valid either for point sensor and actuator or for distributed types such as piezoelectric. Application of the method for different combinations of sensors and actuators has been discussed. Both piezoelectric patch and piezoelectric fiber actuators are used to verify the effectiveness of the proposed index.

The comparison of H_2 and H_∞ norms shows good agreement for beam and plate models with single, three, and six modes. The comparison of H_2 and H_∞ norms is also made for a cantilevered beam with fixed sensor location, and a simply supported plate with a piezoelectric fiber actuator. Agreement between those two norms as well as the proposed index is demonstrated through all the cases.

Imbedded piezoelectric fiber actuators, which are able to supply anisotropic control actuation, have an optimal fiber orientation, which is related to different structures, but independent of the volume fraction of the PZT fibers. Piezoelectric fiber actuator with volume fraction $v_f < 1$ creates twisting moment, which has better performance than that of a monolithic piezoelectric patch actuator in control of twisting mode.

DEDICATION

To my wife Weike and daughter Deana

ACKNOWLEDGMENTS

I would like to express my gratitude to Dr. Thomas E. Alberts for being my advisor. It has been an honor to have him guide my doctoral study. I am very grateful to Dr. Chuh Mei who taught most of my structure courses that were very helpful for this research. I would like to thank Dr. Jeng-Jong Ro for being a member of my guidance committee. He impresses me with his knowledge and expertise in this area. I would also like to thank Dr. Jen-Kuang Huang for his valuable suggestions on this dissertation.

NOMENCLATURE

A	cross-section area of the beam
A_a	area of piezoelectric actuator
A_{mn}	constant
A_s	area of structure
C_a	geometric constant of piezoelectric actuator
C_x, C_y, C_{xy}	piezoelectric material related constants
D	plate flexural rigidity
d_x, d_y	coupling constants between the applied electric field in z direction and normal strains in x, y directions
d_{xy}	coupling constants between the applied electric field in z direction and shear strain in xy plane
d_{31}, d_{32}	coupling constant relating the electric field and the strain in 1, 2 direction
E	Young's Modulus
E_a	Young's modulus of the piezoelectric actuator
e	difference between two impulse response functions
$F_c^{(i)}(t)$	control force
$F_d^{(i)}(t)$	disturbing force
$\{F\}$	$n \times 1$ point force vector
G	open-loop Frequency Response Function
$f_c(x, y, t)$	control force
f_d	distributed disturbing force

$f_i(x,t)$	modal force
$H(s)$	Frequency Response Function
$H(t)$	Heavyside function
h	thickness of the plate
I	moment of inertia
$[I]$	$n \times n$ identical matrix
K	feedback control gain matrix
K_i	constant
$[K]$	$n \times n$ stiffness matrix
k_i	constant
L	length of the beam
M_a	control voltage induced moment
M_{xx}	bending moment in yz plane
M_{yy}	bending moment in zx plane
M_{xy}	twisting moment in xy plane
$[M]$	$n \times n$ mass matrix
m_{xx}	bending moment in yz plane
m_{yy}	bending moment in zx plane
m_{xy}	twisting moment in xy plane
$[p]_f$	constant matrix for PZT fiber
$[\bar{p}]$	transformed piezoelectric constant matrix
$[Q_{ij}]$	stiffness matrices
Q_x, Q_y	plate shear force in z direction

$[\overline{Q}]$	transformed stiffness matrix
$q_i(t)$	modal coordinate
$[T_\sigma(\theta)]$	stress transformation matrix
$[T_\varepsilon(\theta)]$	strain transformation matrix
t_b	thickness of the beam
$\mathbf{u}$	State-Space input force
u	control input
V	proposed index
V_a	voltage applied to the actuating piezoelectric layer
V_s	sensed signal
v_f, v_m	volume fraction of PZT fiber and matrix
$W(x, y, s)$	deflection in frequency domain
w	deflection of the plate in z direction
w_b	width of the beam
w_d	external inputs including disturbances
w_i, w_j	modal deflection
$\mathbf{x}$	State-Space variable
$\dot{\mathbf{x}}$	time derivative of $\mathbf{x}$
$\mathbf{x}_I$, $\mathbf{x}_O$	input, output point coordinate
$\mathbf{x(s)}$	*Laplace Transformation* of $\mathbf{x}$
x_0, x_1, x_2	coordinates
Δx	length of the actuator
$\mathbf{y}$	State-Space output vector

y	observed output
$\{y\}$	$n \times 1$ displacement vector
z	error output.
β_i	constant
δ	Daric delta function (Impulse function)
δ_{ij}	Kronecker delta function
ε_x, ε_y	normal strain in x, y directions
ε_1, ε_2	normal strain in 1, 2 direction
$\Phi_i^{(I)}$, $\Phi_i^{(O)}$	mode shape related function
$[\Phi]$	$n \times n$ mode matrix,
$\phi_i(x)$, $\phi_j(x)$	eigenfunction of beam
$\phi_i(x, y)$, $\phi_j(x, y)$	plate eigenfunction
γ	positive number
γ_{xy}	shear strain in xy plane
γ_{12}	shear strain in 12 plane
η, η_1, η_2	coordinate
ν	Poisson's ratio of the plate
ν_{12}, ν_{21}	major, minor Poisson's ratio
θ	orientation of PZT fiber
ρ	mass density
σ_a	control voltage induced stress
σ_x, σ_y	normal stresses in x, y directions
σ_1, σ_2	normal stress in 1, 2 direction

τ_{xy}	shear stress in xy plane
τ_{12}	shear stress in 12 plane
Ω_i, Ω_j	plate natural frequency
$[\Omega^2]$	$n \times n$ frequency matrix
ω_i	natural frequency of beam
ξ, ξ_1, ξ_2	coordinate
ζ_i	modal damping ratio

Subscript:

m	matrix
f	piezoelectric fiber
c	composite actuator
p	piezoelectric fiber
e	epoxy matrix

TABLE OF CONTENTS

LIST OF TABLES

LIST OF FIGURES

CHAPTER I

INTRODUCTION

The approach to a typical flexible structure vibration control problem using piezoelectric actuators consists of following steps:

1. Selection of piezoelectric materials with the proper properties
2. Model of the flexible structure
3. Application of control methods
4. Prediction of the performance

If parameter optimization is desired, step 4 will be repeated with modified parameters by means of an optimization method until some objective function reaches its optimal value.

In recent years, much research has been devoted to modeling piezoelectric materials for structural control applications, applying stable and effective control methods to the systems, as well as optimizing the dimensions and locations for piezoelectric actuators.

The proliferation of commercially manufactured piezoelectric materials makes it possible to obtain piezoelectric products in many shapes [35]. As smart materials for actuators, however, PZT patches are most commonly used in control of vibration and noise of flexible structures. In many cases, the methods of actuation and sensing use monolithic ceramics that exhibit in-plane isotropy. Thus, it is impossible to distinguish and actuate

---

The format for references in this dissertation is taken from the ASME *Journal of Dynamic Systems, Measurement, and Control*

any single component of in-plane strain with these ceramics. Recently, some researchers have directed their efforts to finding new materials to increase the performance of piezoelectric actuators. Piezoelectric fiber composite actuators are among the new developments that are potentially interesting.

A production of fiber/polymer composites is made possible by a relic-processing technique [46, 47]. This process basically involves impregnating a sacrificial woven carbon-fiber template material with a ceramic precursor, simply by soaking the template in a precursor stock solution. Careful heat treatment removes the carbon and forms a ceramic-fiber relic with the same shape as the original woven-fiber template. After the relics are stintered, they are backfilled with a polymer to form composites. Research indicated that a family of piezoelectric composites with a range of properties could be obtained through combination of various polymer matrix materials and PZT fiber orientations within composites as well as the poling techniques.

Another technique used to produce piezoelectric fibers is the "sol-gel" process, which has received much interest because of its simplicity, low processing temperature, chemical homogeneity and stoichiometry control as well as the ability to produce fibers of uniform microstructure [26, 34, 51]. An investigation of the passive damping properties of composite structures with piezoelectric fibers indicates that resistively shunted piezoceramics appear to offer several advantages, including high stiffness and damping (loss modulus) for a potential composite constituent and tailorable frequency dependence [26].

With the availability of piezoelectric fiber composites, some research has focused on modeling and design of actuators using PZT fiber composites [5, 6]. Generally, the modeling of sensors and actuators is based on classical theory of composite structures [11, 13], where sensors or actuators are treated as composite layers with coupling between the electric fields and the in-plane strains. The difference between a monolithic piezoelectric patch and a piezoelectric fiber lamina is that, the monolithic patch demonstrates isotropy in the in-plane direction while the fiber lamina is orthotropic parallel and perpendicular to the fiber direction within the lamina plane. The combination of two fiber laminae with a ply angle forms an anisotropic actuator. The expression for the effective moment induced by the actuator is derived by the integral of the stresses through the thickness of the laminate plate [1, 33].

The control theories used in active vibration and/or noise control can be classified as feedforward control, feedback control and the combination of both feedforward control and feedback control. In noise control cases, the feedforward control approach has been shown to afford substantial broadband suppression [7, 8, 41]. The utilization of this method for structure dynamic modification has also been demonstrated.

In feedback control, many different control methods have been investigated to pursue a stable and effective control system. PD control [1], LQG control [22, 27, 29, 30, 42, 50], H_2 and H_∞ control [31] are among the methods that have been successfully applied.

With the success of feedforward techniques, feedback control researchers have begun to explore the relationship between feedforward and feedback control methods [17]. In [17] it was shown that, in the case of active noise control, a geometric arrangement of speakers and microphones in the standard feedforward setup allows the control designer to circumvent the inherent limitations of the Bode Integral constraint that identifies situations in which spillover is unavoidable regardless of the control algorithm.

In order to optimize the performance for the control system, a performance index, or objective function, which can properly represent the quality of the control system, is required. For noise control problems, the acoustic pressure [18], or the mean-square of the sound pressure [7, 8] at a selected location is a common choice, while for control of structural vibration, the average mean-square vibration level over the whole structure is adopted [41]. The electric energy required to control the structure is also used as the objective functions to minimize the power requirement for piezoelectric control systems.

Once the performance function is chosen, the optimum placement problem can be solved by choosing parameter values which lead to optimum performance. This process can be done either through computation [43] or experiment [31] and the results depend upon the characteristics of the structure as well as the applied control law.

Kondoh et al. [21] compared the design method of minimizing a quadratic cost function to that of maximizing the dissipative energy due to control action proposed by Schulz and Heimbold. Comparison of two methods on a four mode model of a cantilevered beam

was performed using simulations with a velocity feedback control law. The results showed that the global and local optimum locations of sensors and actuators are very close for both methods.

Lee and Chen [23] presented a design method which calculates sensor/actuator locations and feedback gain via minimization of the integrated total energy W stored in the system. The energy criterion is determined with a quasi-Newton or recursive quadratic programming algorithm.

Kang et al. [20] studied the optimal placement of a collocated piezoelectric sensor/actuator for vibration control of laminated composite beams. The finite element method was used for the analysis of dynamic characteristics of laminated composite beams with piezoelectric sensor/actuator. By means of FEM, the mass, stiffness and damping of all layers (including PZT) were taken into account.

Hać and Liu [15] proposed a methodology for determination of sensor and actuator locations in motion control of flexible structures, which can be used before a control strategy is developed. The proposed approach can be realized by the computation of the eigenvalues of the controllability and observability Grammians, which are independent of control law. Simple indices are given for a simply supported beam and a rectangular plate without comparison of controlled systems.

Redmond and Parker [38] studied the fuel-optimal actuator placement of flexible structures. The computational results, for an assumed two mode Euler-Bernoulli pinned-pinned beam with length L, showed that if the control time is long enough to reach a steady-state, the optimal locations appear in symmetric pairs on either side of the beam midpoint. For disturbances introduced at the outer extents of the beam ($x < 0.25L$ or $x > 0.75L$), the optimal locations coincide with the antinodes of the 2nd mode. In the cases where the disturbance is more centrally located ($0.25L < x < 0.75L$), the optimal locations coincide with the disturbance location and its reflection about the beam midpoint. Finally an *Actuator Location Fitness Function* was suggested.

Lim [31] investigated the effective piezoceramic actuator placement for a flexible wing by experiment. The effectiveness of piezoceramic actuators are expressed in terms of their contributions to the joint controllability and observability. Simulation results based on H_2 and H_∞ control law designs indicate that closed loop performance can be improved significantly by selecting the most suitable locations for the actuators, and the performance improvement is independent of the particular type of control law.

Smith et al. [43] used a mathematical optimization procedure called the *Sequential Quadratic Programming Method* to minimize a suggested cost function which is the H_2 norm of the total system transfer matrix from the disturbance inputs to an output vector formed from the modal acoustic power and the feedback control signals.

Most research about placement optimization is related to particular structures, force excitation and control laws. Thus, an optimal location of piezoelectric actuator for a given structure corresponding to a particular control law and a particular force excitation will not necessarily be the best choice for another case. Here arises the question of whether there are any similarities behind all those results and how to make a good choice which will be suitable to most/all of control and loading cases so that the placement choice can be decided before the application of control laws. That is the motivation of this study.

The objective of this research is to develop a design guideline for placement of piezoelectric actuators for control by means of modal parameters.

The modal parameters referred to here are:

1. natural frequencies
2. modal damping ratios
3. modal shapes

The characteristics of a structure can be exclusively determined by these modal parameters. Some other useful information, e.g. curvatures of the mode shapes and modal sensitivities, can be obtained by simple calculation of the modal parameters.

These parameters could be the results from any of the following analyses:

1. Analytical Modal Analysis

2. Experimental Modal Analysis (Modal Testing)
3. Finite Element Analysis

Analytical solutions are available for simple structures, e.g., beams and plates, while Finite Element Analysis and Modal Testing are used to obtain modal parameters of arbitrarily shaped structures.

In this study, H_2 and H_∞ methods are applied to the chosen structure. Upon comparison of the optimal placement choices for both cases, similarities in both cases are further related to modal parameters (modal deflections, and curvatures of the modal shapes).

An index for placement choice is suggested based on the investigation of the relationships between the modal parameters of the structure and the control properties. This index is verified by case studies for a cantilevered beam and a simply supported rectangular plate. Both piezoelectric patch and piezoelectric fiber composite lamina are utilized to demonstrate the effectiveness of the recommended design method.

CHAPTER II

MODELING OF PIEZOELECTRIC FIBER COMPOSITE ACTUATOR

A piezoelectric fiber composite actuator consists of piezoelectric fibers and a host structure, referred to as the matrix. The PZT fibers provide the predominant composite stiffness, strength and active control effort, while the passive matrix serves to protect the PZT fibers, and facilitates load sharing among the fibers. It is assumed that the piezoelectric fibers are uniformly spaced, and parallel.

2.1 Constitutive Equations for Matrix and Piezoelectric Fiber Materials

In figure 2.1, direction 1 is aligned with the PZT fibers, and the transverse direction is the direction 3. The strain/stress relationship for the matrix can be expressed as [13]:

$$\begin{Bmatrix} \varepsilon_1 \\ \varepsilon_2 \\ \gamma_{12} \end{Bmatrix}_m = \begin{bmatrix} S_{11} & S_{12} & 0 \\ S_{21} & S_{22} & 0 \\ 0 & 0 & S_{66} \end{bmatrix}_m \begin{Bmatrix} \sigma_1 \\ \sigma_2 \\ \tau_{12} \end{Bmatrix}_m \tag{2.1}$$

where ε_1 : normal strain in 1 direction,

ε_2 : normal strain in 2 direction,

γ_{12} : shear strain in 12 plane,

σ_1 : normal stress in 1 direction,

σ_2 : normal stress in 2 direction,

τ_{12} : shear stress in 12 plane,

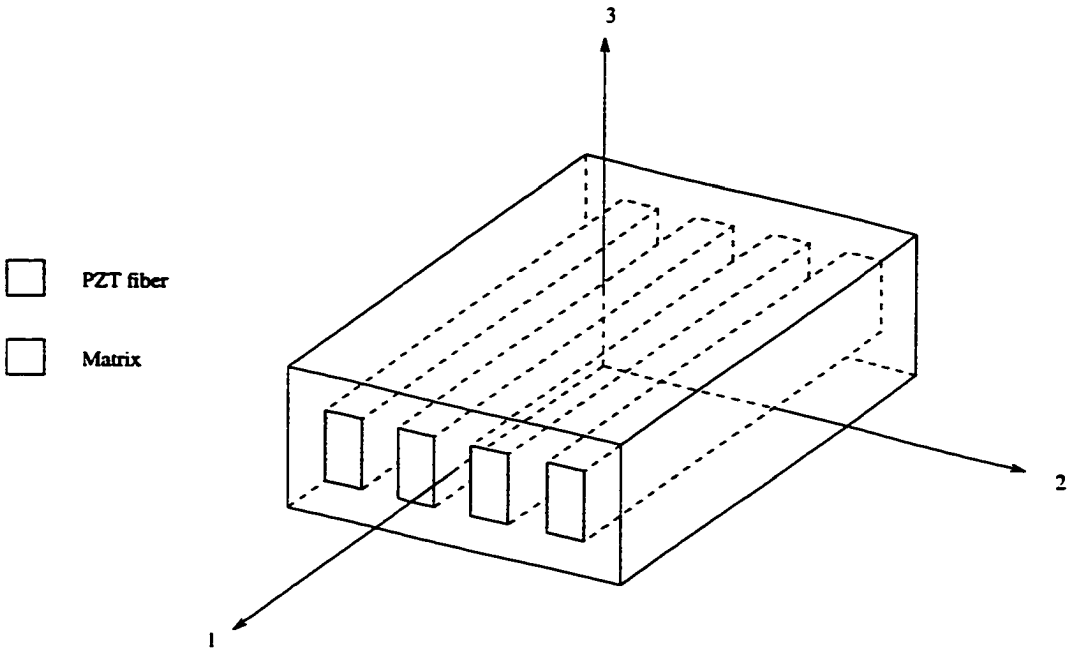

Figure 2.1 Piezoelectric fiber composite actuator

$[S_{ij}]$: compliance matrix.

The subscript m indicates that the subscripted entity is associated with the matrix material. The terms of $[S_{ij}]$ are:

$$S_{11} = \frac{1}{E_1}$$

$$S_{12} = S_{21} = -\frac{\nu_{12}}{E_1} = -\frac{\nu_{21}}{E_2}$$

$$S_{22} = \frac{1}{E_2}$$

$$S_{66} = \frac{1}{G_{12}}$$

where E_1 : Young's modulus in 1 direction,

E_2 : Young's modulus in 2 direction,

G_{12} : shear modulus in 12 plane,

ν_{12} : major Poisson's ratio,

ν_{21} : minor Poisson's ratio.

For isotropic materials, $E_1 = E_2$ and $\nu_{12} = \nu_{21}$. If the fibers are piezoelectric, the coupling between the electric field and the mechanical field is described by an additional term in the constitutive equation, i.e. [49]:

$$\begin{Bmatrix} \varepsilon_1 \\ \varepsilon_2 \\ \gamma_{12} \end{Bmatrix}_f = \begin{bmatrix} S_{11} & S_{12} & 0 \\ S_{21} & S_{22} & 0 \\ 0 & 0 & S_{66} \end{bmatrix}_f \begin{Bmatrix} \sigma_1 \\ \sigma_2 \\ \tau_{12} \end{Bmatrix}_f + \frac{V_a}{t_a} \begin{Bmatrix} d_{31} \\ d_{32} \\ 0 \end{Bmatrix} \tag{2.2}$$

where V_a : electric field in 3 direction,

t_a : thickness of the piezoelectric fiber layer,

d_{31} : coupling constant relating the electric field and the strain in 1 direction,

d_{32} : coupling constant relating the electric field and the strain in 2 direction.

The subscript f indicates that the subscripted entity is associated with the piezoelectric fiber. For isotropic piezoelectric fiber materials $d_{31} = d_{32}$.

The strain/stress relationships (2.1), (2.2) can be also expressed using stiffness matrices as:

$$\begin{Bmatrix} \sigma_1 \\ \sigma_2 \\ \tau_{12} \end{Bmatrix}_m = \begin{bmatrix} Q_{11} & Q_{12} & 0 \\ Q_{21} & Q_{22} & 0 \\ 0 & 0 & Q_{66} \end{bmatrix}_m \begin{Bmatrix} \varepsilon_1 \\ \varepsilon_2 \\ \gamma_{12} \end{Bmatrix}_m \tag{2.3}$$

$$\begin{Bmatrix} \sigma_1 \\ \sigma_2 \\ \tau_{12} \end{Bmatrix}_f = \begin{bmatrix} Q_{11} & Q_{12} & 0 \\ Q_{21} & Q_{22} & 0 \\ 0 & 0 & Q_{66} \end{bmatrix}_f \left(\begin{Bmatrix} \varepsilon_1 \\ \varepsilon_2 \\ \gamma_{12} \end{Bmatrix}_f - \frac{V_a}{t_a} \begin{Bmatrix} d_{31} \\ d_{32} \\ 0 \end{Bmatrix} \right) \tag{2.4}$$

where $[Q_{ij}]_m$ and $[Q_{ij}]_f$ are stiffness matrices for matrix and piezoelectric fiber materials respectively. The terms of $[Q_{ij}]$ are:

$$Q_{11} = \frac{E_1}{1 - \nu_{12}\nu_{21}}$$

$$Q_{12} = Q_{21} = \frac{\nu_{12}E_2}{1 - \nu_{12}\nu_{21}} = \frac{\nu_{21}E_1}{1 - \nu_{12}\nu_{21}}$$

$$Q_{22} = \frac{E_2}{1 - \nu_{12}\nu_{21}}$$

$$Q_{66} = G_{12}$$

2.2 Constitutive Equations For Piezoelectric Fiber Composite Actuator

Based on the *Classical Laminated Plate Theory* [13], perfect bonding at the interface is assumed so no slip occurs between piezoelectric fiber and matrix materials. The fiber and matrix materials are assumed to be linearly elastic and homogeneous, and the piezoelectric fiber is regularly spaced and perfectly aligned.

To combine the PZT fiber and matrix, it is commonly assumed [16] that in the 1 direction:

$$\varepsilon_{c1} = \varepsilon_{f1} = \varepsilon_{m1} \tag{2.5}$$

$$\sigma_{c1} = \sigma_{f1} v_f + \sigma_{m1} v_m \tag{2.6}$$

and in the 2 direction:

$$\sigma_{c2} = \sigma_{f2} = \sigma_{m2} \tag{2.7}$$

$$\varepsilon_{c2} = \varepsilon_{f2} v_f + \varepsilon_{m2} v_m \tag{2.8}$$

with regard to rotation about the 3 axis it is assumed that:

$$\tau_{c12} = \tau_{f12} = \tau_{m12} \tag{2.9}$$

$$\gamma_{c12} = \gamma_{f12} v_f + \gamma_{m12} v_m \tag{2.10}$$

In equations (2.5) to (2.10), subscripts *c, f, m* denote composite actuator, piezoelectric fiber and matrix respectively. The v_f and v_m are volume fraction of PZT fiber and matrix $v_f + v_m = 1$.

To apply equations (2.5) to (2.10), equations (2.3) and (2.4) have to be re-arranged. First solve the second equation in (2.3) and (2.4) for ε_{f2} and ε_{m2}, the third equation in (2.3)

and (2.4) for γ_{f12} and γ_{m12}, then substitute ε_{f2} and γ_{f12} into the first equation of (2.4), ε_{m2} and γ_{m12} into the first equation of (2.3). Equations (2.3) and (2.4) become:

$$\begin{Bmatrix}\sigma_1\\ \varepsilon_2\\ \gamma_{12}\end{Bmatrix}_m = \begin{bmatrix} Q_{11}-\frac{Q_{12}}{Q_{22}} & \frac{Q_{12}}{Q_{22}} & 0\\ -\frac{Q_{12}}{Q_{22}} & \frac{1}{Q_{22}} & 0\\ 0 & 0 & \frac{1}{Q_{66}}\end{bmatrix}_m \begin{Bmatrix}\varepsilon_1\\ \sigma_2\\ \gamma_{12}\end{Bmatrix}_m \tag{2.11}$$

$$\begin{Bmatrix}\sigma_1\\ \varepsilon_2\\ \gamma_{12}\end{Bmatrix}_f = \begin{bmatrix} Q_{11}-\frac{Q_{12}}{Q_{22}} & \frac{Q_{12}}{Q_{22}} & 0\\ -\frac{Q_{12}}{Q_{22}} & \frac{1}{Q_{22}} & 0\\ 0 & 0 & \frac{1}{Q_{66}}\end{bmatrix}_f \begin{Bmatrix}\varepsilon_1\\ \sigma_2\\ \gamma_{12}\end{Bmatrix}_f + \frac{V_a}{t_a}\begin{bmatrix} -Q_{11}+\frac{Q_{12}^2}{Q_{22}} & 0 & 0\\ \frac{Q_{12}}{Q_{22}} & 1 & 0\\ 0 & 0 & 0\end{bmatrix}_f \begin{Bmatrix}d_{31}\\ d_{32}\\ 0\end{Bmatrix} \tag{2.12}$$

From equations (2.5) to (2.10):

$$\begin{Bmatrix}\sigma_1\\ \varepsilon_2\\ \gamma_{12}\end{Bmatrix}_c = \begin{Bmatrix}\sigma_1\\ \varepsilon_2\\ \gamma_{12}\end{Bmatrix}_f v_f + \begin{Bmatrix}\sigma_1\\ \varepsilon_2\\ \gamma_{12}\end{Bmatrix}_m v_m \tag{2.13}$$

and

$$\begin{Bmatrix}\varepsilon_1\\ \sigma_2\\ \gamma_{12}\end{Bmatrix}_c = \begin{Bmatrix}\varepsilon_1\\ \sigma_2\\ \gamma_{12}\end{Bmatrix}_f = \begin{Bmatrix}\varepsilon_1\\ \sigma_2\\ \gamma_{12}\end{Bmatrix}_m \tag{2.14}$$

therefore the combination of equations (2.11) and (2.12) yields:

$$\begin{Bmatrix}\sigma_1\\ \varepsilon_2\\ \gamma_{12}\end{Bmatrix}_c = \left(\begin{bmatrix} Q_{11}-\frac{Q_{12}}{Q_{22}} & \frac{Q_{12}}{Q_{22}} & 0\\ -\frac{Q_{12}}{Q_{22}} & \frac{1}{Q_{22}} & 0\\ 0 & 0 & \frac{1}{Q_{66}}\end{bmatrix}_f v_f + \begin{bmatrix} Q_{11}-\frac{Q_{12}}{Q_{22}} & \frac{Q_{12}}{Q_{22}} & 0\\ -\frac{Q_{12}}{Q_{22}} & \frac{1}{Q_{22}} & 0\\ 0 & 0 & \frac{1}{Q_{66}}\end{bmatrix}_m v_m\right)\begin{Bmatrix}\varepsilon_1\\ \sigma_2\\ \gamma_{12}\end{Bmatrix}_c$$

$$+\frac{v_f V_a}{t_a}\begin{bmatrix} -Q_{11}+\frac{Q_{12}^2}{Q_{22}} & 0 & 0\\ \frac{Q_{12}}{Q_{22}} & 1 & 0\\ 0 & 0 & 0\end{bmatrix}_f \begin{Bmatrix}d_{31}\\ d_{32}\\ 0\end{Bmatrix} \tag{2.15}$$

Finally solve the second equation of (2.15) for σ_2, third equation of (2.15) for τ_{12}, and substitute σ_2, τ_{12} into the first equation of (2.15). Thus equation (2.15) can be re-arranged as:

$$\begin{Bmatrix}\sigma_1\\ \sigma_2\\ \tau_{12}\end{Bmatrix}_c = [Q]_c \begin{Bmatrix}\varepsilon_1\\ \varepsilon_2\\ \gamma_{12}\end{Bmatrix}_c - \frac{V_a}{t_a}[p]_f \begin{Bmatrix}d_{31}\\ d_{32}\\ 0\end{Bmatrix} \tag{2.16}$$

where $[Q]_c$ is the stiffness matrix for composite actuator and $[p]_f$ is the constant matrix for PZT fiber.

For simplicity, the subscripts c, f can be dropped and the equation (2.16) re-written as:

$$\begin{Bmatrix}\sigma_1\\ \sigma_2\\ \tau_{12}\end{Bmatrix} = [Q] \begin{Bmatrix}\varepsilon_1\\ \varepsilon_2\\ \gamma_{12}\end{Bmatrix} - \frac{V_a}{t_a}[p] \begin{Bmatrix}d_{31}\\ d_{32}\\ 0\end{Bmatrix} \tag{2.17}$$

The $[Q]$ and $[p]$ matrices are both 3×3 with elements:

$$Q_{11} = Q_{m11}v_m + Q_{f11}v_f - \frac{(Q_{m12} - Q_{f12})^2 v_m v_f}{Q_{m22}v_f + Q_{f22}v_m}$$

$$Q_{12} = Q_{21} = \frac{Q_{m12}Q_{f22}v_m + Q_{m22}Q_{f12}v_f}{Q_{m22}v_f + Q_{f22}v_m}$$

$$Q_{22} = \frac{Q_{m22}Q_{f22}}{Q_{m22}v_f + Q_{f22}v_m}$$

$$Q_{66} = \frac{Q_{m66}Q_{f66}}{Q_{m66}v_f + Q_{f66}v_m}$$

$$Q_{13} = Q_{23} = Q_{31} = Q_{32} = 0$$

$$p_{11} = \frac{v_f(Q_{m12}Q_{f12}v_m + Q_{m22}Q_{f11}v_f + Q_{f11}Q_{f22}v_m - Q_{f12}^2 v_m)}{Q_{m22}v_f + Q_{f22}v_m}$$

$$p_{12} = \frac{v_f(Q_{m22}Q_{f12}v_f + Q_{m12}Q_{f22}v_m)}{Q_{m22}v_f + Q_{f22}v_m}$$

$$p_{21} = \frac{Q_{m22}Q_{f12}v_f}{Q_{m22}v_f + Q_{f22}v_m}$$

$$p_{22} = \frac{Q_{m22}Q_{f22}v_f}{Q_{m22}v_f + Q_{f22}v_m}$$

$$p_{13} = p_{23} = p_{33} = p_{31} = p_{32} = 0$$

$[Q]$ is a symmetric matrix but $[p]$ is not ($p_{12} \neq p_{21}$).

2.3 Transformation of Fiber Orientation

If the piezoelectric fibers remain parallel to one-another, but are rotated by angle θ such that their principal material coordinates 1,2 are oriented with respect to the global structural coordinates x, y as shown in figure 2.2, the stresses and strains corresponding to the coordinates x, y can be calculated by the Mohr's circle. For stress relationship:

$$\begin{Bmatrix} \sigma_1 \\ \sigma_2 \\ \tau_{12} \end{Bmatrix} = [T_\sigma(\theta)] \begin{Bmatrix} \sigma_x \\ \sigma_y \\ \tau_{xy} \end{Bmatrix} \tag{2.18}$$

For strain and piezoelectric coupling constant:

$$\begin{Bmatrix} \varepsilon_1 \\ \varepsilon_2 \\ \gamma_{12} \end{Bmatrix} = [T_\varepsilon(\theta)] \begin{Bmatrix} \varepsilon_x \\ \varepsilon_y \\ \gamma_{xy} \end{Bmatrix} \tag{2.19}$$

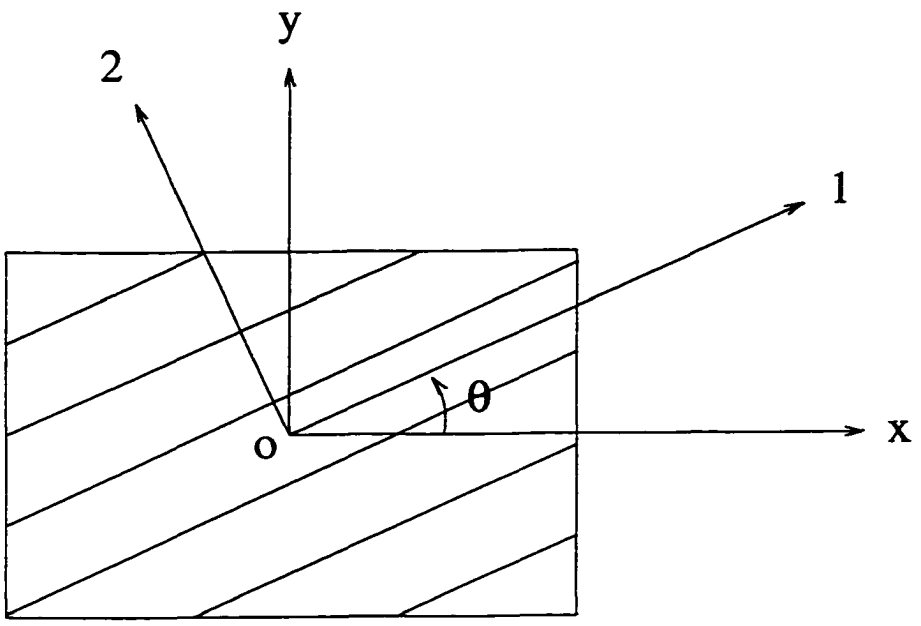

Figure 2.2 Principal material coordinates and global structural coordinates.

$$\begin{Bmatrix} d_{31} \\ d_{32} \\ 0 \end{Bmatrix} = [T_\varepsilon(\theta)] \begin{Bmatrix} d_x \\ d_y \\ d_{xy} \end{Bmatrix} \tag{2.20}$$

where $[T_\sigma(\theta)]$, $[T_\varepsilon(\theta)]$ are the stress transformation matrix and strain transformation matrix respectively; d_x, d_y, d_{xy} are the coupling constants between the applied electric field in z direction and normal strains in x, y directions, and shear strain in xy plane.

$$[T_\sigma(\theta)] = \begin{bmatrix} c^2 & s^2 & 2cs \\ s^2 & c^2 & -2cs \\ -cs & cs & c^2 - s^2 \end{bmatrix} \tag{2.21}$$

$$[T_\varepsilon(\theta)] = \begin{bmatrix} c^2 & s^2 & cs \\ s^2 & c^2 & -cs \\ -2cs & 2cs & c^2 - s^2 \end{bmatrix} \tag{2.22}$$

where $c = \cos\theta$ and $s = \sin\theta$. Substituting equations (2.18), (2.19), (2.20) into equation (2.17):

$$\begin{Bmatrix} \sigma_x \\ \sigma_y \\ \tau_{xy} \end{Bmatrix} = [T_\sigma(\theta)]^{-1}[Q][T_\varepsilon(\theta)] \begin{Bmatrix} \varepsilon_x \\ \varepsilon_y \\ \gamma_{xy} \end{Bmatrix} - \frac{V_a}{t_a}[T_\sigma(\theta)]^{-1}[p][T_\varepsilon(\theta)] \begin{Bmatrix} d_x \\ d_y \\ d_{xy} \end{Bmatrix} \tag{2.23}$$

The transformed stiffness matrix and transformed piezoelectric constant matrix are defined as:

$$[\bar{Q}] = [T_\sigma(\theta)]^{-1}[Q][T_\varepsilon(\theta)] \tag{2.24}$$

$$[\bar{p}] = [T_\sigma(\theta)]^{-1}[p][T_\varepsilon(\theta)] \tag{2.25}$$

Then equation (2.23) becomes:

$$\begin{Bmatrix} \sigma_x \\ \sigma_y \\ \tau_{xy} \end{Bmatrix} = [\bar{Q}] \begin{Bmatrix} \varepsilon_x \\ \varepsilon_y \\ \gamma_{xy} \end{Bmatrix} - \frac{V_a}{t_a}[\bar{p}] \begin{Bmatrix} d_x \\ d_y \\ d_{xy} \end{Bmatrix} \tag{2.26}$$

The terms of above two matrices are:

$$\overline{Q}_{11} = Q_{11}\cos^4\theta + Q_{22}\sin^4\theta + 2(Q_{12} + 2Q_{66})\sin^2\theta\cos^2\theta$$

$$\overline{Q}_{12} = (Q_{11} + Q_{22} - 4Q_{66})\sin^2\theta\cos^2\theta + Q_{12}(\cos^4\theta + \sin^4\theta)$$

$$\overline{Q}_{22} = Q_{11}\sin^4\theta + Q_{22}\cos^4\theta + 2(Q_{12} + 2Q_{66})\sin^2\theta\cos^2\theta$$

$$\overline{Q}_{16} = (Q_{11} - Q_{12} - 2Q_{66})\cos^3\theta\sin\theta - (Q_{22} - Q_{12} - 2Q_{66})\cos\theta\sin^3\theta$$

$$\overline{Q}_{26} = (Q_{11} - Q_{12} - 2Q_{66})\cos\theta\sin^3\theta - (Q_{22} - Q_{12} - 2Q_{66})\cos^3\theta\sin\theta$$

$$\overline{Q}_{66} = (Q_{11} + Q_{22} - 2Q_{12} - 2Q_{66})\sin^2\theta\cos^2\theta + Q_{66}(\cos^4\theta + \sin^4\theta)$$

$$\overline{p}_{11} = p_{11}\cos^4\theta + p_{22}\sin^4\theta + 2(p_{12} + 2P_{66})\sin^2\theta\cos^2\theta$$

$$\overline{p}_{12} = (p_{11} + p_{22} - 4p_{66})\sin^2\theta\cos^2\theta + p_{12}(\cos^4\theta + \sin^4\theta)$$

$$\overline{p}_{22} = p_{11}\sin^4\theta + p_{22}\cos^4\theta + 2(p_{12} + 2P_{66})\sin^2\theta\cos^2\theta$$

$$\overline{p}_{16} = (p_{11} - p_{12} - 2p_{66})\cos^3\theta\sin\theta - (p_{22} - p_{12} - 2p_{66})\cos\theta\sin^3\theta$$

$$\overline{p}_{26} = (p_{11} - p_{12} - 2p_{66})\cos\theta\sin^3\theta - (p_{22} - p_{12} - 2p_{66})\cos^3\theta\sin\theta$$

$$\overline{p}_{66} = (p_{11} + p_{22} - 2p_{12} - 2p_{66})\sin^2\theta\cos^2\theta + p_{66}(\cos^4\theta + \sin^4\theta)$$

From equation (2.20):

$$\begin{Bmatrix} d_x \\ d_y \\ d_{xy} \end{Bmatrix} = [T_\varepsilon(\theta)]^{-1} \begin{Bmatrix} d_{31} \\ d_{32} \\ 0 \end{Bmatrix}$$

$$= \begin{bmatrix} c^2 & s^2 & cs \\ s^2 & c^2 & -cs \\ -2cs & 2cs & c^2 - s^2 \end{bmatrix}^{-1} \begin{Bmatrix} d_{31} \\ d_{32} \\ 0 \end{Bmatrix}$$

$$= \begin{bmatrix} c^2 & s^2 & -cs \\ s^2 & c^2 & cs \\ 2cs & -2cs & c^2 - s^2 \end{bmatrix} \begin{Bmatrix} d_{31} \\ d_{32} \\ 0 \end{Bmatrix} \tag{2.27}$$

for the isotropic PZT fiber: $d_{31} = d_{32} = d$, therefore:

$$\begin{Bmatrix} d_x \\ d_y \\ d_{xy} \end{Bmatrix} = \begin{Bmatrix} d \\ d \\ 0 \end{Bmatrix} \tag{2.28}$$

This implies that an isotropic PZT fiber can not generate shear strain itself. However, it does create shear stress due to the coupling in $[\bar{p}]$ matrix of equation (2.26) after the rotation of angle θ. That represents a significant difference between PZT fiber and PZT patch actuators.

Equation (2.26) can also be applied to PZT patch by letting:

$$\begin{aligned} v_f &= 1 \\ v_m &= 0 \\ c &= \cos\theta = 1 \\ s &= \sin\theta = 0 \end{aligned} \tag{2.29}$$

it is also noted that form equation (2.27):

$$\begin{Bmatrix} d_x \\ d_y \\ d_{xy} \end{Bmatrix} = \begin{Bmatrix} d_{31} \\ d_{32} \\ 0 \end{Bmatrix} \tag{2.30}$$

Equation (2.30) holds for PZT patch which is not necessarily isotropic. When the PZT patch is isotropic, $d_{31} = d_{32}$. For a beam, equation (2.26) reduces to:

$$\sigma_x = Q_{11}\varepsilon_x - \frac{V_a}{t_a} p_{11} d_{31}$$

$$= E\varepsilon_x - \frac{V_a}{t_a} E d_{31} \tag{2.31}$$

or:

$$\varepsilon_x = \frac{1}{E}\sigma_x + \frac{V_a}{t_a} d_{31} \tag{2.32}$$

Equation (2.26) is applicable to piezoelectric fiber or patch actuators, but equation (2.32) is a special case, i.e., for a one-dimensional problem. These two equations will be used to incorporate the piezoelectric actuators into plate and beam structures.

CHAPTER III

DYNAMIC MODEL OF A BEAM WITH PIEZOELECTRIC ACTUATORS

In this chapter, the dynamic model of a cantilevered beam with a pair of piezoelectric patch actuators is derived to study the transfer property between control voltage and response of the beam structure.

3.1 Effectiveness of Piezoelectric Patch

If a voltage $V_a(x,t)$ is applied to a pair of actuating piezoelectric layers, as shown in figure 3.1, it induces a longitudinal stress σ_a given by [37]:

$$\sigma_a(x,t) = \frac{E_a d_{31}}{t_a} V_a(x,t) \tag{3.1}$$

where d_{31} : the electric charge constant of the piezoelectric actuator,

E_a : the Young's modulus of the piezoelectric layer,

t_a : the thickness of the piezoelectric layer.

The bending moment M_a due to this stress can be calculated by:

$$\begin{aligned} M_a(x,t) &= 2\int_{(t_b/2)}^{(t_b/2)+t_a} \sigma_a(x,t) w_b y dy \\ &= E_a d_{31} w_b (t_a + t_b) V_a(x,t) \\ &= C_a V_a(x,t) \end{aligned} \tag{3.2}$$

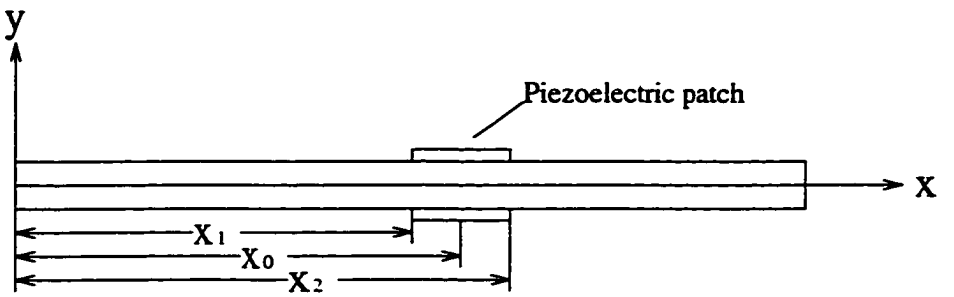

Figure 3.1 A beam with piezoelectric patch

where t_b : the thickness of the beam,

w_b : the width of the beam,

C_a : the geometric constant:

$$C_a = E_a d_{31} w_b (t_a + t_b) \tag{3.3}$$

3.2 Partial Differential Equation and Boundary Conditions

The differential equation of a piezoelectric composite beam is given by:

$$\frac{\partial^2}{\partial x^2}\left[EI(x)\frac{\partial^2 y(x,t)}{\partial x^2} - C_a V_a(x,t)\right] + \rho A \frac{\partial^2 y(x,t)}{\partial t^2} = 0 \tag{3.4}$$

where E : Young's Modulus,

I : moment of inertia,

ρ : mass density,

A : cross-section area of the beam.

The Boundary Conditions for a cantilevered beam clamped at $x = 0$ are:

$$\begin{aligned} y(0,t) &= 0, & \frac{\partial y(0,t)}{\partial x} &= 0 \\ EI\frac{\partial^2 y(L,t)}{\partial x^2} &= 0, & EI\frac{\partial^3 y(L,t)}{\partial x^3} &= 0 \end{aligned} \tag{3.5}$$

where L is the length of the beam.

3.3 Solution to the Partial Differential Equation

The equation (3.4) can be re-written as:

$$\frac{\partial^2}{\partial x^2}\left[EI(x)\frac{\partial^2 y(x,t)}{\partial x^2}\right]+\rho A\frac{\partial^2 y(x,t)}{\partial t^2}=\frac{\partial^2}{\partial x^2}[C_a V_a(x,t)] \tag{3.6}$$

For free vibration $V_a(x,t)\equiv 0$. Separation of variables is assumed in the form:

$$y(x,t)=\sum_{i=1}^{\infty} y_i(x,t)$$

$$=\sum_{i=1}^{\infty}\phi_i(x)q_i(t) \tag{3.7}$$

The modal deflection $y_i(x,t)=\phi_i(x)q_i(t)$ must satisfy the homogeneous part of equation (3.6) and all the Boundary Conditions (3.5), i.e.:

$$\frac{d^2}{dx^2}\left[EI(x)\frac{d^2\phi_i(x)}{dx^2}\right]q_i(t)+\rho A\phi_i(x)\ddot{q}_i(t)=0 \tag{3.8}$$

For harmonic modal deflection $\ddot{q}_i(t)=-\omega_i^2 q_i(t)$, thus:

$$\left\{\frac{d^2}{dx^2}\left[EI(x)\frac{d^2\phi_i(x)}{dx^2}\right]-\rho A\omega_i\phi_i(x)\right\}q_i(t)=0 \tag{3.9}$$

For the non-trivial solution, equation (3.9) reduces to:

$$\frac{d^2}{dx^2}\left[EI(x)\frac{d^2\phi_i(x)}{dx^2}\right]-\rho A\omega_i\phi_i(x)=0 \tag{3.10}$$

For an uniform beam, EI is a constant. The eigenfunction $\phi_i(x)$, satisfying the equation (3.10) and boundary condition (3.5), has the form:

$$\phi_i(x)=\frac{1}{\sqrt{\rho AL}}[\cosh\beta_i x-\cos\beta_i x-k_i(\sinh\beta_i x-\sin\beta_i x)] \qquad i=1,2,\cdots \tag{3.11}$$

where:

$$k_i=\frac{\sinh\beta_i L-\sin\beta_i L}{\cosh\beta_i L+\cos\beta_i L} \qquad i=1,2,\cdots \tag{3.12}$$

and β_i is the ith root of the following equation:

$$1+\cosh\beta_i L\cos\beta_i L=0 \qquad i=1,2,\cdots \qquad (3.13)$$

with corresponding natural frequency:

$$\omega_i=\beta_i^2\sqrt{\frac{EI}{\rho A}} \qquad i=1,2,\cdots \qquad (3.14)$$

The orthogonality of the eigenfunctions are expressed as:

$$\int_0^L \rho A\phi_i(x)\phi_j(x)dx=\delta_{ij} \qquad i,j=1,2,\cdots \qquad (3.15)$$

and

$$\int_0^L \phi_j(x)\frac{d^2}{dx^2}\left[EI(x)\frac{d^2\phi_i(x)}{dx^2}\right]dx=\omega_i^2\delta_{ij} \qquad i,j=1,2,\cdots \qquad (3.16)$$

Therefore, integration of equation (3.8) multiplied by $\phi_j(x)$ leads to:

$$\omega_i^2 q_i(t)+\ddot{q}_i(t)=0 \qquad (3.17)$$

The corresponding non-homogeneous equation (3.6) can be re-written as:

$$\ddot{q}_i(t)+\omega_i^2 q_i(t)=f_i(x,t) \qquad (3.18)$$

Since the piezoelectric actuator covers the beam at the region of $[x_1,x_2]$, the modal force $f_i(x,t)$ can be expressed by the following equation:

$$f_i(x,t)=\int_0^L \phi_i(x)\frac{\partial^2}{\partial x^2}[C_a V_a(x,t)]dx$$

$$=\int_0^L C_a V_a(t)\phi_i(x)\frac{\partial^2}{\partial x^2}[H(x-x_1)-H(x-x_2)]dx \qquad (3.19)$$

where H is Heavyside's step function defined as:

$$H(t-t_0)=\begin{cases}0 & t<t_0\\ 1 & t\geq t_0\end{cases} \qquad (3.20)$$

and

$$\frac{dH(t-t_0)}{dt}=\delta(t-t_0) \tag{3.21}$$

where δ is the *Dirac delta* function (Impulse function) whose n th derivative is defined by [36]. Thus equation (3.19) can be written as:

$$f_i(x,t)=C_aV_a(t)\left\{\int_0^L\left[\frac{\partial\delta(x-x_1)}{\partial x}-\frac{\partial\delta(x-x_2)}{\partial x}\right]\phi_i(x)dx\right\}$$

$$=C_aV_a(t)\left[\frac{\partial\phi_i(x_1)}{\partial x}-\frac{\partial\phi_i(x_2)}{\partial x}\right]$$

$$=C_aV_a(t)\left[\frac{\frac{\partial\phi_i(x_2)}{\partial x}-\frac{\partial\phi_i(x_1)}{\partial x}}{x_2-x_1}\right][-(x_2-x_1)]$$

$$\approx -C_aV_a(t)\frac{\partial^2\phi_i(x_0)}{\partial x^2}\Delta x \tag{3.22}$$

where Δx is the length of the actuator and $x_0=\frac{x_1+x_2}{2}$ is the center point of the actuator. Equation (3.22) is an approximation when the piezoelectric actuator is short in the x dimension. This is generally considered an acceptable approximation when Δx is much less than half the shortest significant wave length. It indicates that the effectiveness of the piezoelectric actuator is proportional to the second derivatives of the mode shape, i.e. the curvature. Thus a piezoelectric actuator at the location corresponding to the mode shape's greatest curvature would have maximum control authority over that mode. This equation permits the discussion of the placement problem without consideration of geometry of the piezoelectric actuators, and without consideration of the discontinuity in the equation (3.19).

The *Laplace Transformation* of equation (3.18) leads to:

$$(s^2+\omega_i^2)Q_i(s) = -C_a \frac{\partial^2 \phi_i(x_0)}{\partial x^2} \Delta x V_a(s)$$

$$\frac{Q_i(s)}{V_a(s)} = -\frac{C_a \Delta x}{(s^2+\omega_i^2)} \frac{\partial^2 \phi_i(x_0)}{\partial x^2} \tag{3.23}$$

From equation (3.7):

$$Y(x,s) = \sum_{i=1}^{\infty} \phi_i(x) Q_i(s)$$

The transfer function between the control voltage (at x_0) and response (at x) is expressed as:

$$\frac{Y(x,s)}{V_a(s)} = \sum_{i=1}^{\infty} \phi_i(x) \frac{Q_i(s)}{V_a(s)}$$

$$= -C_a \Delta x \sum_{i=1}^{\infty} \frac{\phi_i(x) \dfrac{\partial^2 \phi_i(x_0)}{\partial x^2}}{s^2+\omega_i^2} \tag{3.24}$$

The exact form of the transfer function between the control voltage (at x_0) and response (at x) can be written as:

$$\frac{Y(x,s)}{V_a(s)} = C_a \sum_{i=1}^{\infty} \frac{\phi_i(x)\left[\dfrac{\partial \phi_i(x_1)}{\partial x} - \dfrac{\partial \phi_i(x_2)}{\partial x}\right]}{s^2+\omega_i^2} \tag{3.25}$$

The error due to the approximation is evaluated by the following integration:

$$Error = \int_0^t e^2 dt \tag{3.26}$$

where e is the difference between the impulse response of equation (3.24) and that of equation (3.25), and t is the time period. The error is calculated corresponding to the area

of the piezoelectric actuator for a three mode model. The center of the piezoelectric actuator is fixed at the center of the beam. Figure 3.2 shows that the error is relatively small up to $A_a / A_s = 0.3$, where A_a is the area of the piezoelectric actuator, and A_s is the area of the beam. Figure 3.3 shows the impulse response functions corresponding to the approximation and the exact solution for $A_a / A_s = 0.5$. The impulse response function of the approximation is very close to that of the exact solution.

Equation (3.24) shows that the effectiveness of the piezoelectric actuators depends upon the local curvature at the location of the actuator. As is well known, the effectiveness of generalized point force actuators is related to the modal deflections. Equation (3.24) indicates a major difference for placement considerations between generalized point force actuators and piezoelectric actuators. This property will be further verified through plate case in the following chapters.

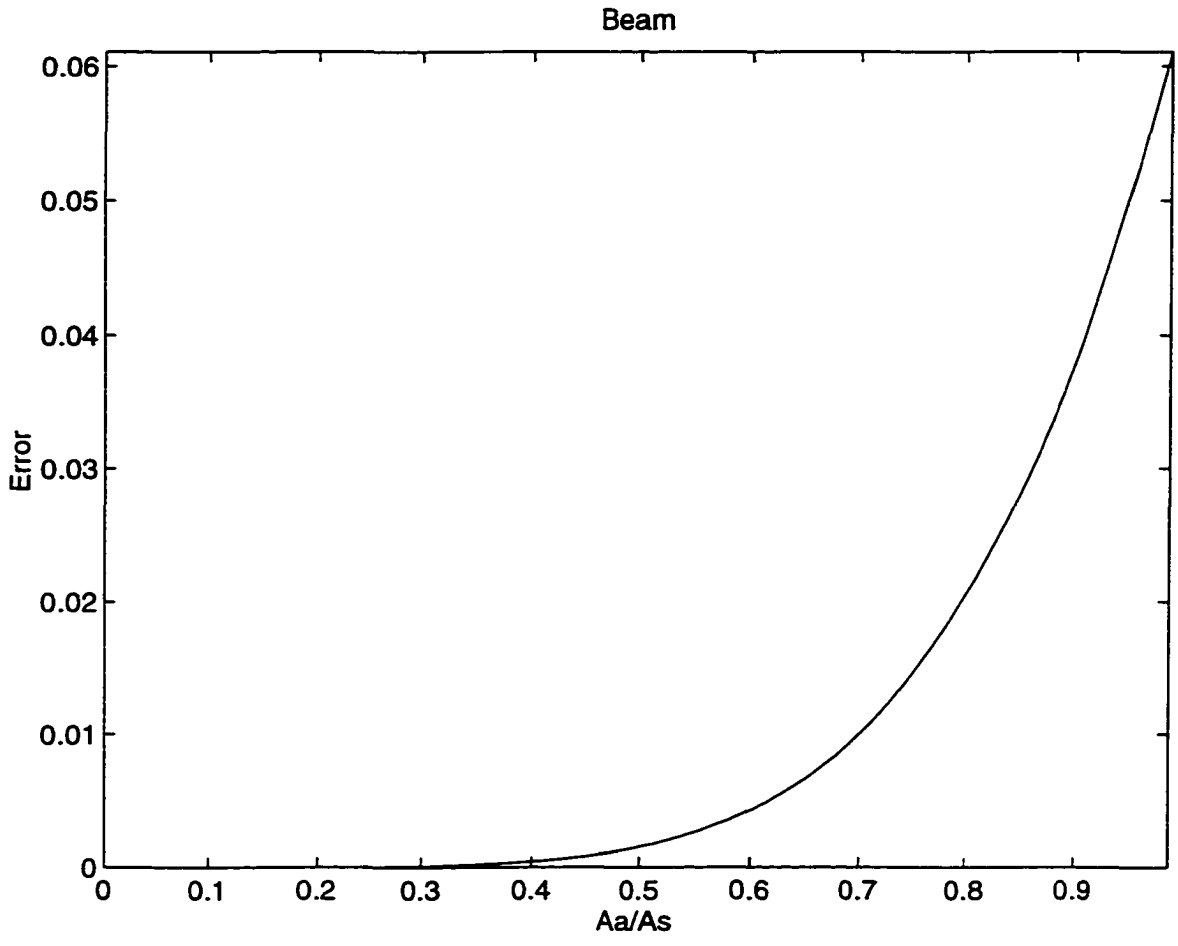

Figure 3.2 Error of the approximation for a cantilevered beam

(Center of the piezoelectric actuator: 0.5 *m*)

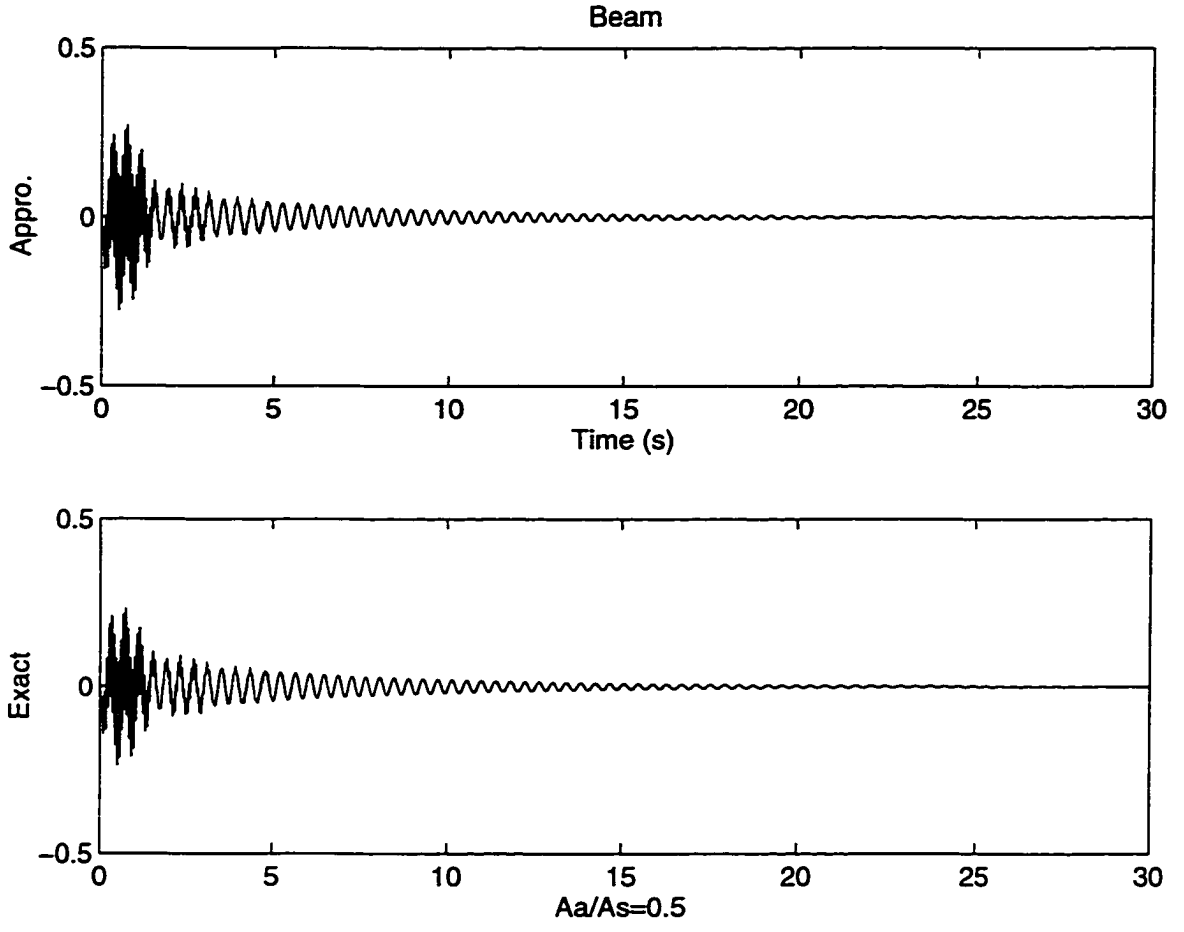

Figure 3.3 Comparison of impulse response functions for a cantilevered beam

CHAPTER IV

DYNAMIC MODEL OF AN ISOTROPIC PLATE WITH PIEZOELECTRIC FIBER COMPOSITE ACTUATORS

4.1 Effectiveness of the Piezoelectric Fiber Composite Actuators

Figure 4.1 shows an isotropic plate with a pair of PZT fiber actuators. The pair of actuators are surface bonded to the plate such that principal material directions of the active fiber in both pieces are parallel and form an angle θ with the x axis. The origin of the coordinates is set at the midplane about the xy plane.

The bending moments and shear forces of the isotropic plate can be expressed as [39]:

$$M_{xx} = -D\left(\frac{\partial^2 w}{\partial x^2} + v\frac{\partial^2 w}{\partial y^2}\right)$$

$$M_{yy} = -D\left(\frac{\partial^2 w}{\partial y^2} + v\frac{\partial^2 w}{\partial x^2}\right)$$

$$M_{xy} = -D(1-v)\frac{\partial^2 w}{\partial x \partial y} \qquad (4.1)$$

$$Q_x = -D\frac{\partial}{\partial x}\left(\frac{\partial^2 w}{\partial x^2} + \frac{\partial^2 w}{\partial y^2}\right)$$

$$Q_y = -D\frac{\partial}{\partial y}\left(\frac{\partial^2 w}{\partial x^2} + \frac{\partial^2 w}{\partial y^2}\right)$$

where M_{xx} : bending moment in yz plane,

M_{yy} : bending moment in zx plane,

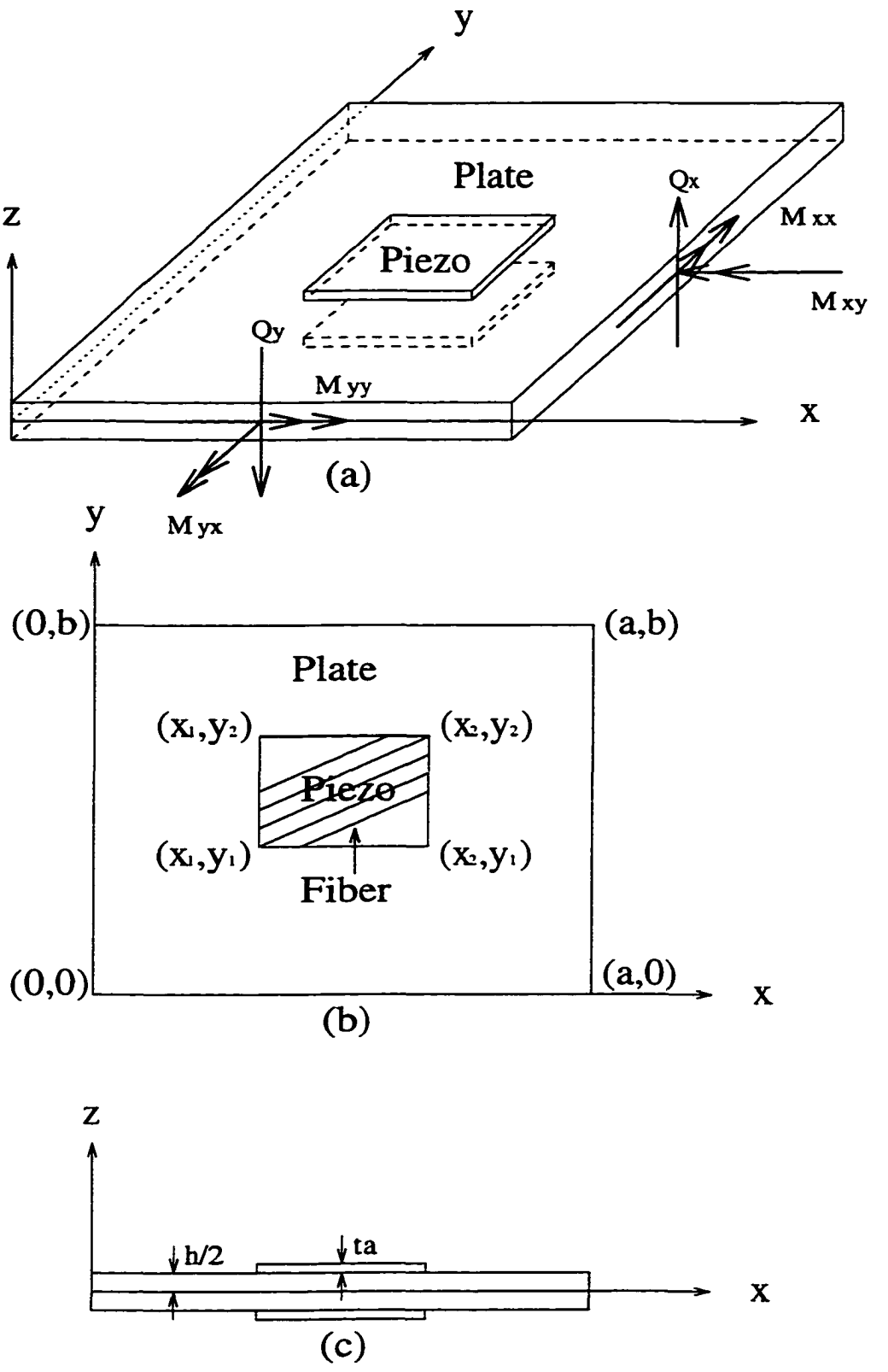

Figure 4.1 An isotropic plate with a pair of PZT fiber actuators

M_{xy} : twisting moment in xy plane,

Q_x : shear force as shown in figure 4.1a,

Q_y : shear force as shown in figure 4.1a,

w : deflection of the plate in z direction,

ν : Poisson's ratio of the plate,

D : plate flexural rigidity which is defined as:

$$D = \frac{Eh^3}{12(1-\nu^2)} \tag{4.2}$$

where E : Young's Modulus of the plate,

h : thickness of the plate.

The bending moment generated by the PZT fiber actuators can be obtained by the following integration:

$$\begin{Bmatrix} m_{xx} \\ m_{yy} \\ m_{xy} \end{Bmatrix} = \int_{(\frac{h}{2}+t_a)}^{\frac{h}{2}+t_a} \begin{Bmatrix} \sigma_x \\ \sigma_y \\ \tau_{xy} \end{Bmatrix} z \, dz \tag{4.3}$$

where m_{xx} : bending moment in yz plane,

m_{yy} : bending moment in zx plane,

m_{xy} : twisting moment in xy plane,

h : thickness of the isotropic plate,

t_a : thickness of the PZT fiber actuators as shown in figure 4.1c.

The stress vector in equation (4.3) is expressed in equation (2.26) which includes two parts: a passive stress term due to the stiffness of the actuator and an active voltage-induced stress term. The passive stress term changes the local stiffness of the structure and leads to discontinuity of the structural properties at the actuator's edge which renders the problem untractable unless Finite Element Method is used. The active term represents the coupling between the mechanical field and electric field which is the output of the controller in practice. Customarily, the stiffness of the actuators is neglected in the analytical approach [4, 32] because, compared with the structure, the thickness of the actuators is relatively small. In addition, the PZT actuators considered (either isotropic or fiber composite) are small relative to the size of the structure. Thus it is reasonable to assume that the stiffness of the patch is small enough to be neglected. Therefore equation (2.26) can be approximated as:

$$\begin{Bmatrix} \sigma_x \\ \sigma_y \\ \tau_{xy} \end{Bmatrix} = -\frac{V_a}{t_a}[\bar{p}]\begin{Bmatrix} d_x \\ d_y \\ d_{xy} \end{Bmatrix} \tag{4.4}$$

Substituting equation (4.4) into equation (4.3) leads to:

$$\begin{Bmatrix} m_{xx} \\ m_{yy} \\ m_{xy} \end{Bmatrix} = \int_{(\frac{h}{2}+t_a)}^{\frac{h}{2}+t_a} -\frac{V_a}{t_a}[\bar{p}]\begin{Bmatrix} d_x \\ d_y \\ d_{xy} \end{Bmatrix} z\, dz \tag{4.5}$$

To obtain bending moments, the poling directions of the pair of PZT fiber actuators and the applied control voltage must be correctly connected.

In figure 4.2 either of poling arrangements (a) or (b) ensures a pure bending moment [52], and in either case equation (4.5) can be written as:

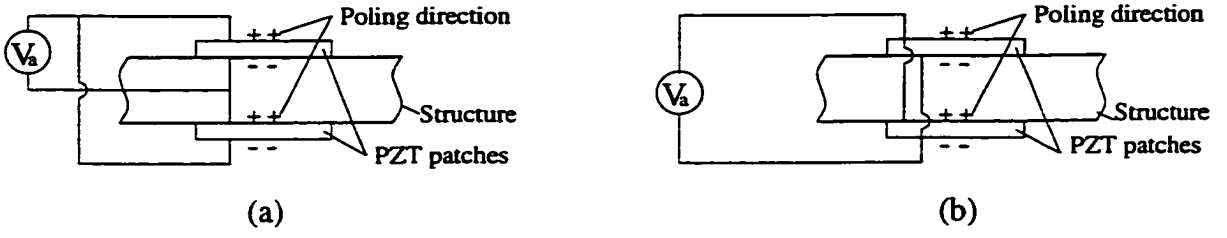

Figure 4.2 Poling directions and the applied control voltages.

$$\begin{Bmatrix} m_{xx} \\ m_{yy} \\ m_{xy} \end{Bmatrix} = \int_{\frac{h}{2}}^{(\frac{h}{2}+t_a)} -\frac{2V_a}{t_a}[\bar{p}]\begin{Bmatrix} d_x \\ d_y \\ d_{xy} \end{Bmatrix} z\,dz$$

$$= -(h+t_a)V_a[\bar{p}]\begin{Bmatrix} d_x \\ d_y \\ d_{xy} \end{Bmatrix}$$

$$= -V_a\begin{Bmatrix} C_x \\ C_y \\ C_{xy} \end{Bmatrix} \tag{4.6}$$

where : $C_x = (h+t_a)(\bar{p}_{11}d_x + \bar{p}_{12}d_y + \bar{p}_{16}d_{xy})$

$$C_y = (h+t_a)(\bar{p}_{21}d_x + \bar{p}_{22}d_y + \bar{p}_{26}d_{xy}) \tag{4.7}$$

$$C_{xy} = (h+t_a)(\bar{p}_{61}d_x + \bar{p}_{62}d_y + \bar{p}_{66}d_{xy})$$

For piezoelectric patch actuator, $C_x = C_y$ and $C_{xy} = 0$.

4.2 Partial Differential Equation of Motion for a Plate

The equation of motion for a plate with actuators can be written as:

$$\frac{\partial^2(M_{xx} - m_{xx})}{\partial x^2} + 2\frac{\partial^2(M_{xy} - m_{xy})}{\partial x \partial y} + \frac{\partial^2(M_{yy} - m_{yy})}{\partial y^2} = \rho h\frac{\partial^2 w}{\partial t^2} - f_d(x,y,t) \tag{4.8}$$

where w : deflection of plate in z direction as shown in figure 4.1c,

ρ : mass density,

h : thickness of plate,

f_d : distributed disturbance force.

Since m_{xx}, m_{yy}, m_{xy} represent control effort, re-arrange the equation (4.8) as:

$$-\left(\frac{\partial^2 M_{xx}}{\partial x^2}+2\frac{\partial^2 M_{xy}}{\partial x\partial y}+\frac{\partial^2 M_{yy}}{\partial y^2}\right)+\rho h\frac{\partial^2 w}{\partial t^2}$$

$$=-\left(\frac{\partial^2 m_{xx}}{\partial x^2}+2\frac{\partial^2 m_{xy}}{\partial x\partial y}+\frac{\partial^2 m_{yy}}{\partial y^2}\right)+f_d(x,y,t) \tag{4.9}$$

Substituting equation (4.6) into equation (4.9) and noticing equation (4.1), the equation of Motion for the plate vibration can be written as:

$$D\nabla^4 w+\rho h\ddot{w}=f_c(x,y,t)+f_d(x,y,t) \tag{4.10}$$

where ∇^2 is the *Laplacian Operator*:

$$\nabla^2 w=\frac{\partial^2 w}{\partial x^2}+\frac{\partial^2 w}{\partial y^2}$$

$$\nabla^4 w=\nabla^2\left(\nabla^2 w\right)=\frac{\partial^4 w}{\partial x^4}+2\frac{\partial^4 w}{\partial x^2\partial y^2}+\frac{\partial^4 w}{\partial y^4}$$

and $f_c(x,y,t)$ is the control force which has the form of:

$$f_c(x,y,t)=C_x\frac{\partial^2 V_a}{\partial x^2}+2C_{xy}\frac{\partial^2 V_a}{\partial x\partial y}+C_y\frac{\partial^2 V_a}{\partial y^2} \tag{4.11}$$

since the piezoelectric actuators cover only a small rectangular area $x=[x_1,x_2]$ and $y=[y_1,y_2]$ as shown in figure 4.1, the control electric field V_a is a function of coordinates and time. The Heavyside function can be introduced to V_a to describe such a discontinuity [9, 48]:

$$V_a=V_a(t)[H(x-x_1)-H(x-x_2)][H(y-y_1)-H(y-y_2)] \tag{4.12}$$

where $V_a(t)$ is the magnitude of the control voltage applied to actuators.

Substitution of equation (4.12) into equation (4.11) leads to:

$$f_c(x,y,t)=V_a(t)\left\{C_x\left[\frac{d^2H(x-x_1)}{dx^2}-\frac{d^2H(x-x_2)}{dx^2}\right][H(y-y_1)-H(y-y_2)]\right.$$

$$+2C_{xy}\left[\frac{dH(x-x_1)}{dx}-\frac{dH(x-x_2)}{dx}\right]\left[\frac{dH(y-y_1)}{dy}-\frac{dH(y-y_2)}{dy}\right]$$

$$\left.+C_y[H(x-x_1)-H(x-x_2)]\left[\frac{d^2H(y-y_1)}{dy^2}-\frac{d^2H(y-y_2)}{dy^2}\right]\right\}$$

$$=V_a(t)\left\{C_x\left[\frac{d\delta(x-x_1)}{dx}-\frac{d\delta(x-x_2)}{dx}\right][H(y-y_1)-H(y-y_2)]\right.$$

$$+2C_{xy}[\delta(x-x_1)-\delta(x-x_2)][\delta(y-y_1)-\delta(y-y_2)]$$

$$\left.+C_y[H(x-x_1)-H(x-x_2)]\left[\frac{d\delta(y-y_1)}{dy}-\frac{d\delta(y-y_2)}{dy}\right]\right\} \qquad (4.13)$$

Note that the n th derivative of the *Dirac delta function* is defined:

$$\int_{-\infty}^{\infty}\frac{d^n\delta(t-t_0)}{dt^n}\varphi(t)\,dt=(-1)^n\frac{d^n\varphi(t_0)}{dt^n} \qquad (4.14)$$

where $\varphi(t)$ is an arbitrary function. Equation (4.13) is widely used to model the piezoelectric actuators for vibration control of plate structures. The Heaveside function and Dirac delta function in equation (4.13) cause discontinuity within the plate structure. Analysis of the system using equation (4.13) requires the Finite Element Method [40, 45], which can be computationally expensive. This problem will be solved in the next chapter.

CHAPTER V

VIBRATION ANALYSIS OF A SIMPLY SUPPORTED RECTANGULAR PLATE

The dynamic model of piezoelectric actuators has been created in the preceding chapter. The control force due to piezoelectric actuation is to be transferred into modal coordinates. Discontinuity at the edge of the piezoelectric actuators will be eliminated by approximation based on the Cauchy Integration Theory. An unique equation is to be derived to simplify the transfer function between the piezoelectric actuators and the response of the structures.

5.1 Equation of Motion

The Equation of Motion for the plate vibration is given by equations (4.10), and (4.13). For convenience, the equation is repeated here:

$$D\nabla^4 w + \rho h\ddot{w} = f_c(x,y,t) + f_d(x,y,t) \tag{5.1}$$

where D : plate flexural rigidity defined by equation (4.2),

ρ : mass density,

h : thickness of plate,

f_d : disturbance force,

f_c : control force which has the form of equation (4.13).

The deflection of the plate can be written as the summation of harmonic displacements of each mode:

$$w(x,y,t)=\sum_{i=1}^{\infty} w_i(x,y,t)=\sum_{i=1}^{\infty}\phi_i(x,y)q_i(t) \tag{5.2}$$

Therefore, the bending moments M_{xx} and M_{yy}, the twisting moment M_{xy}, the shear forces Q_x and Q_y can be expressed as:

$$M_{xx}(x,y,t)=\sum_{i=1}^{\infty} M_{xx}^{(i)}(x,y)q_i(t)$$

$$M_{yy}(x,y,t)=\sum_{i=1}^{\infty} M_{yy}^{(i)}(x,y)q_i(t)$$

$$M_{xy}(x,y,t)=\sum_{i=1}^{\infty} M_{xy}^{(i)}(x,y)q_i(t) \tag{5.3}$$

$$Q_x(x,y,t)=\sum_{i=1}^{\infty} Q_x^{(i)}(x,y)q_i(t)$$

$$Q_y(x,y,t)=\sum_{i=1}^{\infty} Q_y^{(i)}(x,y)q_i(t)$$

5.2 Free Vibration

According to equation (5.2),

$$w_i(x,y,t)=\phi_i(x,y)q_i(t) \tag{5.4}$$

where $\phi_i(x,y)$ is the ith modal shape with natural frequency Ω_i. For harmonic motion:

$$\ddot{q}_i(t)=-\Omega_i^2 q_i(t) \tag{5.5}$$

Substitution of equation (5.4) into equation (5.1) leads to:

$$D\nabla^4\phi_i(x,y)=\rho h\Omega_i^2\phi_i(x,y) \tag{5.6}$$

The orthogonality relation and normalization condition can be stated as:

$$\int_A \rho h \phi_i(x,y)\phi_j(x,y)dA = \delta_{ij} \tag{5.7}$$

where δ_{ij} is the *Kronecker delta* symbol with property:

$$\delta_{ij} = \begin{cases} 1 & i = j \\ 0 & i \neq j \end{cases}$$

Equation (5.7) is known as the orthonormality relation of the free vibration modes associated with equation (5.6).

If the x dimension of the plate is a, and the y dimension of the plate is b, as shown in figure 4.1, the boundary conditions for simply supported case are:

$$\begin{aligned} \phi_i(x,0) &= M_{yy}^{(i)}(x,0) = 0 \\ \phi_i(x,b) &= M_{yy}^{(i)}(x,b) = 0 \\ \phi_i(0,y) &= M_{xx}^{(i)}(0,y) = 0 \\ \phi_i(a,y) &= M_{xx}^{(i)}(a,y) = 0 \end{aligned} \tag{5.8}$$

The solution of equation (5.6), subject to the boundary condition (5.8), is given by:

$$\phi_i(x,y) = A_{mn} \sin\frac{m\pi x}{a}\sin\frac{n\pi y}{b} \qquad m = 1,2,3,\cdots; \quad n = 1,2,3,\cdots \tag{5.9}$$

where A_{mn} are constants, and the natural frequencies of the plate are:

$$\Omega_i = \Omega_{mn} = \sqrt{\frac{D}{\rho h}}\left[\left(\frac{m\pi}{a}\right)^2 + \left(\frac{n\pi}{b}\right)^2\right] \tag{5.10}$$

Substituting the eigenfunctions $\phi_i(x,y)$ into the normalization condition (5.8) leads to:

$$A_{mn} = \left[\int_0^a \int_0^b \rho h \sin^2 \frac{m\pi x}{a} \sin^2 \frac{n\pi y}{b} dxdy \right]^{-\frac{1}{2}} = \frac{2}{\sqrt{ab\rho h}}$$

thus, equation (5.9) results in:

$$\phi_i(x, y) = \phi_{mn}(x, y) = \frac{2}{\sqrt{ab\rho h}} \sin \frac{m\pi x}{a} \sin \frac{n\pi y}{b}$$

$$m = 1,2,3,\cdots; \quad n = 1,2,3,\cdots \tag{5.11}$$

5.3 Forced Vibration

Substituting equation (5.2) into equation (5.1) leads to:

$$\sum_{i=1}^{\infty} \rho h \phi_i(x, y) \left[\ddot{q}_i(t) + \Omega_i^2 q_i(t) \right] = f_c(x, y, t) + f_d(x, y, t) \tag{5.12}$$

multiplying both sides of equation (5.12) by $\phi_j(x, y)$ and integrating over the area A of the plate leads to:

$$\sum_{i=1}^{\infty} \left[\ddot{q}_i(t) + \Omega_i^2 q_i(t) \right] \int_A \rho h \phi_i(x, y) \phi_j(x, y) dA$$

$$= \int_A f_c(x, y, t) \phi_j(x, y) dA + \int_A f_d(x, y, t) \phi_j(x, y) dA \tag{5.13}$$

Upon application of the orthogonality relation (5.7), equation (5.13) becomes:

$$\ddot{q}_i(t) + \Omega_i^2 q_i(t) = F_c^{(i)}(t) + F_d^{(i)}(t) \tag{5.14}$$

where

$$F_c^{(i)}(t) = \int_A f_c(x, y, t) \phi_i(x, y) dA \tag{5.15}$$

$$F_d^{(i)}(t) = \int_A f_d(x, y, t) \phi_i(x, y) dA \tag{5.16}$$

For linear systems, the solution of equation (5.14) can be considered as superposition of the responses to the disturbance force $F_d^{(i)}(t)$ and that to the control force $F_c^{(i)}(t)$.

5.3.1 Excited by a Point Force

Notice that the $f_d(x, y, t)$ in equation (5.16) is a distributed force. If the disturbance comes from a point control force $f_0(x, y, t)$ at location (x_0, y_0), it can be presented as:

$$f_d(x, y, t) = f_0(x, y, t)\delta(x - x_0)\delta(y - y_0) \tag{5.17}$$

where δ is the *Dirac delta function*. substituting equation (5.17) into equation (5.16) results in:

$$\begin{aligned} \overline{F}_d^{(i)}(x, y, t) &= \int_A f_d(x, y, t)\phi_i(x, y)dA \\ &= f_0(t)\phi_i(x_0, y_0) \end{aligned} \tag{5.18}$$

Substituting equation (5.11) into equation (5.18) results in:

$$\begin{aligned} F_d^{(i)}(x, y, t) &= \frac{2f_0(t)}{\sqrt{ab\rho h}} \sin\frac{m\pi x_0}{a} \sin\frac{n\pi y_0}{b} \\ &= C_d^{(i)} f_0(t) \end{aligned} \tag{5.19}$$

where

$$C_d^{(i)} = \frac{2}{\sqrt{ab\rho h}} \sin\frac{m\pi x_0}{a} \sin\frac{n\pi y_0}{b} \tag{5.20}$$

Therefore, in the absence of control effort, equation (5.14) becomes:

$$\ddot{q}_i(t) + \Omega_i^2 q_i(t) = C_d^{(i)} f_0(t) \tag{5.21}$$

The *Laplace Transform* of equation (5.21) yields:

$$\left(s^2 + \Omega_i^2\right) Q_i(s) = C_d^{(i)} F_0(s) \tag{5.22}$$

From equation (5.22), the transfer function between the disturbance force and the ith modal response is found:

$$H_d^{(i)}(s) = \frac{Q_i(s)}{F_0(s)} = \frac{C_d^{(i)}}{s^2 + \Omega_i^2} \tag{5.23}$$

The *Laplace Transform* of equation (5.2) yields:

$$W(x, y, s) = \sum_{i=1}^{\infty} \phi_i(x, y) Q_i(s) \tag{5.24}$$

Substituting equation (5.23) into equation (5.24) results in:

$$H_d(s) = \frac{W(x, y, s)}{F_0(s)} = \sum_{i=1}^{\infty} \phi_i(x, y) \frac{C_d^{(i)}}{s^2 + \Omega_i^2} \tag{5.25}$$

Substituting equation (5.11), equation (5.20) into equation (5.25) leads to:

$$H_d(s) = \frac{W(x, y, s)}{F_0(x_0, y_0, s)}$$

$$= \sum_{i=1}^{\infty} \frac{4}{ab\rho h\left(s^2 + \Omega_i^2\right)} \sin\frac{m\pi x_0}{a} \sin\frac{n\pi y_0}{b} \sin\frac{m\pi x}{a} \sin\frac{n\pi y}{b} \tag{5.26}$$

where (x_0, y_0) and (x, y) are the coordinates of the driving and response points, respectively.

5.3.2 Excited by Voltage

The modal control force $F_c^{(i)}(t)$ can be calculated by substituting equation (4.13) into equation (5.15) and taking note of equation (4.14):

$$F_c^{(i)}(t) = \int_A f_c(x,y,t)\phi_i(x,y)dA$$

$$= V_a(t)\left\{C_x \int_A \left[\frac{d\delta(x-x_1)}{dx} - \frac{d\delta(x-x_2)}{dx}\right][H(y-y_1) - H(y-y_2)]\phi_i(x,y)\,dA\right.$$

$$+ 2C_{xy} \int_A [\delta(x-x_1) - \delta(x-x_2)][\delta(y-y_1) - \delta(y-y_2)]\phi_i(x,y)\,dA$$

$$\left. + C_y \int_A [H(x-x_1) - H(x-x_2)]\left[\frac{d\delta(y-y_1)}{dy} - \frac{d\delta(y-y_2)}{dy}\right]\phi_i(x,y)\,dA\right\}$$

$$= V_a(t)\left\{C_x \int_0^b \left[\frac{\partial\phi_i(x_2,y)}{\partial x} - \frac{\partial\phi_i(x_1,y)}{\partial x}\right][H(y-y_1) - H(y-y_2)]dy\right.$$

$$+ 2C_{xy} \int_0^b [\phi_i(x_1,y) - \phi_i(x_2,y)][\delta(y-y_1) - \delta(y-y_2)]dy$$

$$\left. + C_y \int_0^a [H(x-x_1) - H(x-x_2)]\left[\frac{\partial\phi_i(x,y_2)}{\partial y} - \frac{\partial\phi_i(x,y_1)}{\partial y}\right]dx\right\}$$

$$= V_a(t)\left\{C_x \int_{y_1}^{y_2} \left[\frac{\partial\phi_i(x_2,y)}{\partial x} - \frac{\partial\phi_i(x_1,y)}{\partial x}\right]dy\right.$$

$$+ 2C_{xy}[\phi_i(x_1,y_1) - \phi_i(x_2,y_1) - \phi_i(x_1,y_2) + \phi_i(x_2,y_2)]$$

$$\left. + C_y \int_{x_1}^{x_2} \left[\frac{\partial\phi_i(x,y_2)}{\partial y} - \frac{\partial\phi_i(x,y_1)}{\partial y}\right]dx\right\}$$

$$= V_a(t)C_c^{(i)} \tag{5.27}$$

where

$$C_c^{(i)} = \left\{C_x \int_{y_1}^{y_2} \left[\frac{\partial\phi_i(x_2,y)}{\partial x} - \frac{\partial\phi_i(x_1,y)}{\partial x}\right]dy\right.$$

$$+ 2C_{xy}[\phi_i(x_1,y_1) - \phi_i(x_2,y_1) - \phi_i(x_1,y_2) + \phi_i(x_2,y_2)]$$

$$\left. + C_y \int_{x_1}^{x_2} \left[\frac{\partial\phi_i(x,y_2)}{\partial y} - \frac{\partial\phi_i(x,y_1)}{\partial y}\right]dx\right\} \tag{5.28}$$

Equation (5.28) is an exact expression for $C_c^{(i)}$, which can be used to determine the constant for rectangular shaped structures with analytical expressions for the mode shapes.

Recall the Cauchy Integration Theory:

If function $f(x)$ is a continuous and integrable function defined in area [a, b], there exists a point $\xi \in [a,b]$ such that the following equation holds:

$$\int_a^b f(x)dx = (b-a)f(\xi)$$

Equation (5.28) can be modified by applying the above integration theory:

$$\begin{aligned} C_c^{(i)} = \Bigg\{ & C_x \left[\frac{\partial \phi_i(x_2,\eta_2)}{\partial x} - \frac{\partial \phi_i(x_1,\eta_1)}{\partial x} \right](y_2 - y_1) \\ & + 2C_{xy}\left[\phi_i(x_1,y_1) - \phi_i(x_2,y_1) - \phi_i(x_1,y_2) + \phi_i(x_2,y_2)\right] \\ & + C_y \left[\frac{\partial \phi_i(\xi_2,y_2)}{\partial y} - \frac{\partial \phi_i(\xi_1,y_1)}{\partial y} \right](x_2 - x_1) \Bigg\} \end{aligned} \tag{5.29}$$

where $\xi_1, \xi_2 \in [x_1, x_2]$; $\eta_1, \eta_2 \in [y_1, y_2]$. Equation (5.29) is also an exact form as long as the appropriate points $\xi_1, \xi_2, \eta_1, \eta_2$ are found. An alternative choice is to select the midpoints such that:

$$\xi = \xi_1 = \xi_2 = \frac{x_1 + x_2}{2}$$

$$\eta = \eta_1 = \eta_2 = \frac{y_1 + y_2}{2}$$

then an approximation of equation (5.29) is written as:

$$C_c^{(i)} \approx \left\{ C_x \left[\frac{\partial \phi_i(x_2,\eta)}{\partial x} - \frac{\partial \phi_i(x_1,\eta)}{\partial x} \right] (y_2 - y_1) \right.$$

$$+ 2C_{xy} \left[\phi_i(x_1, y_1) - \phi_i(x_2, y_1) - \phi_i(x_1, y_2) + \phi_i(x_2, y_2) \right]$$

$$\left. + C_y \left[\frac{\partial \phi_i(\xi, y_2)}{\partial y} - \frac{\partial \phi_i(\xi, y_1)}{\partial y} \right] (x_2 - x_1) \right\} \tag{5.30}$$

As the purpose of this research, the location is under investigation in which the application of PZT actuators leads to an optimal solution in a sense of effectiveness for most control methods. Therefore, it is reasonable to assume that the applied PZT actuators have relatively small dimensions by comparison to the modal wave length. When (x_1, y_1) approaches (x_2, y_2), equation (5.30) can be further approximated as:

$$C_c^{(i)} \approx \left\{ C_x \left[\frac{\dfrac{\partial \phi_i(x_2,\eta)}{\partial x} - \dfrac{\partial \phi_i(x_1,\eta)}{\partial x}}{(x_2 - x_1)} \right] (x_2 - x_1)(y_2 - y_1) \right.$$

$$+ 2C_{xy} \left[\frac{\phi_i(x_1, y_1) - \phi_i(x_2, y_1)}{x_1 - x_2} - \frac{\phi_i(x_1, y_2) - \phi_i(x_2, y_2)}{x_1 - x_2} \right] (x_1 - x_2)$$

$$\left. + C_y \left[\frac{\dfrac{\partial \phi_i(\xi, y_2)}{\partial y} - \dfrac{\partial \phi_i(\xi, y_1)}{\partial y}}{y_2 - y_1} \right] (x_2 - x_1)(y_2 - y_1) \right\}$$

$$\approx A_a \left\{ C_x \frac{\partial^2 \phi_i(\xi,\eta)}{\partial x^2} + 2C_{xy} \frac{\partial^2 \phi_i(\xi,\eta)}{\partial x \partial y} + C_y \frac{\partial^2 \phi_i(\xi,\eta)}{\partial y^2} \right\} \tag{5.31}$$

where $A_a = (x_2 - x_1)(y_2 - y_1)$ is the area of an actuator and (ξ,η) is chosen as the central point of A_a. The coefficients C_x, C_{xy}, and C_y in equation (5.31) are determined by the properties of the piezoelectric actuators (either piezoelectric fiber actuators or

piezoelectric patch actuators) while the effectiveness of the modal force also depends upon the second derivatives of the mode shapes. Equation (5.31) is a continuous function over the entire structure, which solves the discontinuity problem in equation (4.13) and can be computed without application of Finite Element Method, even for complicated structures. This is a significant benefit for the calculation of the indices over an entire structure with very large number of nodes. By taking A_a as a constant, one is able to compare the actuation performance of piezoelectric actuators with fixed area.

The modal response to the control voltage is governed by:

$$\ddot{q}_i(t) + \Omega_i^2 q_i(t) = C_c^{(i)} V_a(t) \tag{5.32}$$

Similar to the steps from equation (5.21) to equation (5.26), the transfer function between the control voltage and ith modal response can be easily written as:

$$H_c^{(i)}(s) = \frac{Q_i(s)}{V_a(s)} = \frac{C_c^{(i)}}{s^2 + \Omega_i^2} \tag{5.33}$$

The transfer function from control voltage to global response is:

$$H_c(s) = \frac{W(x, y, s)}{V_a(s)} = \sum_{i=1}^{\infty} \phi_i(x, y) \frac{C_c^{(i)}}{s^2 + \Omega_i^2} \tag{5.34}$$

Using the approximate form equation (5.31), equation (5.34) results in:

$$H_c(s) = \frac{W(x, y, s)}{V_a(\xi, \eta, s)}$$

$$= \sum_{i=1}^{\infty} \phi_i(x, y) \frac{A_a}{s^2 + \Omega_i^2} \left[C_x \frac{\partial^2 \phi_i(\xi, \eta)}{\partial x^2} + 2C_{xy} \frac{\partial^2 \phi_i(\xi, \eta)}{\partial x \partial y} + C_y \frac{\partial^2 \phi_i(\xi, \eta)}{\partial y^2} \right] \tag{5.35}$$

If a rectangular piezoelectric actuator covers the area $x \in [x_1, x_2]$ and $y \in [y_1, y_2]$, the exact form of the transfer function between the control voltage and response can be derived using equation (5.28):

$$H_c(s) = \sum_{i=1}^{\infty} \phi_i(x,y) \frac{A_a}{s^2 + \Omega_i^2} \left\{ +2C_{xy} \left[\phi_i(x_1, y_1) - \phi_i(x_2, y_1) - \phi_i(x_1, y_2) + \phi_i(x_2, y_2) \right] \right.$$

$$\left. - \frac{2}{\sqrt{abph}} \left(\frac{mb}{na} C_x + \frac{na}{mb} C_y \right) \left(\cos\frac{m\pi x_2}{a} - \cos\frac{m\pi x_1}{a} \right) \left(\cos\frac{n\pi y_2}{b} - \cos\frac{n\pi y_1}{b} \right) \right\} \quad (5.36)$$

The error due to the approximation can be evaluated by equation (3.26). The error is calculated corresponding to the area of the piezoelectric actuator for a three mode model. The center of the piezoelectric actuator is fixed at the center of the rectangular plate and the ratio of the widths of the piezoelectric actuator is fixed as $\frac{y_2 - y_1}{x_2 - x_1} = \frac{b}{a}$, where a and b are the widths of the rectangular plate. Figure 5.1 shows that the error is relatively small up to $A_a / A_s = 0.1$, where A_a is the area of the piezoelectric actuator, and A_s is the area of the plate. Figure 5.2 shows the impulse response functions corresponding to the approximation and the exact solution for $A_a / A_s = 0.25$.

Similar to the equation (3.24) for the beam case, equation (5.35) shows that the effectiveness of the piezoelectric actuators depends upon the local modal curvature where the actuators are placed, which is different in actuation mechanism from the generalized point force actuators whose effectiveness is related to the mode deflections. This is an important distinction which will significantly affect the placement consideration for different types of actuators in the applications of vibration control.

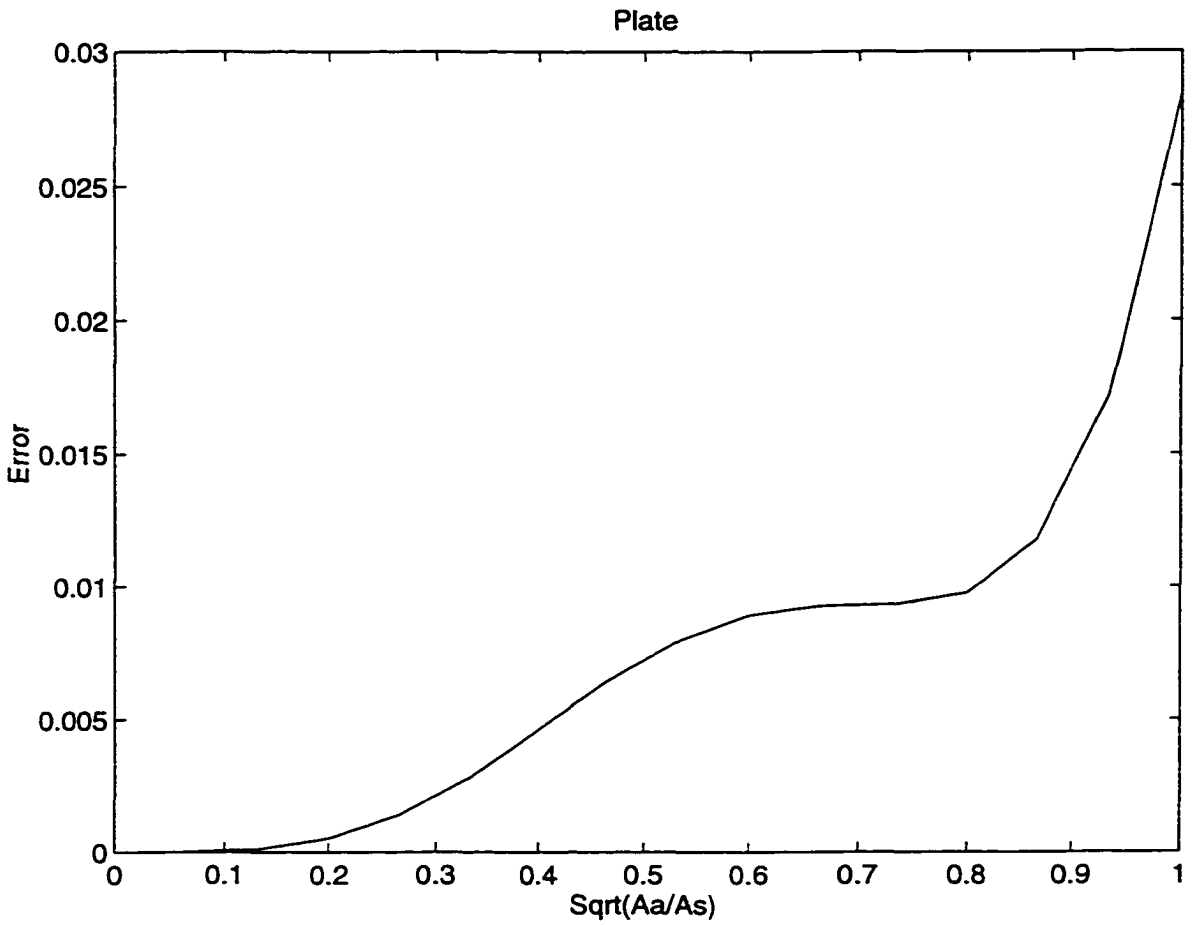

Figure 5.1 Error of the approximation for a rectangular plate

(Center of the piezoelectric actuator: (0.5m, 0.3m))

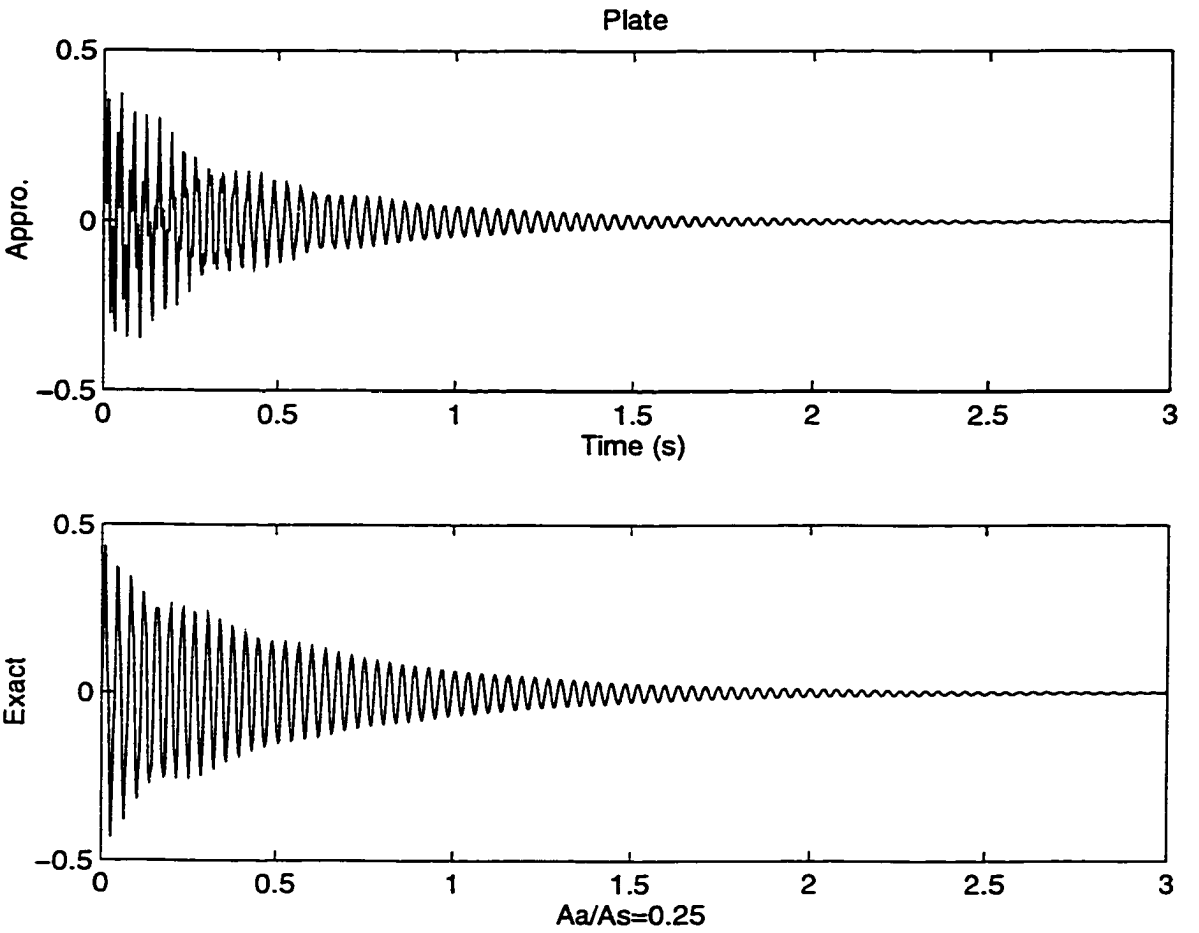

Figure 5.2 Comparison of impulse response functions for a rectangular plate

CHAPTER VI

STATE-SPACE REPRESENTATION OF DYNAMIC SYSTEMS

The vibration equations for beam and plate are transferred into State-Space in order to apply modern control methods. The transfer functions are calculated using State-Space matrices to verify the derivation of equations by comparison with the results from the preceding chapters.

6.1 General Form of State-Space Representation of Dynamic Systems

A governing equation of motion of n degree of freedom dynamic system can be written as [12]:

$$[M]\{\ddot{y}\}+[K]\{y\}=\{F\} \tag{6.1}$$

where $[M]$: the $n\times n$ mass matrix,

$[K]$: the $n\times n$ stiffness matrix,

$\{y\}$: the $n\times 1$ displacement vector,

$\{F\}$: the $n\times 1$ point force vector.

If the mode vectors are mass normalized, i.e.:

$$[\Phi]^T[M][\Phi]=[I] \tag{6.2}$$

$$[\Phi]^T[K][\Phi]=[\Omega^2] \tag{6.3}$$

where $[\Phi]$: the $n\times n$ mode matrix,

$[I]$: the $n \times n$ identical matrix,

$[\Omega^2]$: the $n \times n$ frequency matrix.

which have the following forms respectively:

$$[\Phi]=[\{\phi_1\} \cdots \{\phi_i\} \cdots \{\phi_n\}] \tag{6.4}$$

$$[I]=\begin{bmatrix} 1 & & & & \\ & \ddots & & & \\ & & 1 & & \\ & & & \ddots & \\ & & & & 1 \end{bmatrix} \tag{6.5}$$

$$[\Omega^2]=\begin{bmatrix} \omega_1^2 & & & & \\ & \ddots & & & \\ & & \omega_i^2 & & \\ & & & \ddots & \\ & & & & \omega_n^2 \end{bmatrix} \tag{6.6}$$

where $\{\phi_i\}$: the ith mode shape,

ω_i : the ith natural frequency.

Transformation of coordinates of equation (6.1) into modal coordinates:

$$\{y\}=[\Phi]\{q\} \tag{6.7}$$

$$\{\ddot{y}\}=[\Phi]\{\ddot{q}\} \tag{6.8}$$

leads to:

$$\ddot{q}_i + \omega_i^2 q_i = f_i \tag{6.9}$$

where q_i : the ith modal displacement,

f_i : the ith modal force which has the form:

$$\{f\}=[\Phi]^T\{F\} \tag{6.10}$$

If the damping of the system is under consideration, equation (6.9) can be modified by adding a damping term as:

$$\ddot{q}_i + 2\zeta_i\omega_i\dot{q}_i + \omega_i^2 q_i = f_i \tag{6.11}$$

where ζ_i is the modal damping ratio.

Re-write equation (6.11) as:

$$\ddot{q}_i = -2\zeta_i\omega_i\dot{q}_i - \omega_i^2 q_i + f_i \tag{6.12}$$

and add another equation:

$$\omega_i\dot{q}_i = \omega_i\dot{q}_i \tag{6.13}$$

Equations (6.12) and (6.13) can be combined to:

$$\begin{Bmatrix} \ddot{q}_i \\ \omega_i\dot{q}_i \end{Bmatrix} = \begin{bmatrix} -2\zeta_i\omega_i & -\omega_i \\ \omega_i & 0 \end{bmatrix} \begin{Bmatrix} \dot{q}_i \\ \omega_i q_i \end{Bmatrix} + \begin{Bmatrix} f_i \\ 0 \end{Bmatrix} \tag{6.14}$$

For the whole system with n degree of freedom, the equation in state-space becomes:

$$\dot{\mathbf{x}} = \mathbf{A}\mathbf{x} + \mathbf{B}\mathbf{u} \tag{6.15}$$

where:

$$\mathbf{x} = [\dot{q}_1 \quad \omega_1 q_1 \quad \cdots \quad \dot{q}_n \quad \omega_n q_n]^T \tag{6.16}$$

$$\mathbf{A} = diag(\mathbf{A}_i) \tag{6.17}$$

$$\mathbf{A}_i = \begin{bmatrix} -2\zeta_i\omega_i & -\omega_i \\ \omega_i & 0 \end{bmatrix} \tag{6.18}$$

$$\mathbf{u} = [f_1 \quad 0 \quad \cdots \quad f_n \quad 0]^T \tag{6.19}$$

$$\mathbf{B} = diag(\mathbf{B}_i) \tag{6.20}$$

$$\mathbf{B}_i = \begin{bmatrix} 1 & 0 \\ 0 & 0 \end{bmatrix} \tag{6.21}$$

The **B** matrix in equation (6.20) holds for point force inputs. The equation (6.7) can be re-written as:

$$\mathbf{y} = \mathbf{C}\mathbf{x} \tag{6.22}$$

where **y** is the output vector.

$$\mathbf{y} = [y_1 \quad y_2 \quad \cdots \quad y_{n-1} \quad y_n]^T \tag{6.23}$$

$$\mathbf{C} = \left[\{0\} \quad \frac{\{\phi_1\}}{\omega_1} \quad \cdots \quad \{0\} \quad \frac{\{\phi_n\}}{\omega_n} \right] \tag{6.24}$$

A standard state-space representation is expressed as:

$$\dot{\mathbf{x}} = \mathbf{A}\mathbf{x} + \mathbf{B}\mathbf{u} \tag{6.25}$$

$$\mathbf{y} = \mathbf{C}\mathbf{x} + \mathbf{D}\mathbf{u} \tag{6.26}$$

Laplace Transform of the equations (6.25) and (6.26) yields to:

$$\mathbf{s}\mathbf{x}(\mathbf{s}) = \mathbf{A}\mathbf{x}(\mathbf{s}) + \mathbf{B}\mathbf{u}(\mathbf{s}) \tag{6.27}$$

$$\mathbf{y}(\mathbf{s}) = \mathbf{C}\mathbf{x}(\mathbf{s}) + \mathbf{D}\mathbf{u}(\mathbf{s}) \tag{6.28}$$

Solve equation (6.27) for $\mathbf{x}(\mathbf{s})$:

$$\mathbf{x}(\mathbf{s}) = (\mathbf{s}\mathbf{I} - \mathbf{A})^{-1}\mathbf{B}\mathbf{u}(\mathbf{s}) \tag{6.29}$$

Substituting equation (6.29) into equation (6.28) gives:

$$\mathbf{y}(\mathbf{s}) = \mathbf{C}(\mathbf{s}\mathbf{I} - \mathbf{A})^{-1}\mathbf{B}\mathbf{u}(\mathbf{s}) + \mathbf{D}\mathbf{u}(\mathbf{s})$$

$$= [\mathbf{C}(\mathbf{s}\mathbf{I} - \mathbf{A})^{-1}\mathbf{B} + \mathbf{D}]\,\mathbf{u}(\mathbf{s}) \tag{6.30}$$

The transfer function matrix between the control force $\mathbf{u(s)}$ and response $\mathbf{y(s)}$ is thus written as:

$$[H(s)] = \frac{\mathbf{y(s)}}{\mathbf{u(s)}} = \mathbf{C(sI - A)^{-1}B + D} \tag{6.31}$$

6.2 State-Space Representation for a Cantilevered Beam

For a cantilevered beam with piezoelectric actuator, the control force is approximately proportional to the second derivative of the mode shapes. The control input $\mathbf{u}$ is:

$$\mathbf{u} = V_a(t) \tag{6.32}$$

The $\mathbf{B}$ matrix in equation (6.15) becomes:

$$\mathbf{B} = -C_a \Delta x \begin{bmatrix} \frac{\partial^2 \phi_1(x_0)}{\partial x^2} \\ 0 \\ \vdots \\ \frac{\partial^2 \phi_n(x_0)}{\partial x^2} \\ 0 \end{bmatrix} \tag{6.33}$$

where C_a is the geometric constant of the beam defined by equation (3.3) and Δx is the length of the piezoelectric actuator.

Substituting equations (6.17), (6.18), (6.24), and (6.33) into equation (6.31) with $\mathbf{D} = [\mathbf{0}]$, the transfer function matrix between the control force and the response is found as:

$$[H(s)] = \mathbf{C}(\mathbf{sI} - \mathbf{A})^{-1}\mathbf{B}$$

$$= \begin{bmatrix} \{0\} & \frac{\{\phi_1(x)\}}{\omega_1} & \cdots & \{0\} & \frac{\{\phi_n(x)\}}{\omega_n} \end{bmatrix} \begin{bmatrix} s + 2\zeta_1\omega_1 & \omega_1 & & & \\ -\omega_1 & s & & & \\ & & \ddots & & \\ & & & s + 2\zeta_n\omega_n & \omega_n \\ & & & -\omega_n & s \end{bmatrix}^{-1}$$

$$\cdot(-C_a\Delta x) \begin{bmatrix} \frac{\partial^2\phi_1(x_0)}{\partial x^2} \\ 0 \\ \vdots \\ \frac{\partial^2\phi_n(x_0)}{\partial x^2} \\ 0 \end{bmatrix}$$

$$= -C_a\Delta x \left[\frac{\{\phi_1(x)\}\frac{\partial^2\phi_1(x_0)}{\partial x^2}}{s^2 + 2\zeta_1\omega_1 s + \omega_1^2} + \cdots + \frac{\{\phi_n(x)\}\frac{\partial^2\phi_n(x_0)}{\partial x^2}}{s^2 + 2\zeta_n\omega_n s + \omega_n^2} \right]$$

$$= -C_a\Delta x \sum_{i=1}^{n} \frac{\{\phi_i(x)\}\frac{\partial^2\phi_i(x_0)}{\partial x^2}}{s^2 + 2\zeta_i\omega_i s + \omega_i^2} \tag{6.34}$$

Equation (6.34) is consistent with equation (3.24) except for the addition of damping and the truncation of the number of modes to *n*.

6.3 State-Space Representation for a Simply Supported Rectangular Plate

The vibration equations of a simply supported rectangular plate are derived in Chapter IV and Chapter V. Comparing equation (6.15) to equation (5.32), the control input **u** and **B** matrix in equation (6.15) can be written as:

$$\mathbf{u} = V_a(t) \tag{6.35}$$

$$\mathbf{B} = \begin{bmatrix} C_c^{(1)} \\ 0 \\ \vdots \\ C_c^{(n)} \\ 0 \end{bmatrix} = A_a \begin{bmatrix} C_x \dfrac{\partial^2 \phi_1(\xi,\eta)}{\partial x^2} + 2C_{xy} \dfrac{\partial^2 \phi_1(\xi,\eta)}{\partial x \partial y} + C_y \dfrac{\partial^2 \phi_1(\xi,\eta)}{\partial y^2} \\ 0 \\ \vdots \\ C_x \dfrac{\partial^2 \phi_n(\xi,\eta)}{\partial x^2} + 2C_{xy} \dfrac{\partial^2 \phi_n(\xi,\eta)}{\partial x \partial y} + C_y \dfrac{\partial^2 \phi_n(\xi,\eta)}{\partial y^2} \\ 0 \end{bmatrix} \tag{6.36}$$

where A_a is the area of the piezoelectric actuator; C_x, C_{xy}, C_y are constants relating piezoelectric field and bending moments, which are defined by equation (4.7).

Substituting equations (6.17), (6.18), (6.24) and (6.36) into equation (6.31) with $\mathbf{D} = [\mathbf{0}]$, the transfer function matrix between the control force and the response is found as:

$$[H(s)] = \mathbf{C}(\mathbf{sI} - \mathbf{A})^{-1}\mathbf{B}$$

$$= \left[\{0\} \quad \frac{\{\phi_1(x,y)\}}{\omega_1} \quad \cdots \quad \{0\} \quad \frac{\{\phi_n(x,y)\}}{\omega_n} \right] \begin{bmatrix} s+2\zeta_1\omega_1 & \omega_1 & & & \\ -\omega_1 & s & & & \\ & & \ddots & & \\ & & & s+2\zeta_n\omega_n & \omega_n \\ & & & -\omega_n & s \end{bmatrix}^{-1}$$

$$\cdot A_a \begin{bmatrix} C_x \dfrac{\partial^2\phi_1(\xi,\eta)}{\partial x^2} + 2C_{xy} \dfrac{\partial^2\phi_1(\xi,\eta)}{\partial x \partial y} + C_y \dfrac{\partial^2\phi_1(\xi,\eta)}{\partial y^2} \\ 0 \\ \vdots \\ C_x \dfrac{\partial^2\phi_n(\xi,\eta)}{\partial x^2} + 2C_{xy} \dfrac{\partial^2\phi_n(\xi,\eta)}{\partial x \partial y} + C_y \dfrac{\partial^2\phi_n(\xi,\eta)}{\partial y^2} \\ 0 \end{bmatrix}$$

$$= A_a \sum_{i=1}^{n} \frac{\{\phi_i(x,y)\}\left\{ C_x \dfrac{\partial^2\phi_i(\xi,\eta)}{\partial x^2} + 2C_{xy} \dfrac{\partial^2\phi_i(\xi,\eta)}{\partial x \partial y} + C_y \dfrac{\partial^2\phi_i(\xi,\eta)}{\partial y^2} \right\}}{s^2 + 2\zeta_i\omega_i s + \omega_i^2} \qquad (6.37)$$

Equation (6.37) is consistent with Equation (5.35) except for the addition of damping and the truncation of the number of modes to *n*.

CHAPTER VII

APPLICATION OF H_2 AND H_∞ CONTROL THEORIES

The modern approach to characterizing closed-loop performance is to evaluate the value of various matrix norms [3]. Matrix norms provide a measure of how large output signals can get for certain classes of input signals. The use of matrix norms as performance objectives is the main thrust of recent optimal control theory, such as H_2 and H_∞ optimal control.

Figure 7.1 is a block diagram of a closed-loop feedback control system [10], where

G : Open-loop Frequency Response Function,

K : Feedback control gain matrix,

u : Control input,

y : Observed output,

w_d : External inputs including disturbances,

z : Error output.

This system can be described by the following form of State-Space equation:

$$\begin{bmatrix} \dot{\mathbf{x}} \\ \mathbf{y} \end{bmatrix} = \begin{bmatrix} \mathbf{A} & \mathbf{B} \\ \mathbf{C} & \mathbf{D} \end{bmatrix} \begin{bmatrix} \mathbf{x} \\ \mathbf{u} \end{bmatrix} \tag{7.1}$$

and the open-loop Frequency Response Function $H(s)$ is related to the State-Space equation (7.1) as:

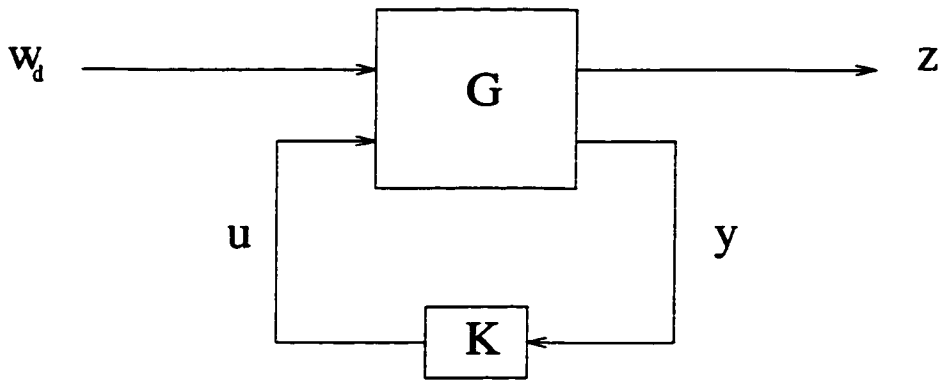

Figure 7.1 Block diagram of a closed-loop feedback control system

$$H(s) = \mathbf{C}(s\mathbf{I} - \mathbf{A})^{-1}\mathbf{B} + \mathbf{D} \tag{7.2}$$

This is equation (6.31).

In order to optimize the control system, a performance index, or cost function, is needed to evaluate the system. In this research, two of the most popular performance measures, H_2 and H_∞, are used as references to develop proposed index.

7.1 H_2 Control

The H_2 norm of a system H is defined as [43]:

$$\|H\|_2 := \left(\mathbf{Tr}\left[\frac{1}{2\pi} \int_{-\infty}^{\infty} H(j\omega) H^*(j\omega) d\omega \right] \right)^{1/2} \tag{7.3}$$

where: $H(j\omega)$ is the Frequency Response Function and $\mathbf{Tr}[\bullet]$ is the trace operator. The physical interpretation is that the H_2 norm is the RMS output when all the input is driven by independent white noise input signals. H_2 optimal control theory was studied extensively in the 1960's as the *Linear Quadratic Gaussian (LQG)* optimal control problem [3].

For the system described by State-Space equation (7.1), the H_2 norm of the system is:

$$\|H\|_2 = \sqrt{\mathbf{Tr}[\mathbf{C}\mathbf{X}\mathbf{C}^T]} \tag{7.4}$$

where X is the solution to the *Lyapunov equation:*

$$\mathbf{A}\mathbf{X} + \mathbf{X}\mathbf{A}^T + \mathbf{B}\mathbf{B}^T = \mathbf{0} \tag{7.5}$$

7.2 H_∞ Control

The H_∞ norm of a system H is defined as [10]:

$$\|H\|_\infty := \sup_\omega \sigma_{max}[H(j\omega)] \tag{7.6}$$

(σ_{max} := maximum singular value)

where $H(j\omega)$ is the Frequency Response Function. The physical meaning of the H_∞ norm can be stated as the maximal output energy for all inputs with unit energy [28]. For the system with transfer matrix:

$$G(s) = \begin{bmatrix} \mathbf{A} & \mathbf{B} \\ \\ \mathbf{C} & \mathbf{0} \end{bmatrix} \tag{7.7}$$

calculation of the H_∞ norm involves determining eigenvalues of the following *Hamiltonian matrix:*

$$H_\gamma := \begin{bmatrix} \mathbf{A} & \gamma^{-2}\mathbf{B}\mathbf{B}^T \\ \\ -\mathbf{C}^T\mathbf{C} & -\mathbf{A}^T \end{bmatrix} \tag{7.8}$$

where γ is a positive number. The calculation is an iteration procedure to find the maximum singular value of the transfer matrix G by adjusting the γ value.

7.3 Comparison of H_2 and H_∞ Norms for Beam and Plate

The definitions of H_2 and H_∞ norms are given by equation (7.3) and equation (7.6) respectively. Finding the relationship between those two norms is beyond the scope of this research. For the purpose of this research, however, a convenient index, which should be consistent with those two widely used indices, is to be developed. Thus a

cantilevered beam and a simply supported rectangular plate are used as case studies to verify the proposed index.

7.3.1 H_2 and H_∞ Norms for a Cantilevered Beam

The cantilevered beam has the following parameters:

Young's modulus:	$E = 1.95 \times 10^{11}$	(N/m^2)
Volumetric mass density:	$\rho = 7700$	(kg/m^3)
Length	$L = 1$	(m)
Width:	$b = 0.025$	(m)
Thickness:	$h = 0.003$	(m)

The beam is clamped at $x = 0$ and free at $x = L$. The $\beta_i L$ values and natural frequencies of the first six modes are listed in table 7.1:

i	$\beta_i L$	$f_i (Hz)$
1	1.87510406871196	2.439
2	4.69409113297417	15.284
3	7.85475743823761	42.795
4	10.99554073487546	83.860
5	14.13716839104647	138.627
6	17.21875953208824	207.085

Table 7.1 $\beta_i L$ values and natural frequencies of a cantilevered beam

The corresponding mode shapes and their derivatives are plotted in figure 7.2 to figure 7.7. It can be seen that for all six modes the deflections have maximum values at the

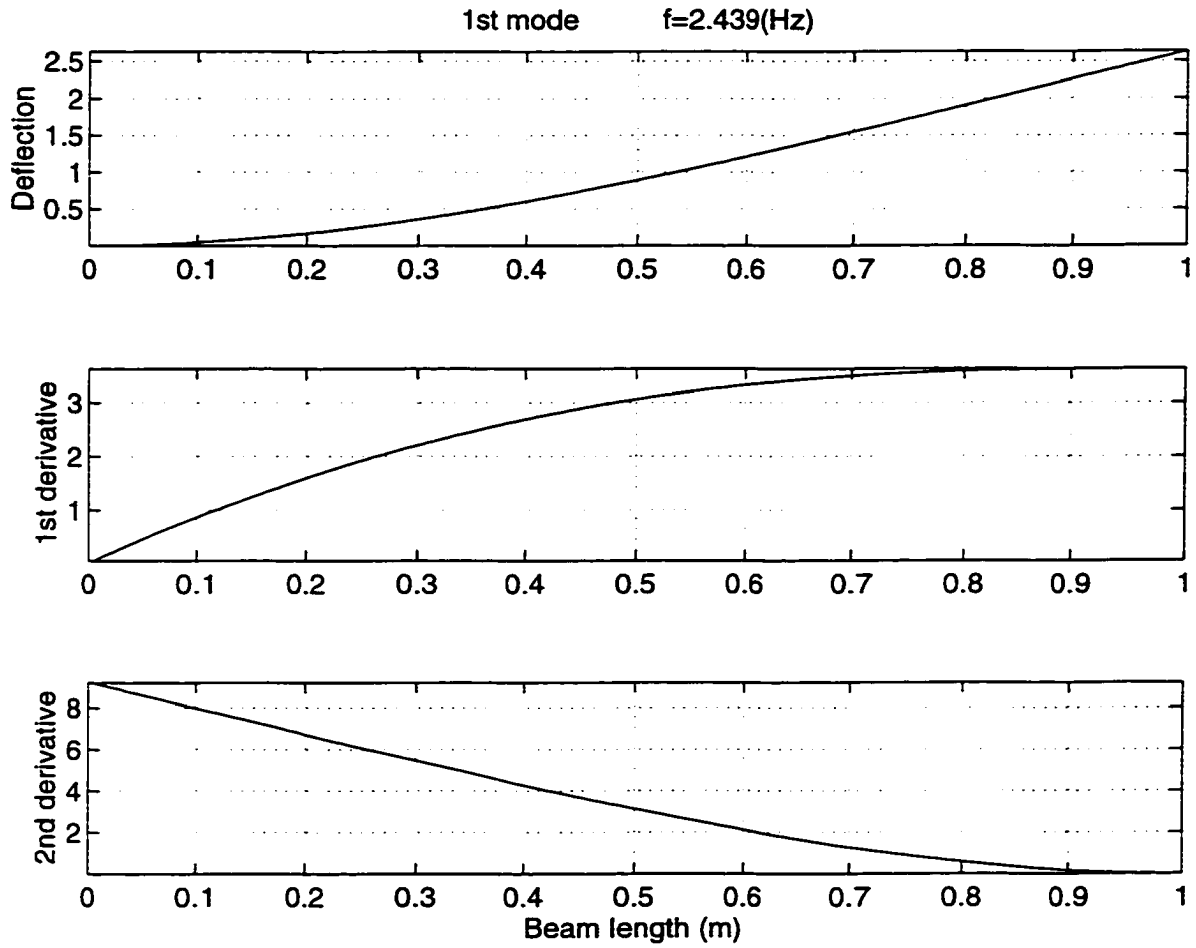

Figure 7.2 1st mode and its derivatives of a cantilevered beam

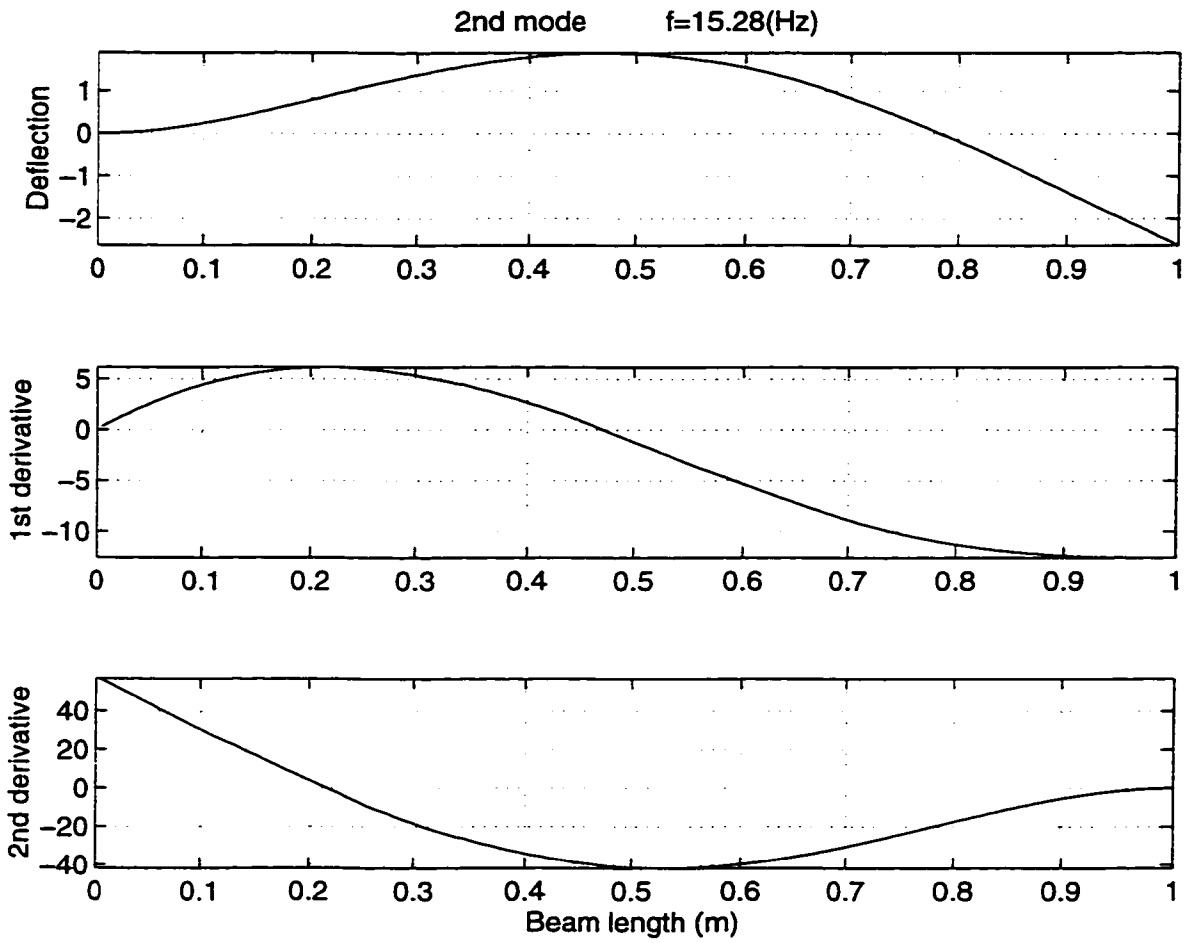

Figure 7.3 2nd mode and its derivatives of a cantilevered beam

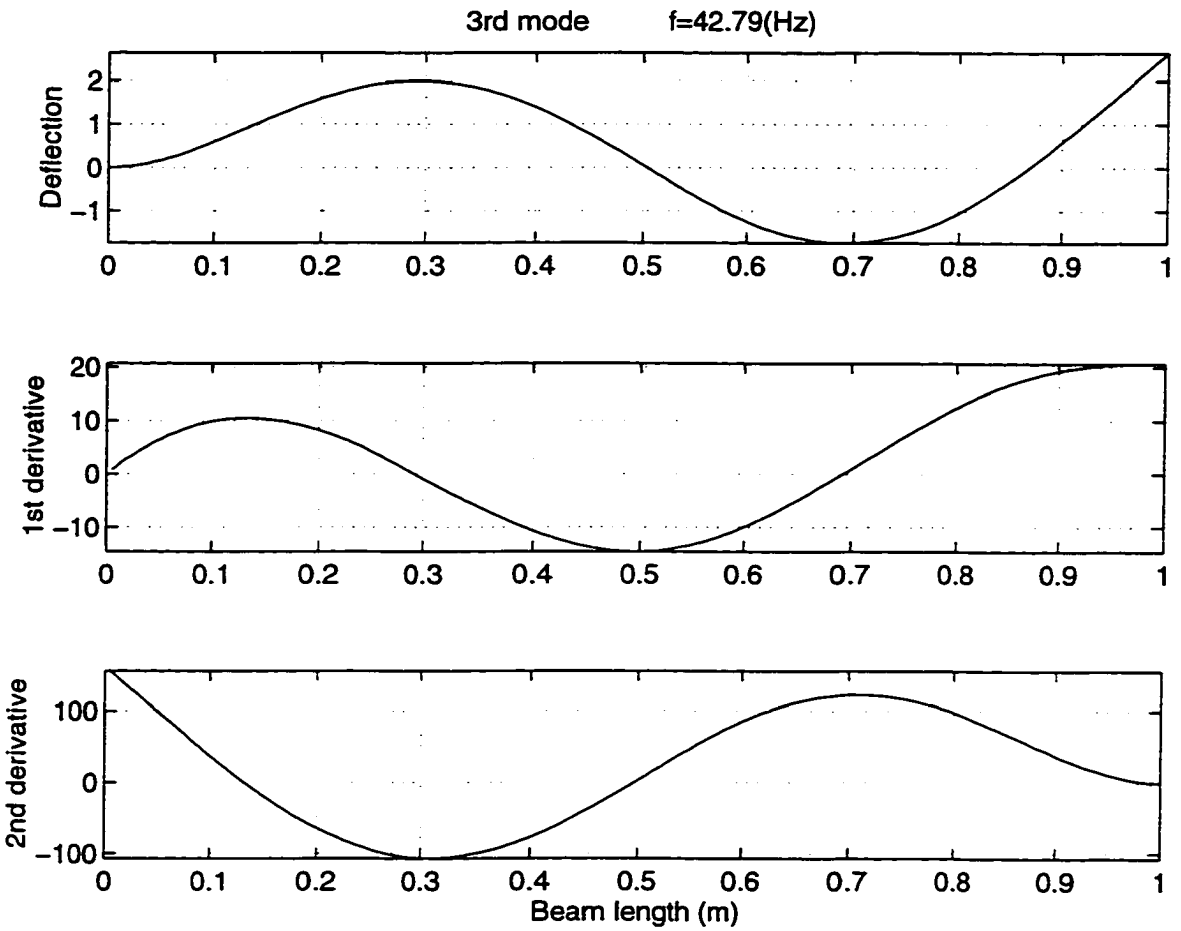

Figure 7.4 3rd mode and its derivatives of a cantilevered beam

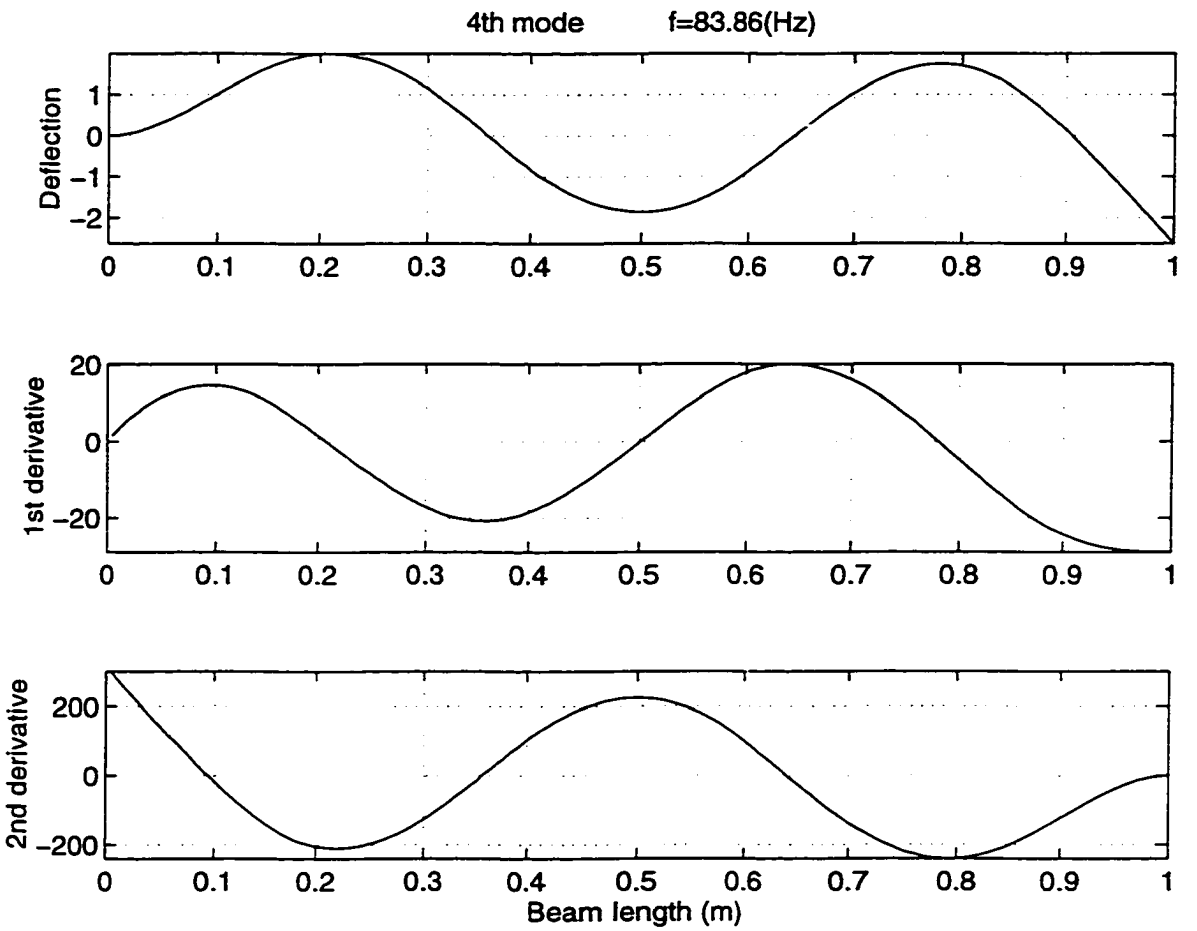

Figure 7.5 4th mode and its derivatives of a cantilevered beam

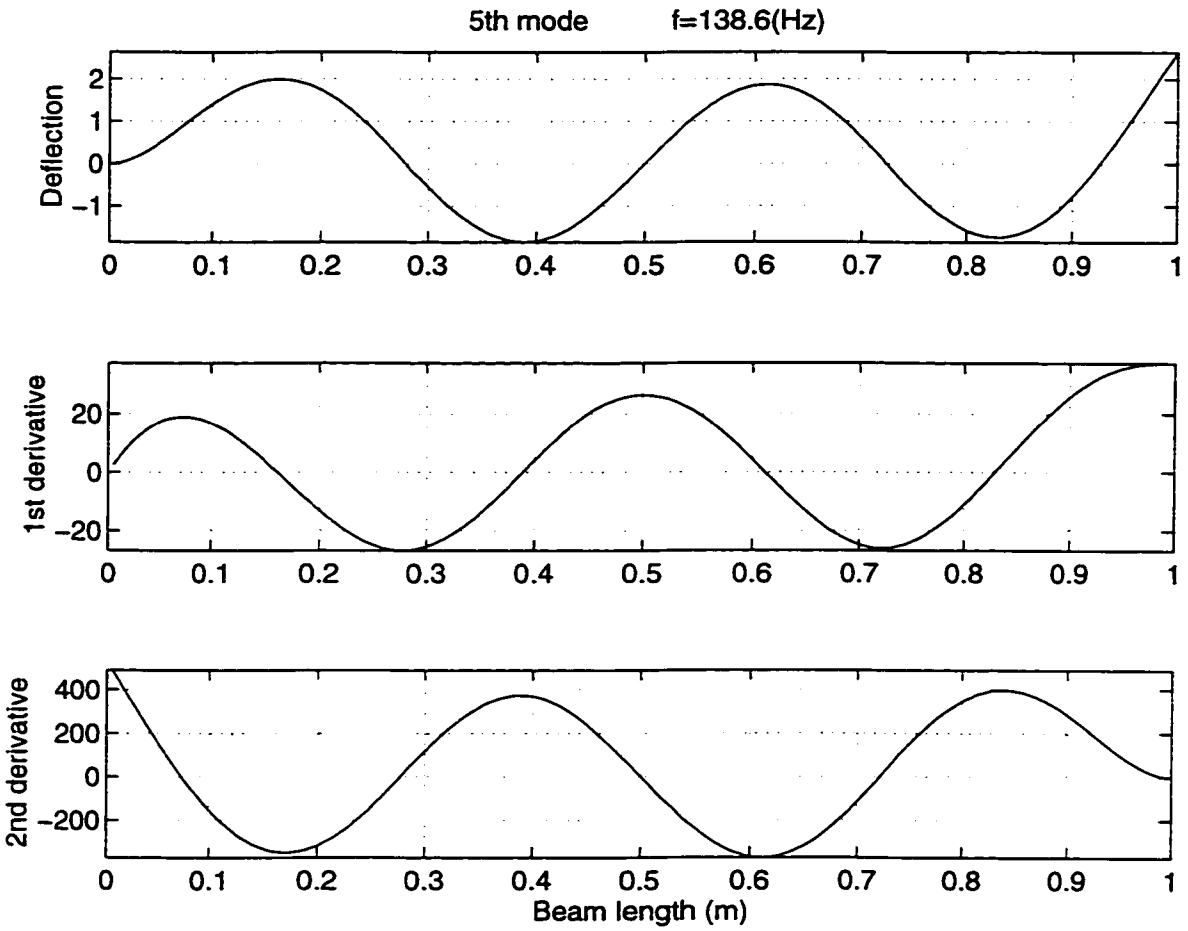

Figure 7.6 5th mode and its derivatives of a cantilevered beam

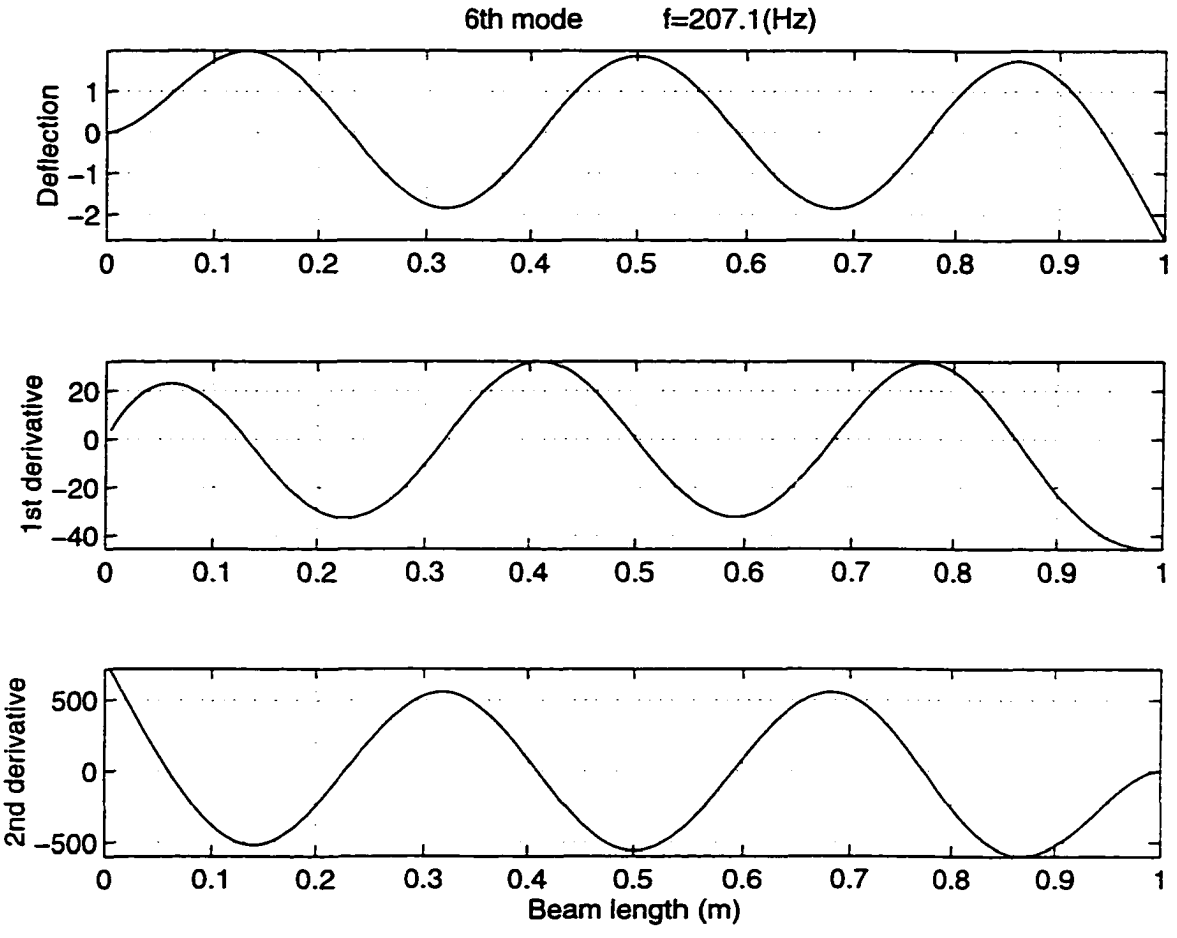

Figure 7.7 6th mode and its derivatives of a cantilevered beam

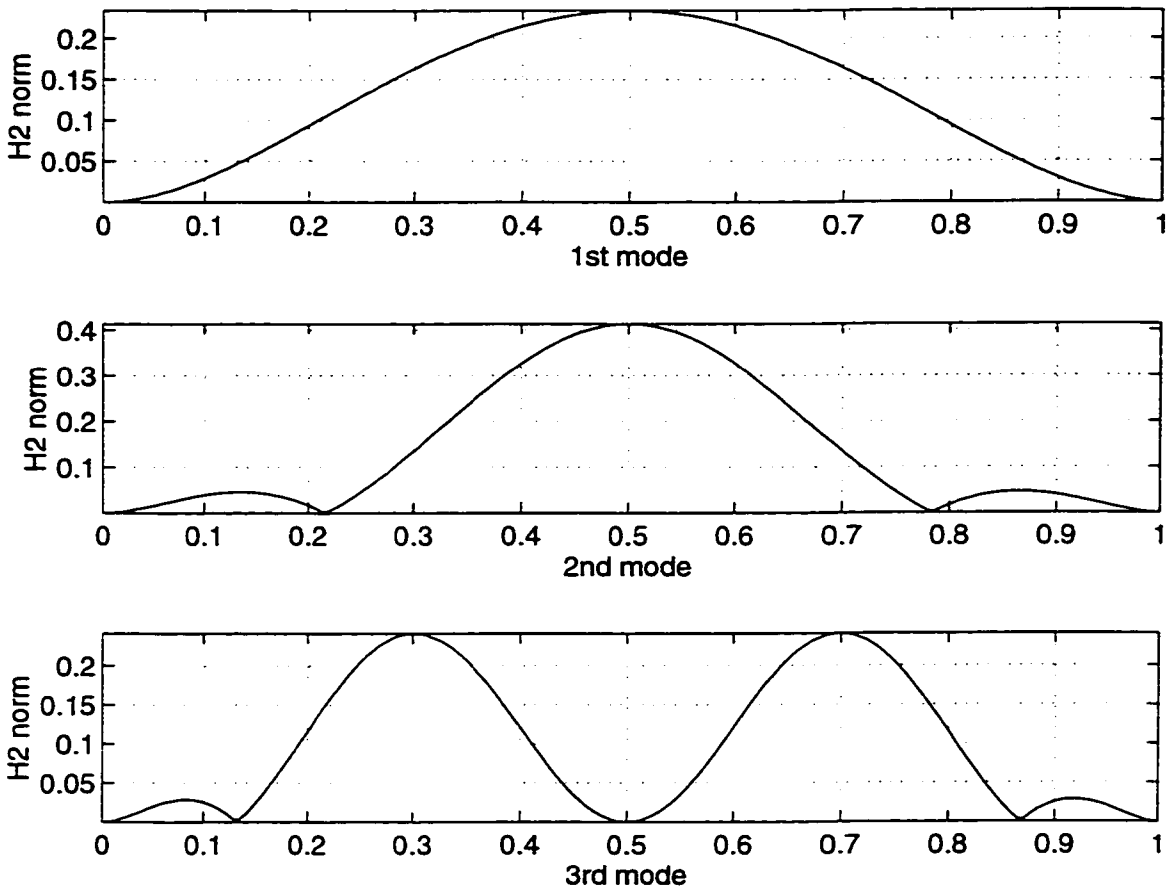

Figure 7.8 H_2 norm of single mode model

(Collocated sensor and actuator)

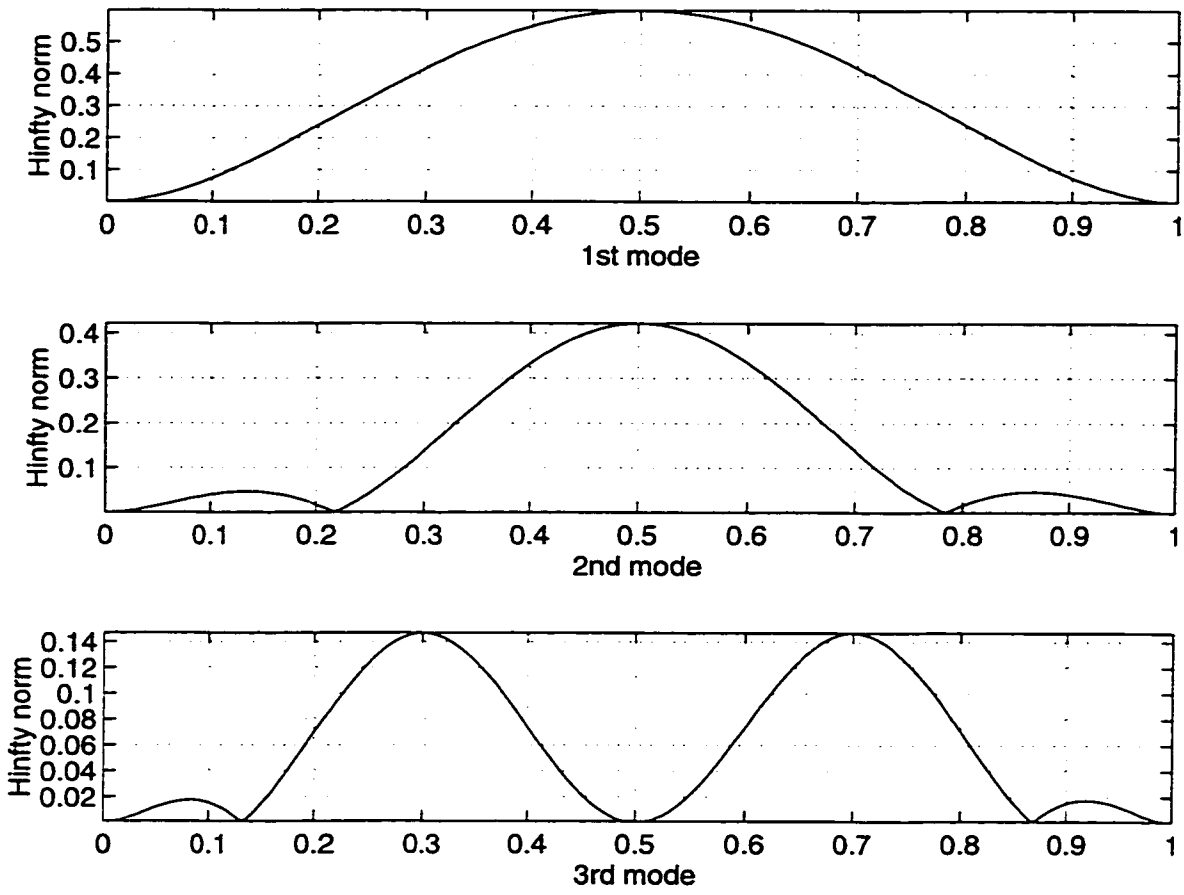

Figure 7.9 H_∞ norm of single mode model

(Collocated sensor and actuator)

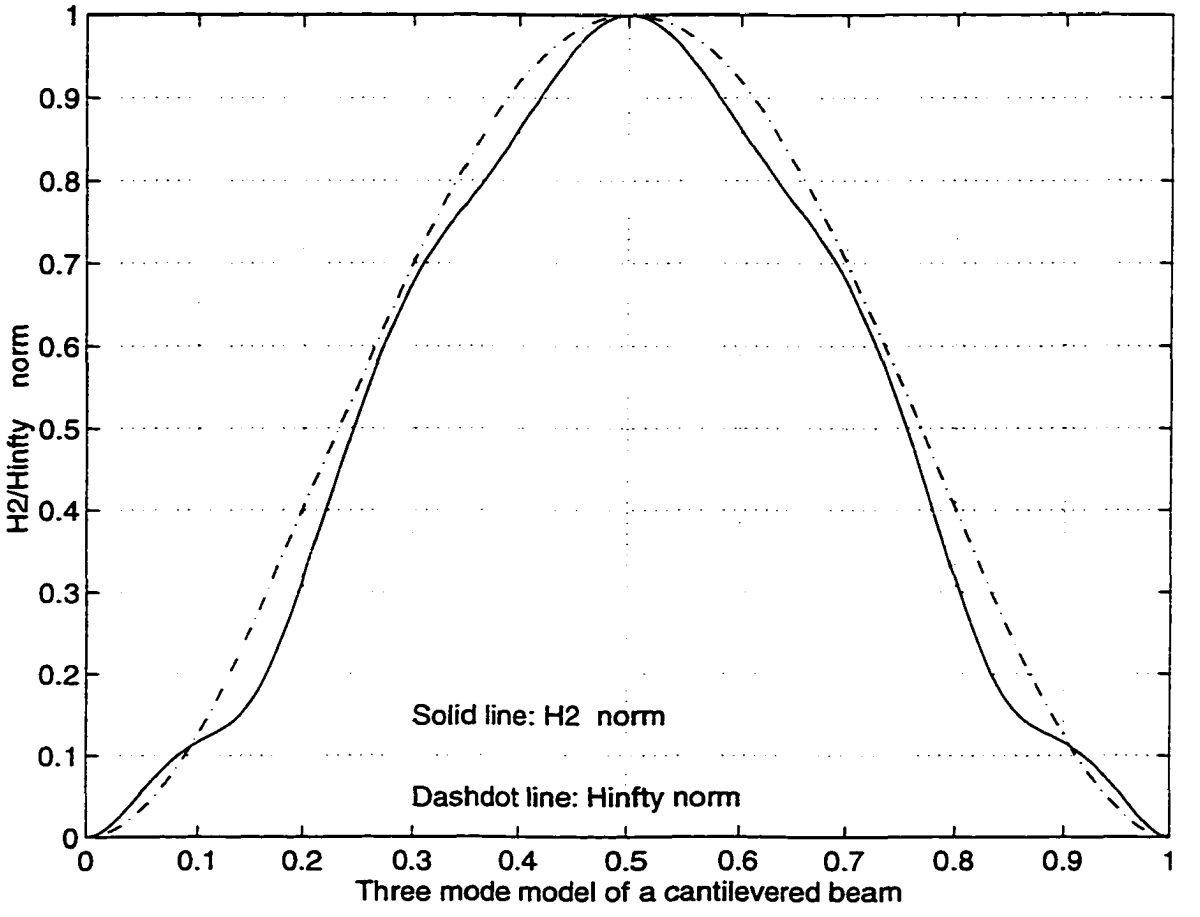

Figure 7.10 Comparison of H_2 and H_∞ norms for three mode model of a cantilevered beam (Collocated sensor and actuator)

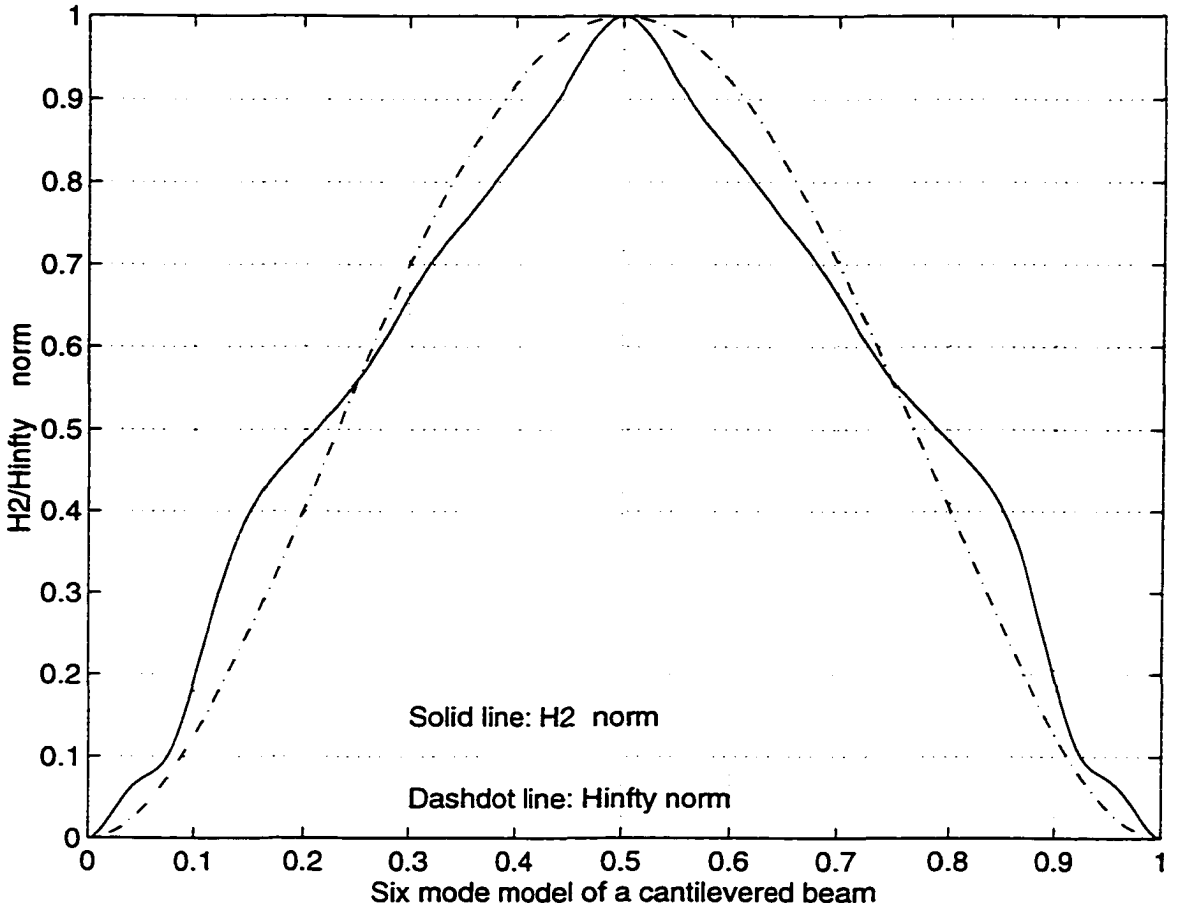

Figure 7.11 Comparison of H_2 and H_∞ norms for six mode model of a cantilevered beam (Collocated sensor and actuator)

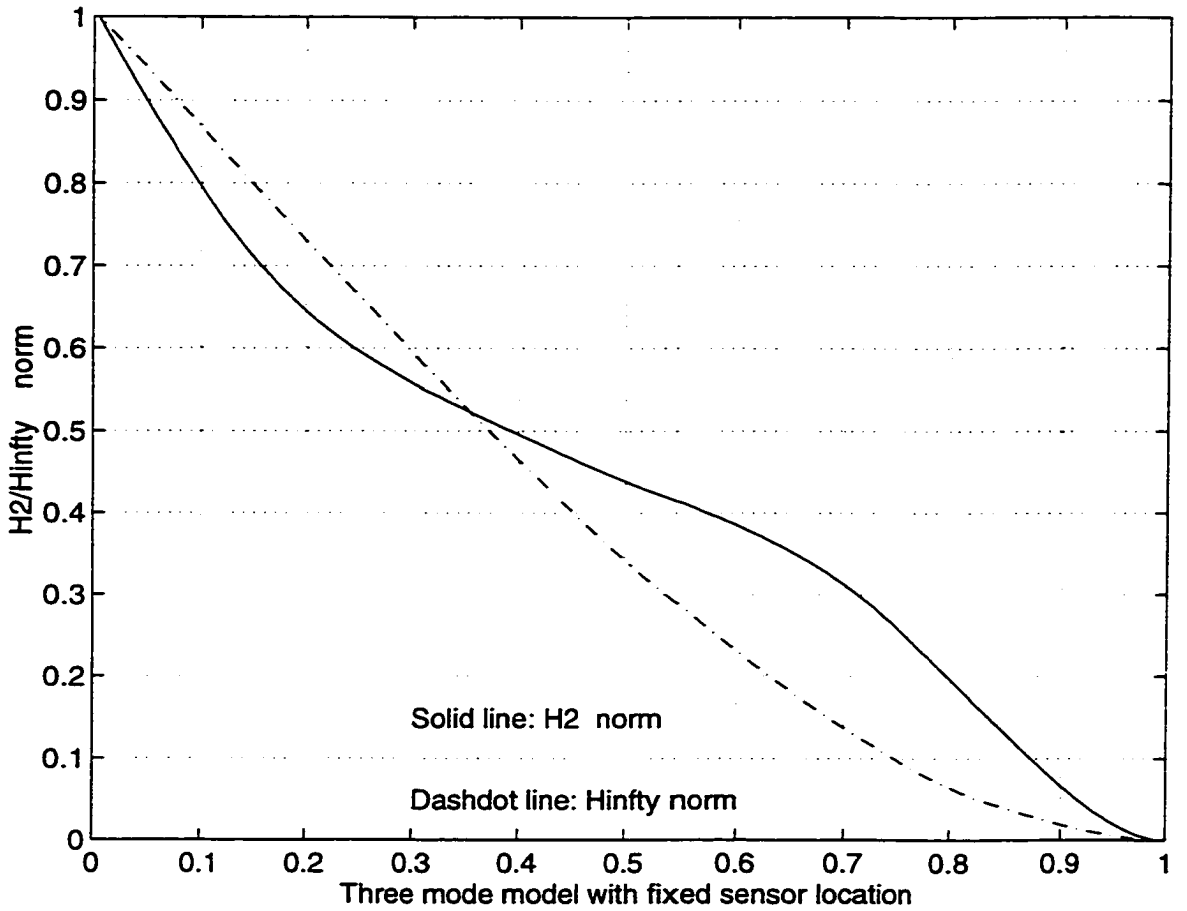

Figure 7.12 Comparison of H_2 and H_∞ norms for three mode model with fixed sensor location ($x = 0.6m$)

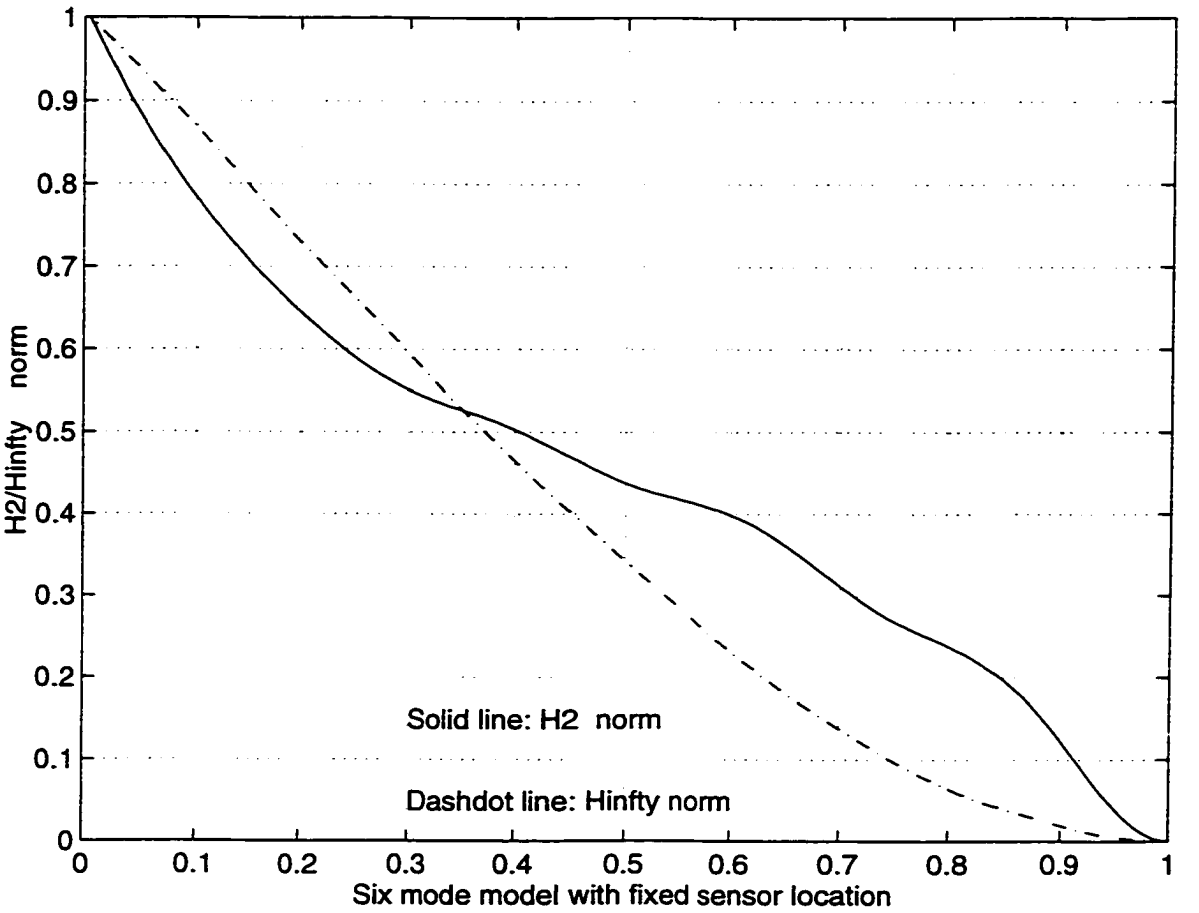

Figure 7.13 Comparison of H_2 and H_∞ norms for six mode model with fixed sensor location ($x = 0.6m$)

free end while the maximum curvatures are found at the clamped end. This is obviously due to the boundary conditions of the structure.

Figures 7.8, 7.9 are H_2 and H_∞ norms for single mode model, i.e., only one mode is included in the system. The sensor and actuator are collocated. The indices appear to be identical except for difference in scales for all three modes. For placement problems the relative index, rather than absolute value, is of interest. Normalizing the norms by setting the maximum value to unity, H_2 and H_∞ norms appear to be exactly same for these single mode cases.

Comparisons are also made for beam models with first three modes and first six modes respectively, as shown in figures 7.10, 7.11. The sensor and actuator are collocated too. In both figures, H_2 and H_∞ norms have the same tendency in so far as both norms reach their maximum and minimum values at the same points. Both indices monotonically-increase from $x = 0$ to $x = 0.5m$, and monotonically-decrease from $x = 0.5m$ to $x = 1m$. The results in figures 7.8 to 7.11 are obtained for collocated sensor/actuator cases. For fixed sensor location (x = 0.6m), similar tendency is also found between H_2 and H_∞ norms, as shown in figure 7.12 for the three mode model and figure 7.13 for six mode model.

7.3.2 H_2 and H_∞ Norms of a Simply Supported Plate

The simply supported plate has the following parameters:

Young's modulus:	$E = 1.95 \times 10^{11}$	(N/m^2)
Volumetric mass density:	$\rho = 7700$	(kg/m^3)
Poisson's ratio:	$\nu = 0.3$	
Width in x direction:	$a = 1$	(m)
Width in y direction:	$b = 0.6$	(m)
Thickness:	$h = 0.003$	(m)

The first six natural frequencies are listed in table 7.2:

i	m	n	$f_i(Hz)$
1	1	1	27.111
2	2	1	48.639
3	3	1	84.521
4	1	2	86.913
5	2	2	108.442
6	4	1	134.755

Table 7.2 Natural frequencies of a simply supported rectangular plate

The corresponding mode shape and its derivatives are shown in figures 7.14 to 7.19. Assuming a monolithic piezoelectric patch actuator is used, i.e. $C_x = C_y$ and $C_{xy} = 0$ in equation (6.36), H_2 and H_∞ norms are calculated. Just as in the beam case, the H_2 and H_∞ norms for single mode models appear to be exactly same if the maximum values of both indices are set to unity. The H_2 and H_∞ norms for three mode and six mode models are shown in figure 7.20 and figure 7.21 respectively, in which the H_2 norm is offset by 2 for clarity.

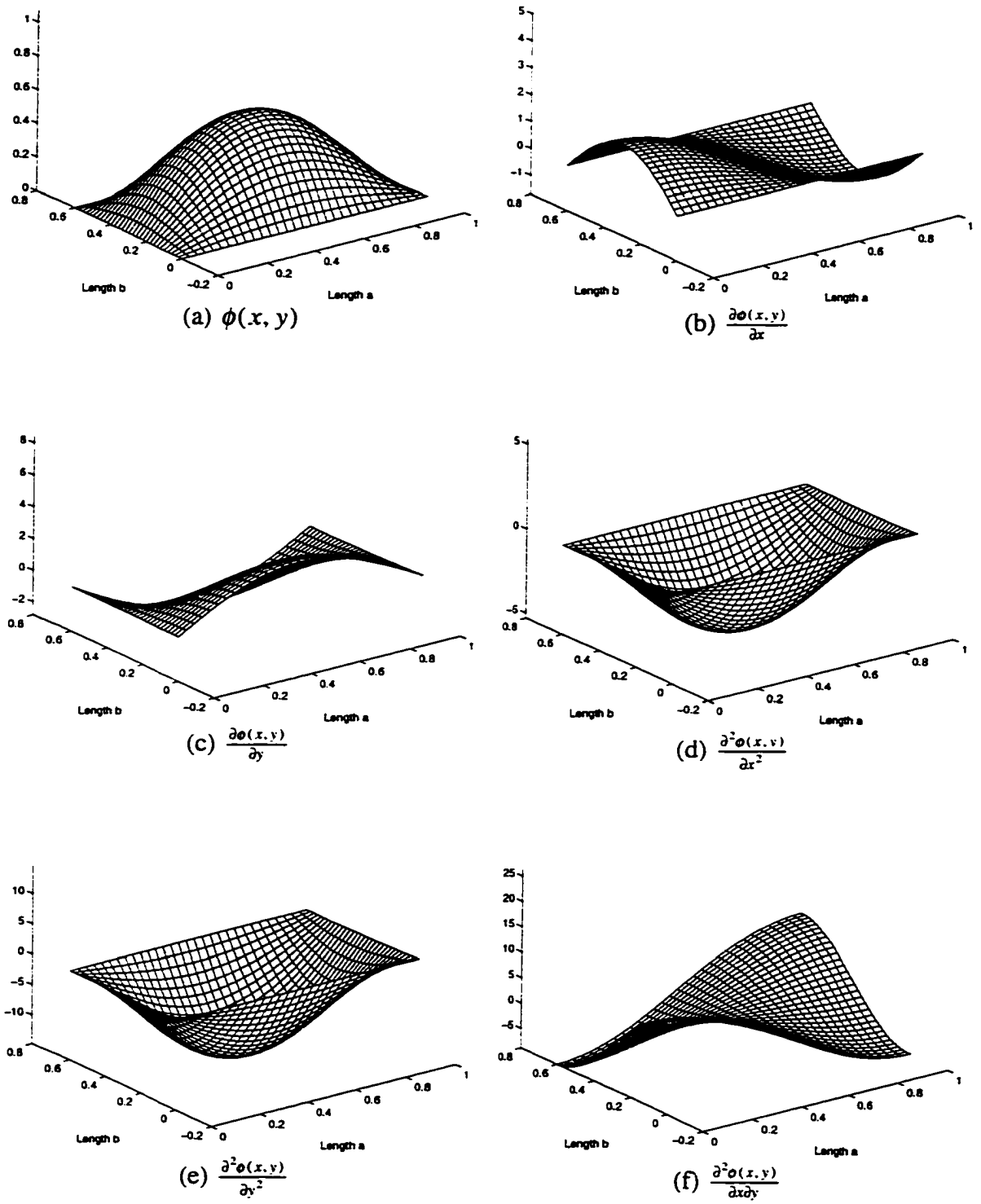

(a) $\phi(x, y)$ (b) $\frac{\partial \phi(x,y)}{\partial x}$

(c) $\frac{\partial \phi(x,y)}{\partial y}$ (d) $\frac{\partial^2 \phi(x,y)}{\partial x^2}$

(e) $\frac{\partial^2 \phi(x,y)}{\partial y^2}$ (f) $\frac{\partial^2 \phi(x,y)}{\partial x \partial y}$

Figure 7.14 1st mode and its derivatives of a simply supported plate

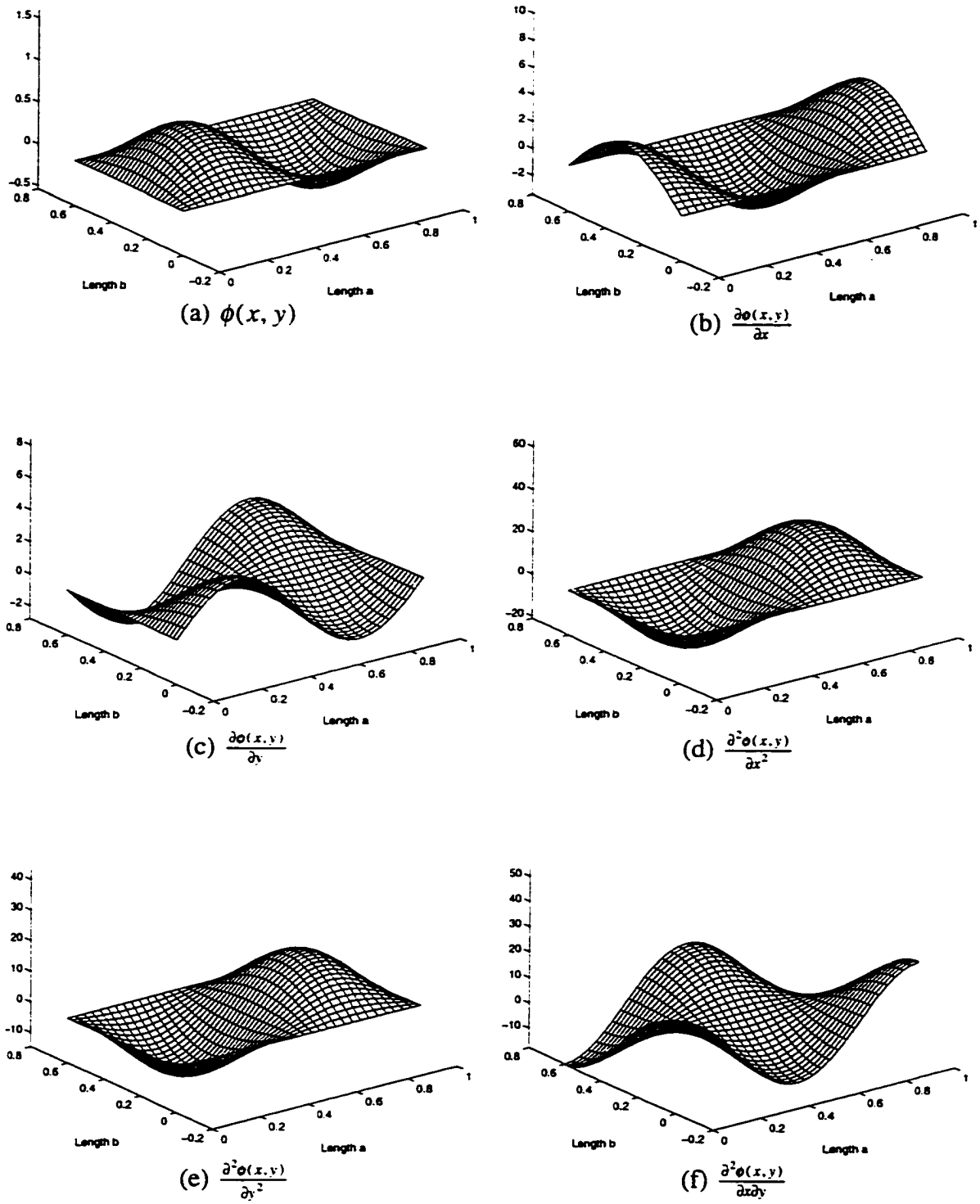

(a) $\phi(x, y)$ (b) $\frac{\partial \phi(x,y)}{\partial x}$

(c) $\frac{\partial \phi(x,y)}{\partial y}$ (d) $\frac{\partial^2 \phi(x,y)}{\partial x^2}$

(e) $\frac{\partial^2 \phi(x,y)}{\partial y^2}$ (f) $\frac{\partial^2 \phi(x,y)}{\partial x \partial y}$

Figure 7.15 2nd mode and its derivatives of a simply supported plate

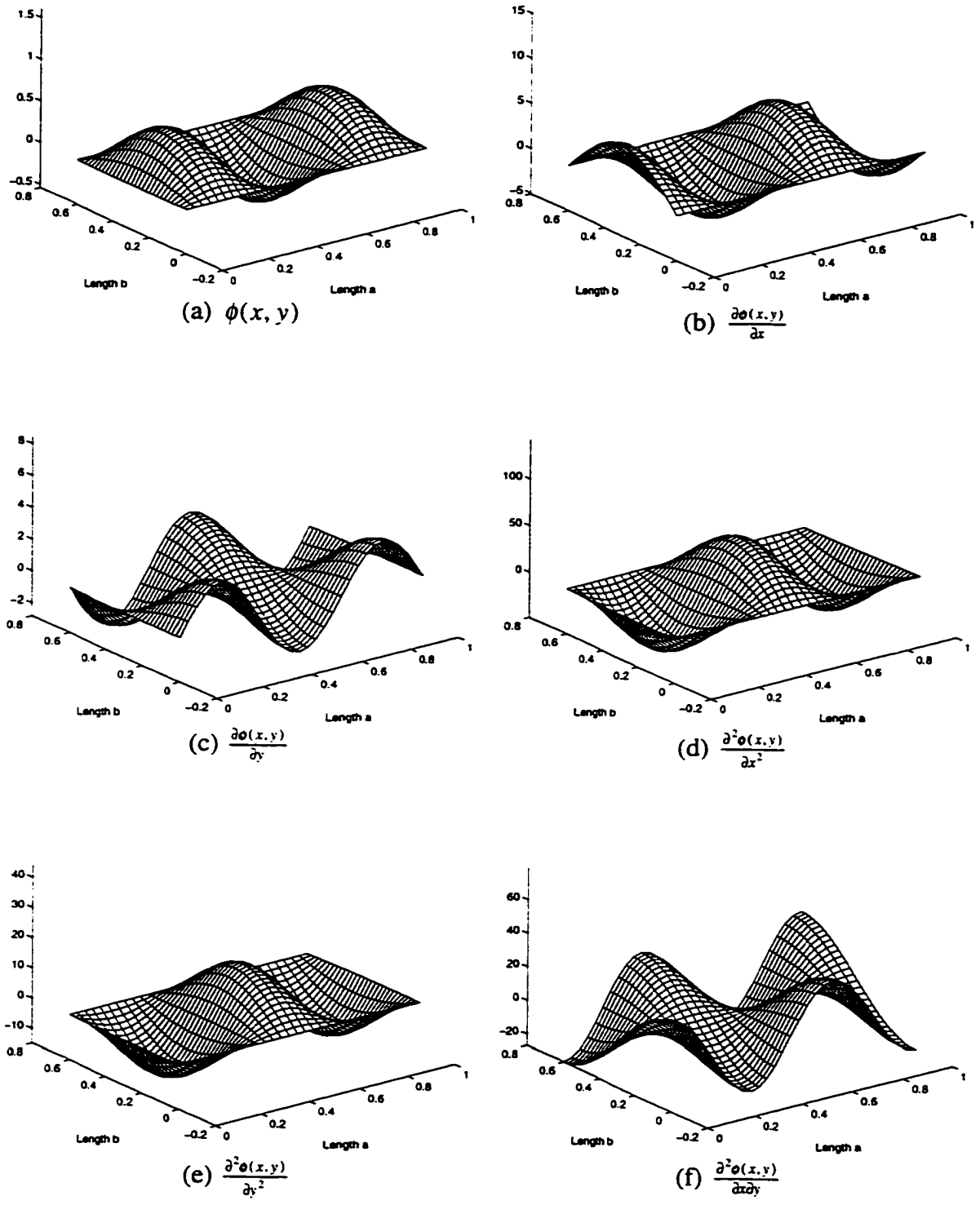

Figure 7.16 3rd mode and its derivatives of a simply supported plate

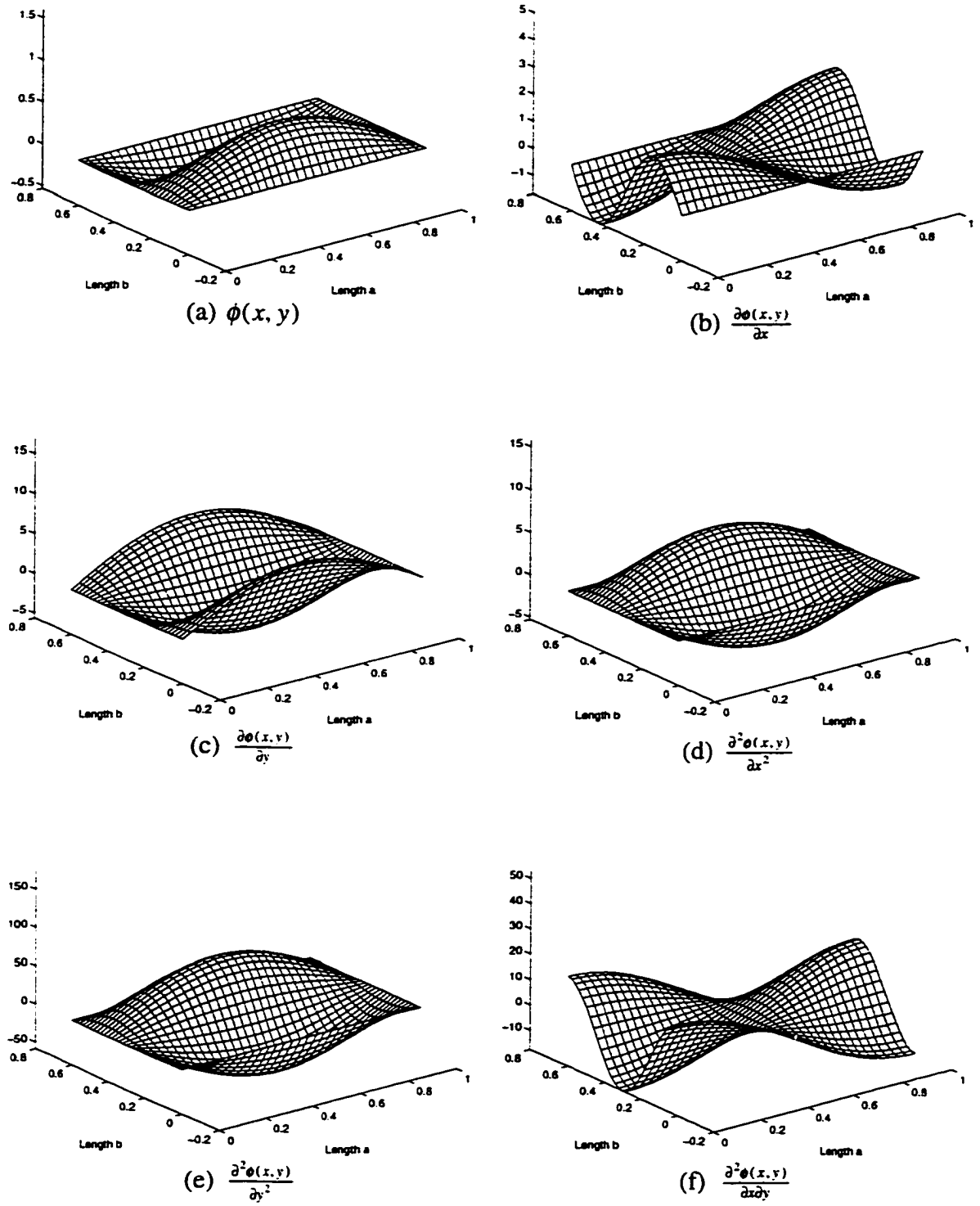

(a) $\phi(x, y)$ (b) $\frac{\partial \phi(x,y)}{\partial x}$

(c) $\frac{\partial \phi(x,y)}{\partial y}$ (d) $\frac{\partial^2 \phi(x,y)}{\partial x^2}$

(e) $\frac{\partial^2 \phi(x,y)}{\partial y^2}$ (f) $\frac{\partial^2 \phi(x,y)}{\partial x \partial y}$

Figure 7.17 4th mode and its derivatives of a simply supported plate

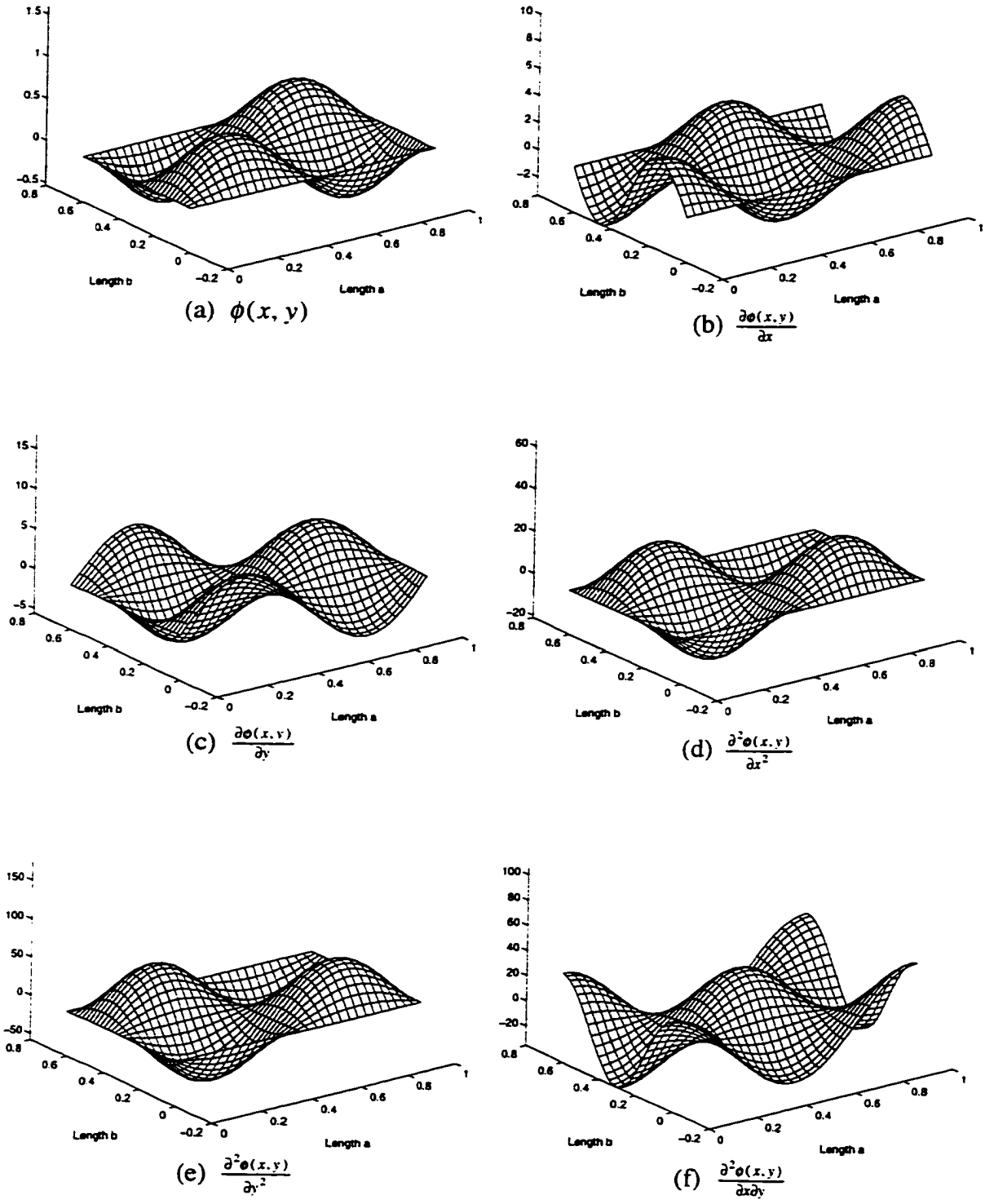

(a) $\phi(x, y)$ (b) $\frac{\partial \phi(x,y)}{\partial x}$

(c) $\frac{\partial \phi(x,y)}{\partial y}$ (d) $\frac{\partial^2 \phi(x,y)}{\partial x^2}$

(e) $\frac{\partial^2 \phi(x,y)}{\partial y^2}$ (f) $\frac{\partial^2 \phi(x,y)}{\partial x \partial y}$

Figure 7.18 5th mode and its derivatives of a simply supported plate

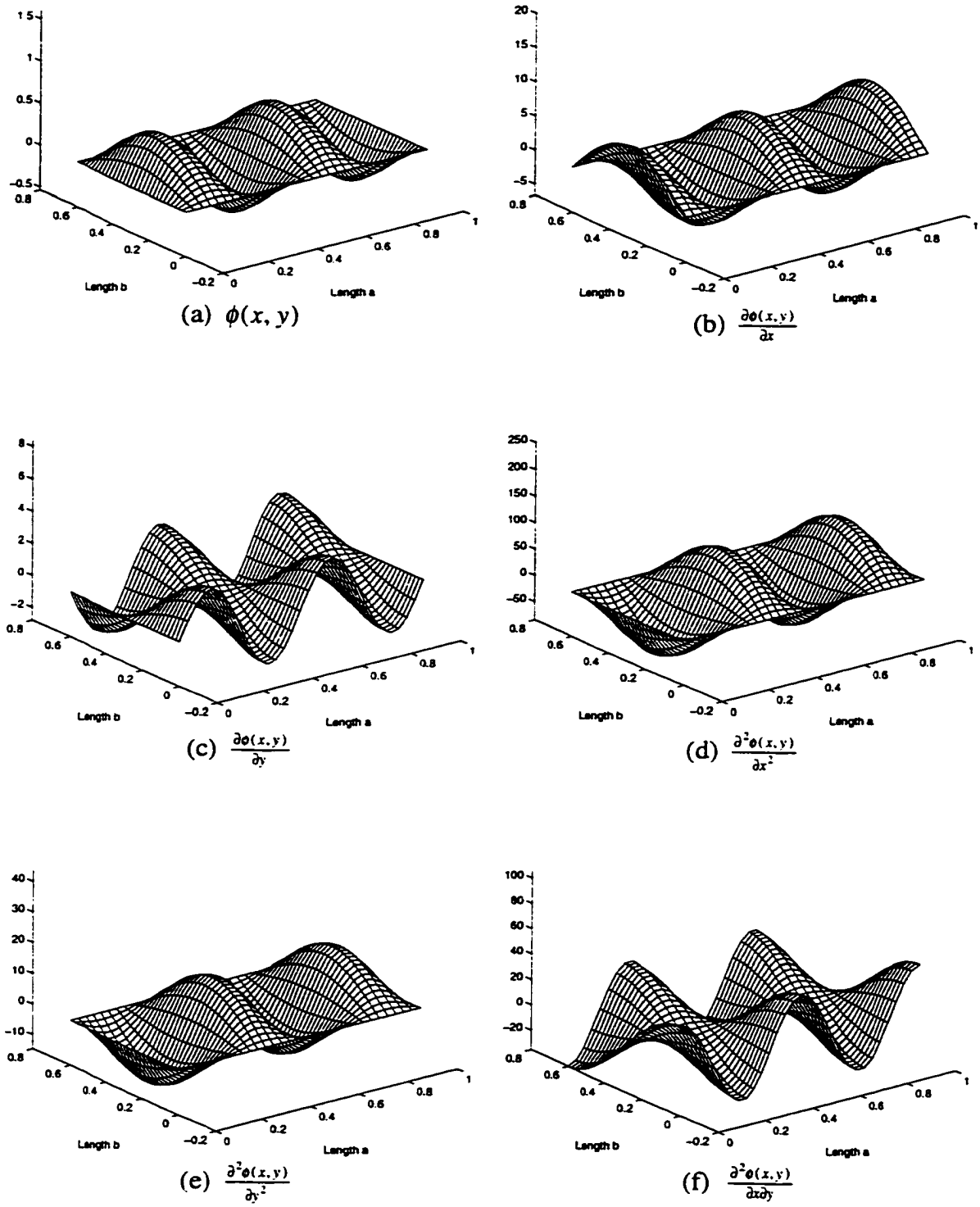

Figure 7.19 6th mode and its derivatives of a simply supported plate

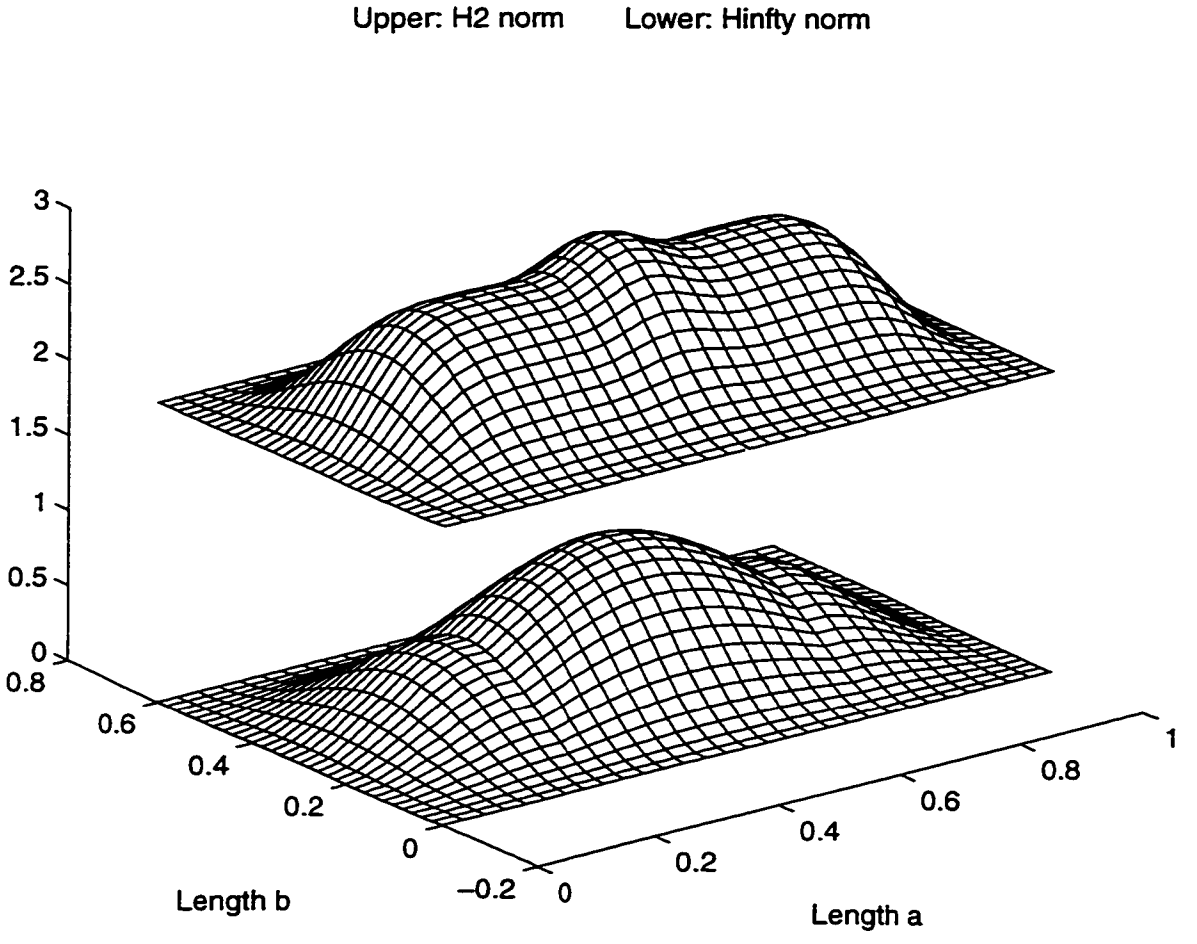

Figure 7.20 Comparison of H_2 and H_∞ norms for three mode model of a simply supported plate (Collocated sensor and actuator)

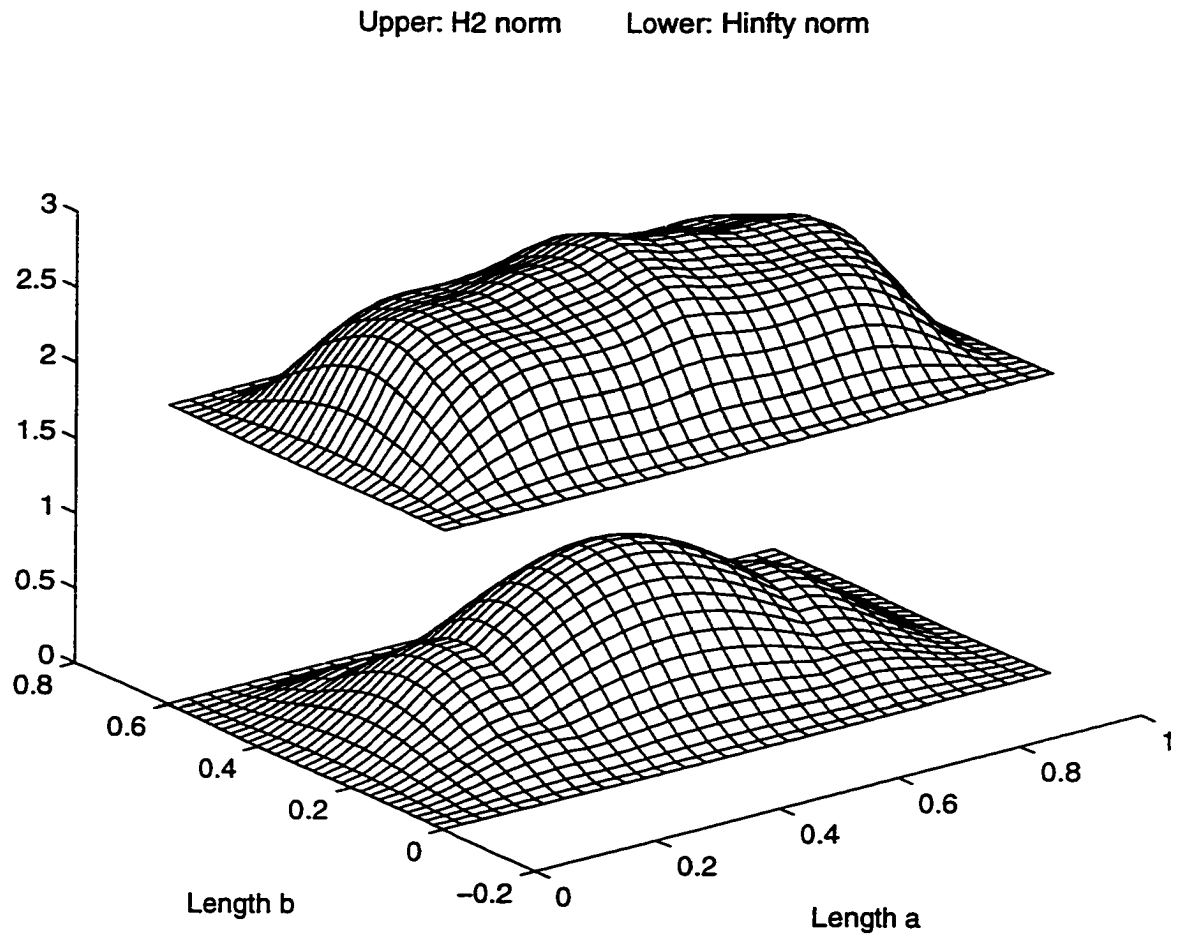

Figure 7.21 Comparison of H_2 and H_∞ norms for six mode model of a simply supported plate (Collocated sensor and actuator)

In both cases, H_2 and H_∞ norms have good agreement over the entire plate and the maximum value is found at the center of the plate.

7.3.3 H_2 and H_∞ Norms Versus Volume Fraction v_f and Orientation of Piezoelectric Fiber θ for a Simply Supported Plate

The piezoelectric fiber and epoxy matrix have the following material properties:

PZT fiber

Young's modulus:	$E_p = 6\times10^{10}$	(N/m^2)
Poisson's ratio:	$v_p = 0.3$	
Shear modulus:	$G_p = 2.31\times10^{10}$	(N/m^2)
Strain-to-voltage constant:	$d_{31} = d_{32} = -2.73\times10^{-10}$	(m/V)

Epoxy

Young's modulus:	$E_e = 2.7\times10^{9}$	(N/m^2)
Poisson's ratio:	$v_e = 0.3$	
Shear modulus:	$G_e = 1.04\times109$	(N/m^2)

The collocated point sensor and piezoelectric fiber actuator is located at (0.367m, 0.22m). A single mode model, with the first, second, and third mode, is used to study the effectiveness of the actuator. Figure 7.22, 7.23, and 7.24 show that the H_2 and H_∞ norms increase with the increase of volume fraction of PZT fiber while the optimal

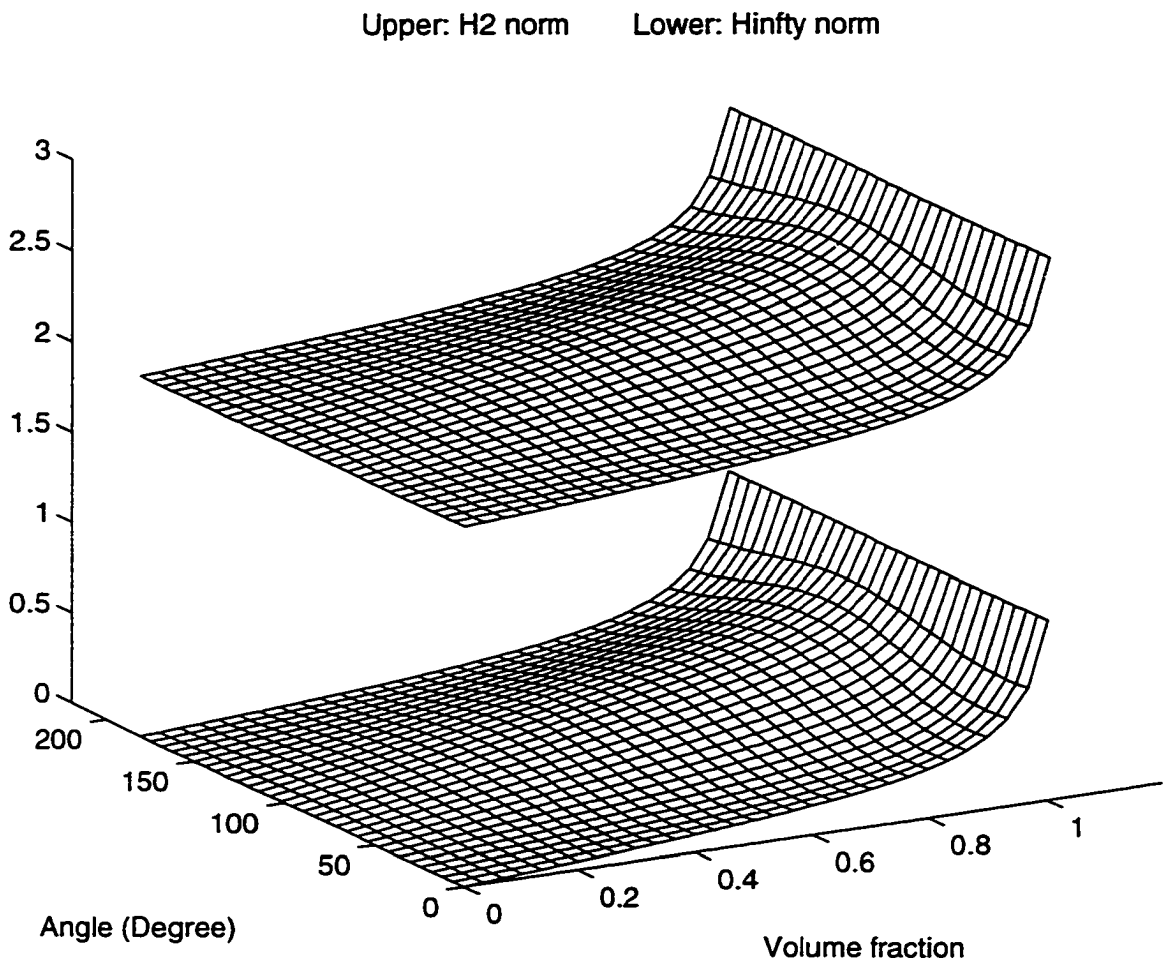

Figure 7.22 H_2 and H_∞ norms of the 1st mode versus volume fraction v_f and orientation of piezoelectric fiber θ

(Collocated sensor and actuator at $(0.367m, 0.22m)$)

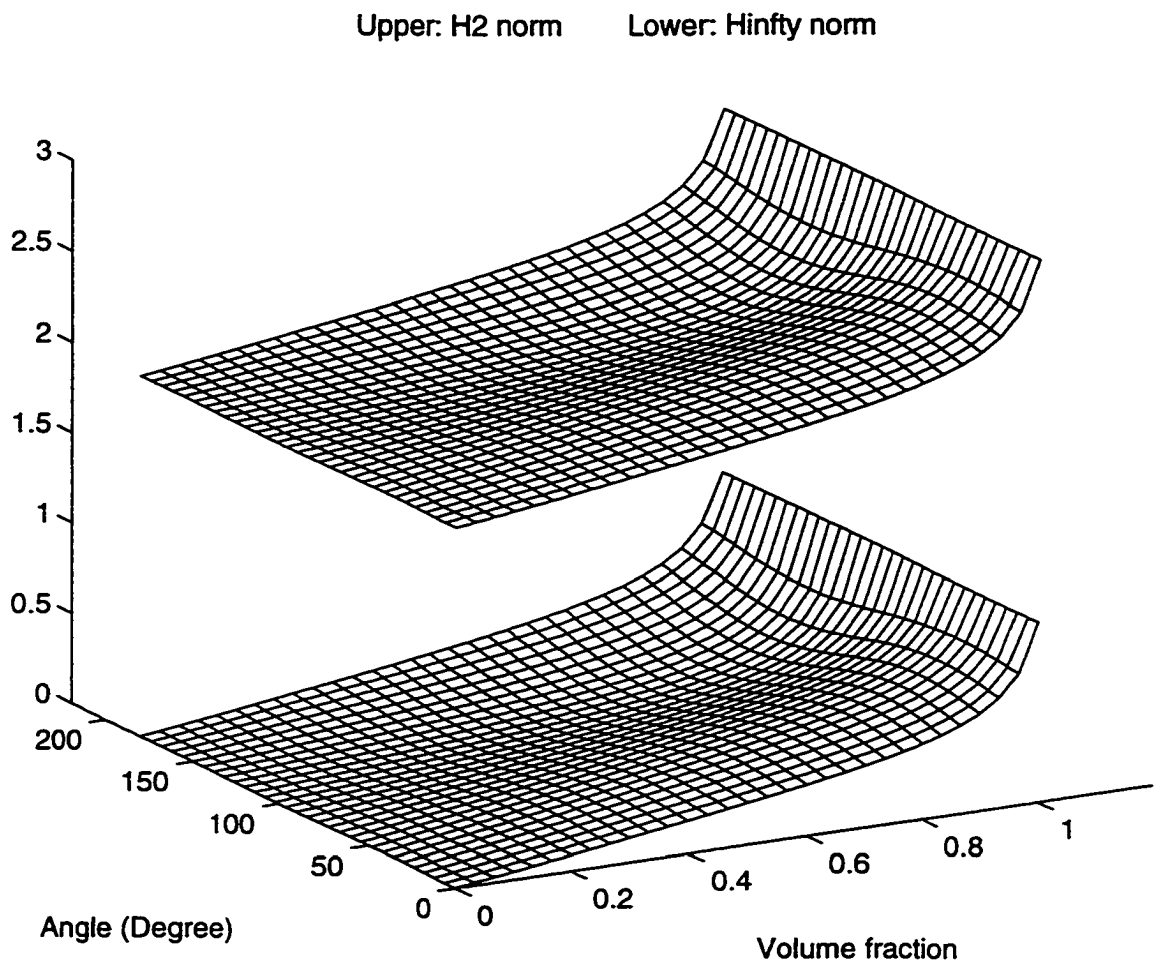

Figure 7.23 H_2 and H_∞ norms of the 2nd mode versus volume fraction v_f and orientation of piezoelectric fiber θ

(Collocated sensor and actuator at $(0.367m, 0.22m)$)

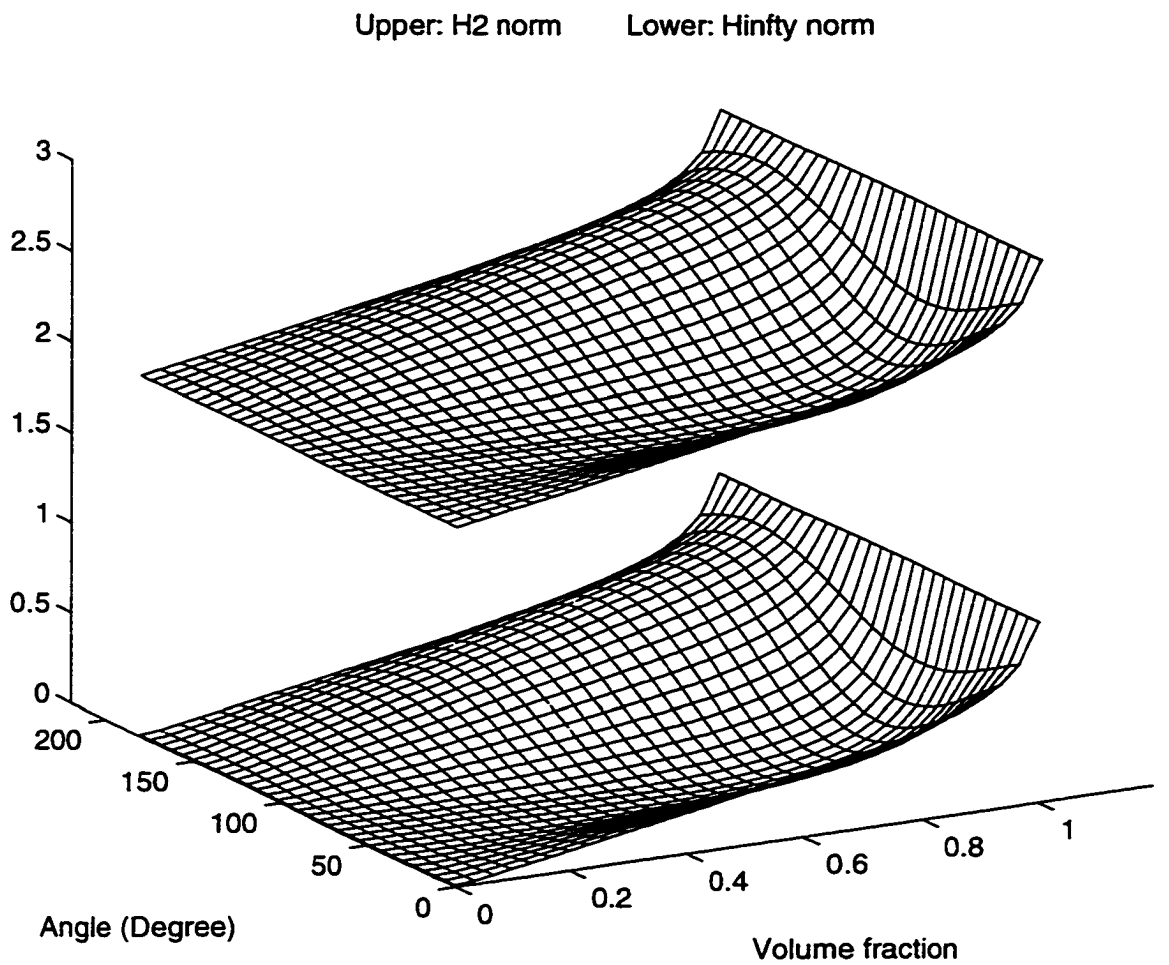

Figure 7.24 H_2 and H_∞ norms of the 3rd mode versus volume fraction v_f and orientation of piezoelectric fiber θ

(Collocated sensor and actuator at $(0.367m, 0.22m)$)

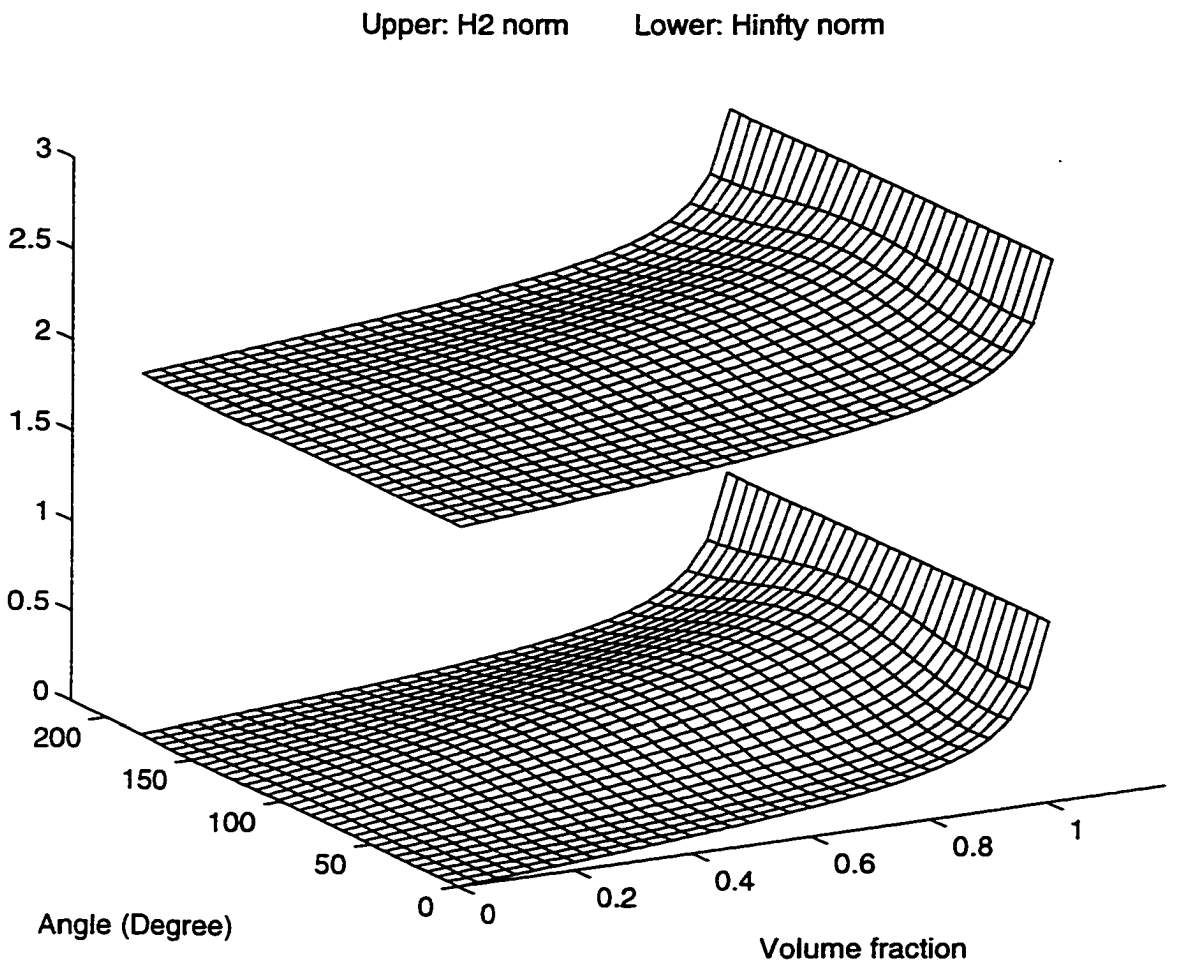

Figure 7.25 H_2 and H_∞ norms of a three mode model versus volume fraction v_f and orientation of piezoelectric fiber θ

(Collocated sensor and actuator at $(0.367m, 0.22m)$)

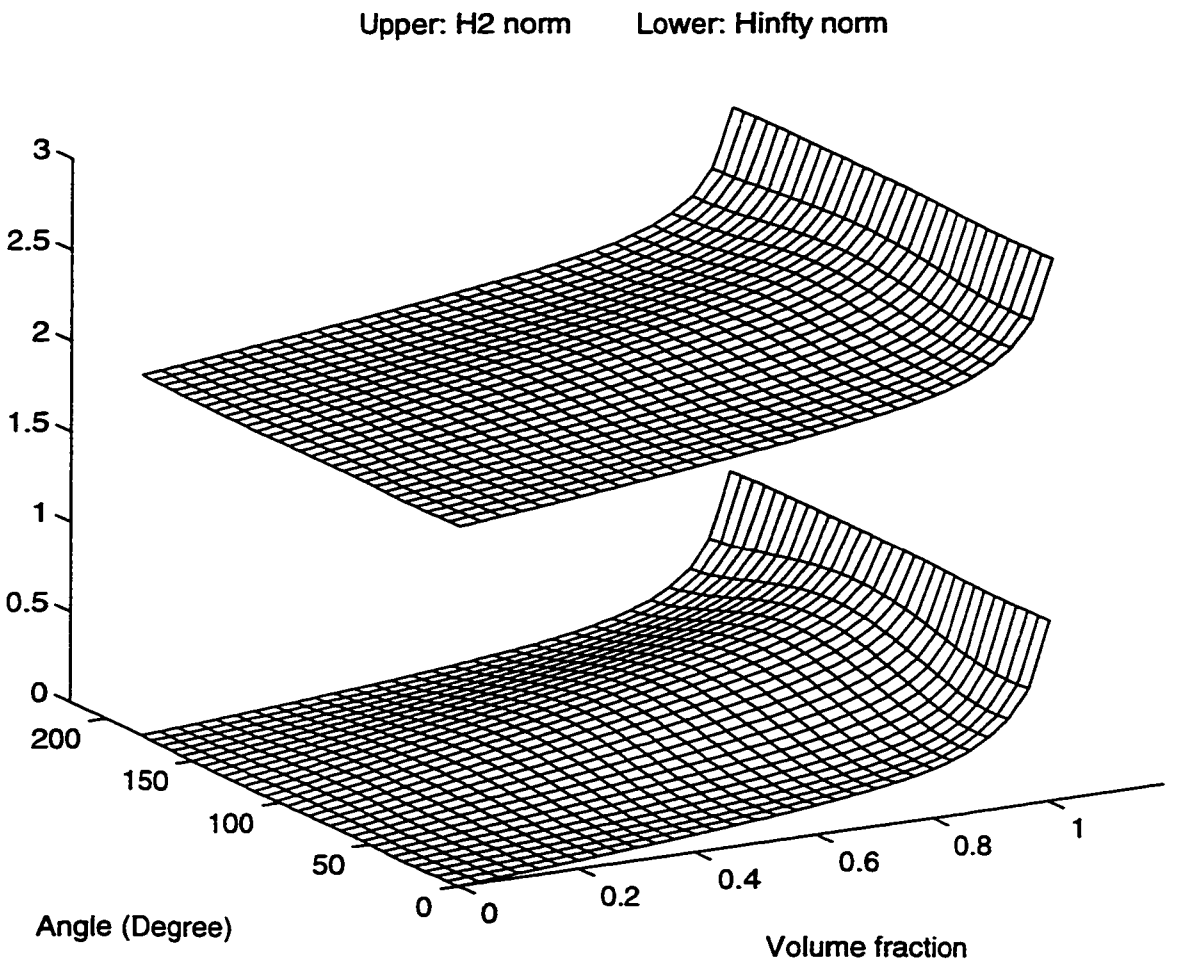

Figure 7.26 H_2 and H_∞ norms of a six mode model versus volume fraction v_f and orientation of piezoelectric fiber θ

(Collocated sensor and actuator at $(0.367m, 0.22m)$)

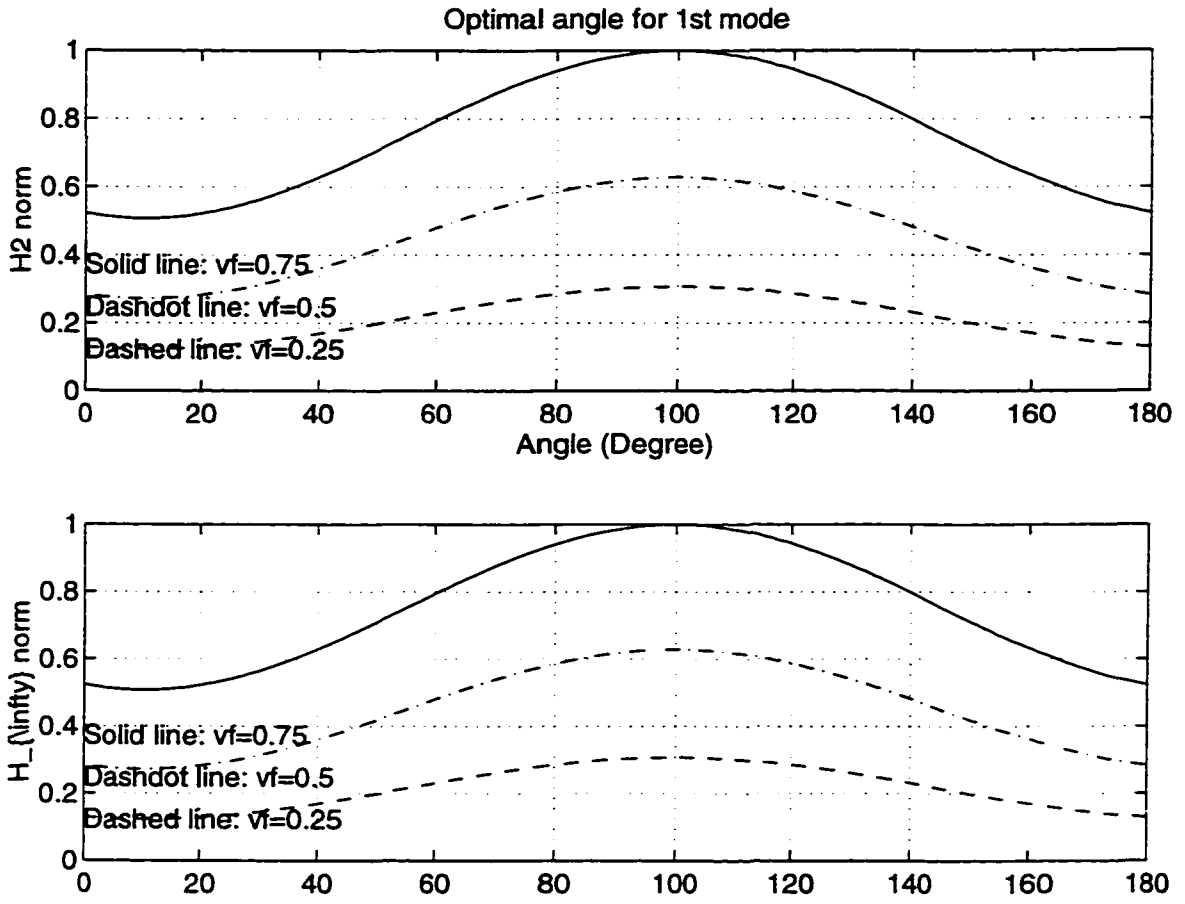

Figure 7.27 H_2 and H_∞ norms of the 1st mode versus orientation of piezoelectric fiber θ

(Collocated sensor and actuator at $(0.367m, 0.22m)$)

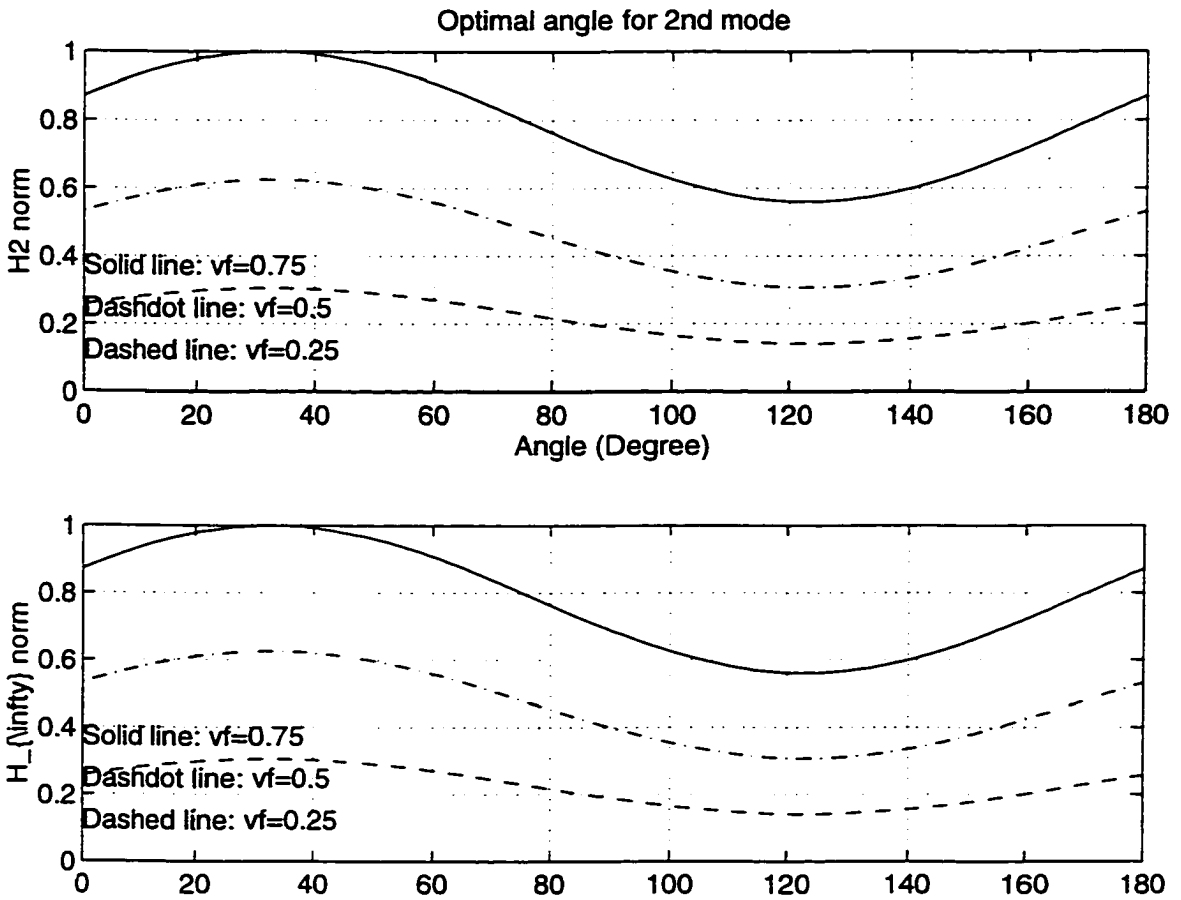

Figure 7.28 H_2 and H_∞ norms of the 2nd mode versus orientation of piezoelectric fiber θ

(Collocated sensor and actuator at $(0.367m, 0.22m)$)

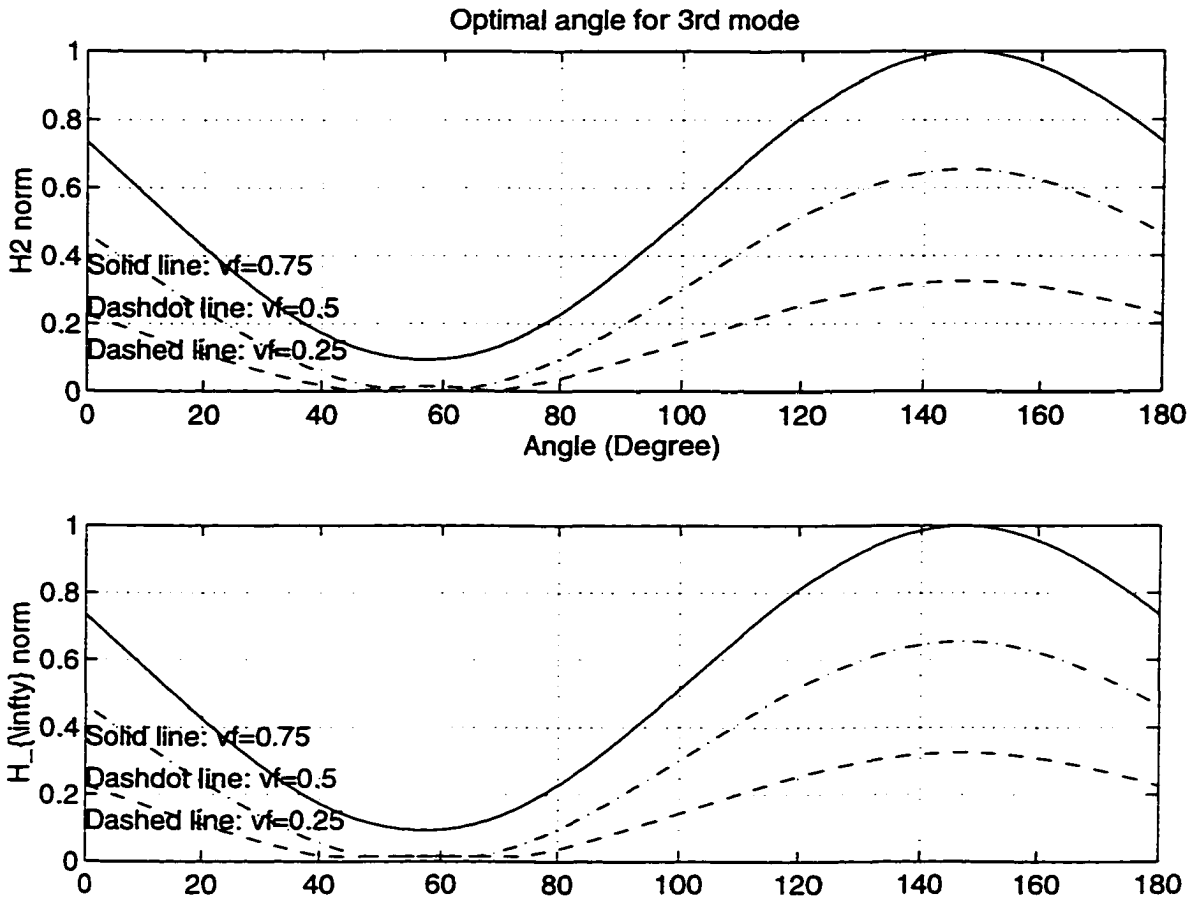

Figure 7.29 H_2 and H_∞ norms of the 3rd mode versus orientation of piezoelectric fiber θ

(Collocated sensor and actuator at $(0.367m, 0.22m)$)

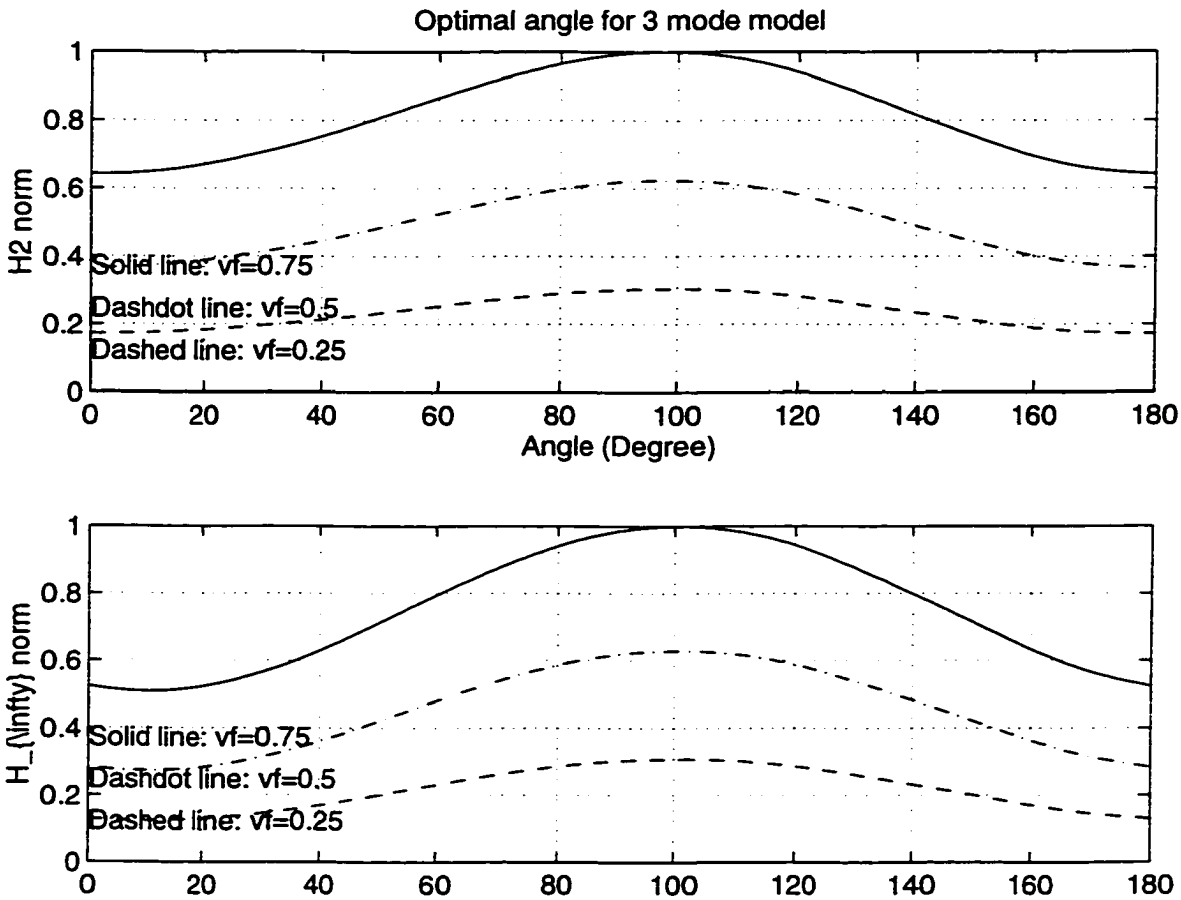

Figure 7.30 H_2 and H_∞ norms of a three mode model versus orientation of piezoelectric fiber θ

(Collocated sensor and actuator at $(0.367m, 0.22m)$)

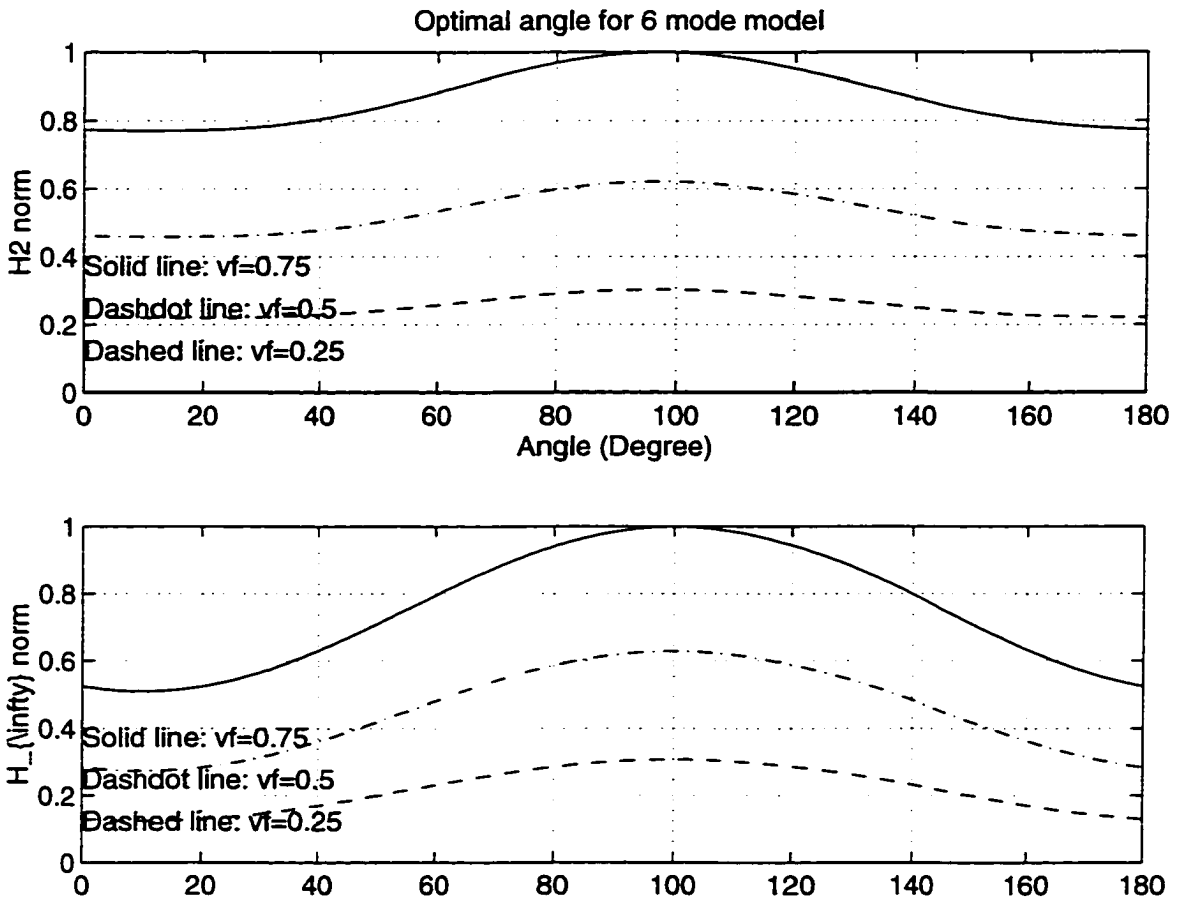

Figure 7.31 H_2 and H_∞ norms of a six mode model versus orientation of piezoelectric fiber θ

(Collocated sensor and actuator at $(0.367m, 0.22m)$)

orientation of the PZT fiber varies with the different modes, and is independent of the volume fraction of PZT fiber. H_2 and H_∞ norms have very good agreement over the entire plate. These properties can also be seen through the indices for three and six mode model in figures 7.25 and 7.26. Figures 7.27 to 7.31 are 2-D figures with fixed volume fraction ($v_f = 0.25$, 0.5, and 0.75). The optimal orientations for each case are listed in table 7.3.

System	1st mode	2nd mode	3rd mode	1-3 modes	1-6 modes
Optimal θ	100	32	148	98	98

Table 7.3 Optimal orientation θ (Degree) for piezoelectric fibers

The optimal orientations for three and six mode models are same and close to the optimal value for the first mode. This shows that the system is dominated by low order modes, especially, the first mode.

7.3.4 Comparison of Monolithic Piezoelectric Patch and Piezoelectric Fiber Actuators in Control of Twisting Mode

Equation (5.31) indicates that the modal control force of a control voltage is proportional to the modal curvature $C_x \frac{\partial^2 \phi_i(x,y)}{\partial x^2} + 2C_{xy} \frac{\partial^2 \phi_i(x,y)}{\partial x \partial y} + C_y \frac{\partial^2 \phi_i(x,y)}{\partial y^2}$. Constants C_x, C_y, and C_{xy} are defined in equation (4.7). For monolithic piezoelectric patch actuator, $C_x = C_y$ and $C_{xy} = 0$. If a monolithic piezoelectric patch actuator is located at a point where $\frac{\partial^2 \phi_i(x,y)}{\partial x^2} = \frac{\partial^2 \phi_i(x,y)}{\partial y^2} = 0$, the actuator will not be able to control the system. If a piezoelectric fiber actuator is used, however, control force can be applied to the system through the twisting term $2C_{xy} \frac{\partial^2 \phi_i(x,y)}{\partial x \partial y}$. This is the case when a piezoelectric actuator is placed at the

center of a simply supported plate to control the 5th mode shown in figure 7.18. Figure 7.32 to 7.35 shows the H_2 and H_∞ norms versus volume fraction v_f and orientation of piezoelectric fiber θ with different collocated sensor and actuator locations. If the location is close to the center of the structure, the H_2 and H_∞ norms have maximum values corresponding to optimal volume fraction v_f and orientation of piezoelectric fiber θ as listed in table 7.4:

Location	Optimal v_f	Optimal θ	θ at the 2nd peak
(0.475m, 0.285m)	0.833	135	45
(0.45m, 0.27m)	0.867	133	43
(0.425m, 0.255m)	0.9	131	41

Table 7.4 Optimal volume fraction v_f and orientation of piezoelectric fiber θ (Degree)

Figures 7.36 to 7.38 are 2D plots to show the optimal orientations. For all the cases listed in the table 7.4, piezoelectric fiber actuators demonstrate better performance than that of monolithic piezoelectric patch actuators, in terms of the H_2 and H_∞ norms. If the location of the sensor and actuator is far enough from the center of the plate, as shown in figure 7.35, monolithic patch ($v_f = 1$) is more effective than piezoelectric fiber actuator, which is also verified in figures 7.22 to 7.26.

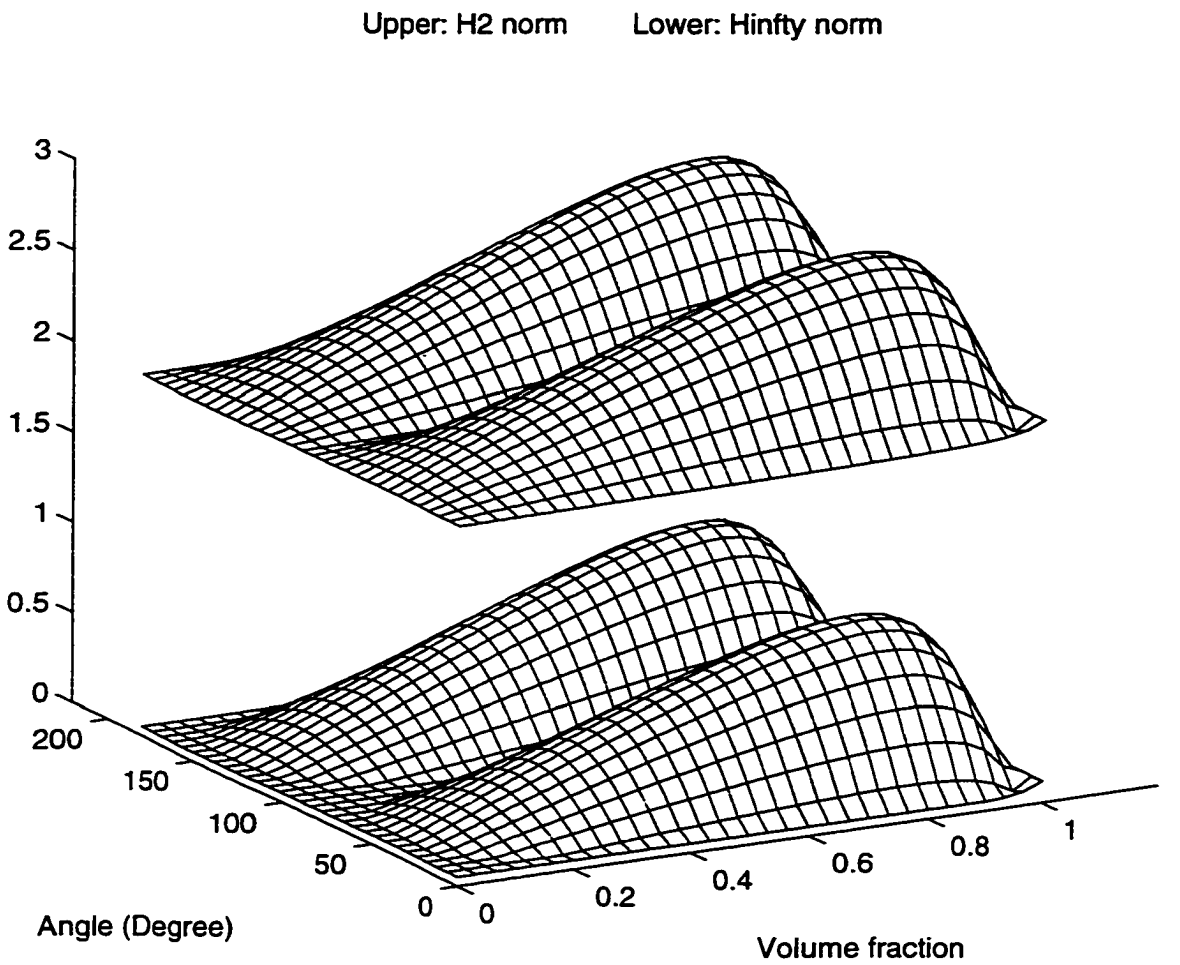

Figure 7.32 H_2 and H_∞ norms of the 5th mode versus volume fraction v_f and orientation of piezoelectric fiber θ

(Collocated sensor and actuator at (0.475m, 0.285m))

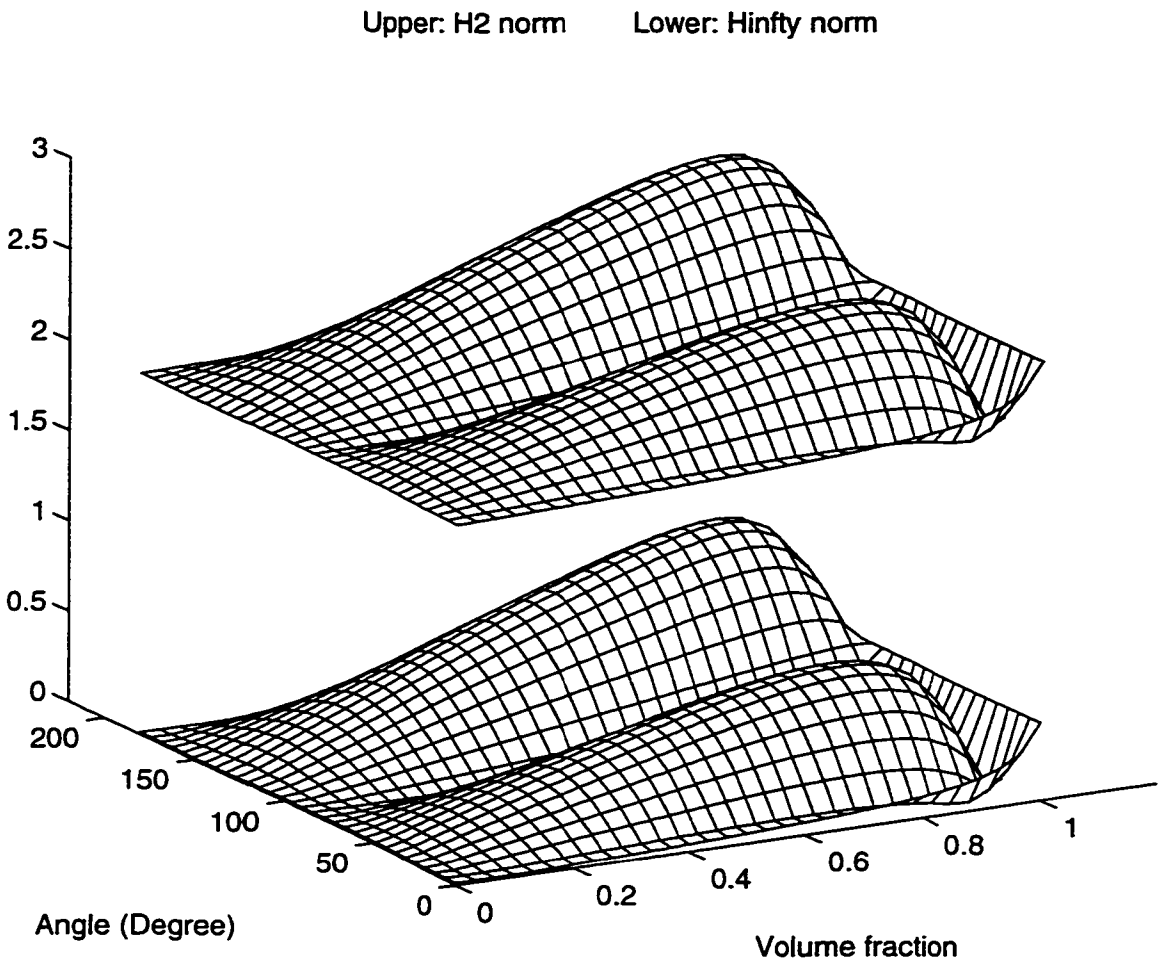

Figure 7.33 H_2 and H_∞ norms of the 5th mode versus volume fraction v_f and orientation of piezoelectric fiber θ

(Collocated sensor and actuator at (0.45m, 0.27m))

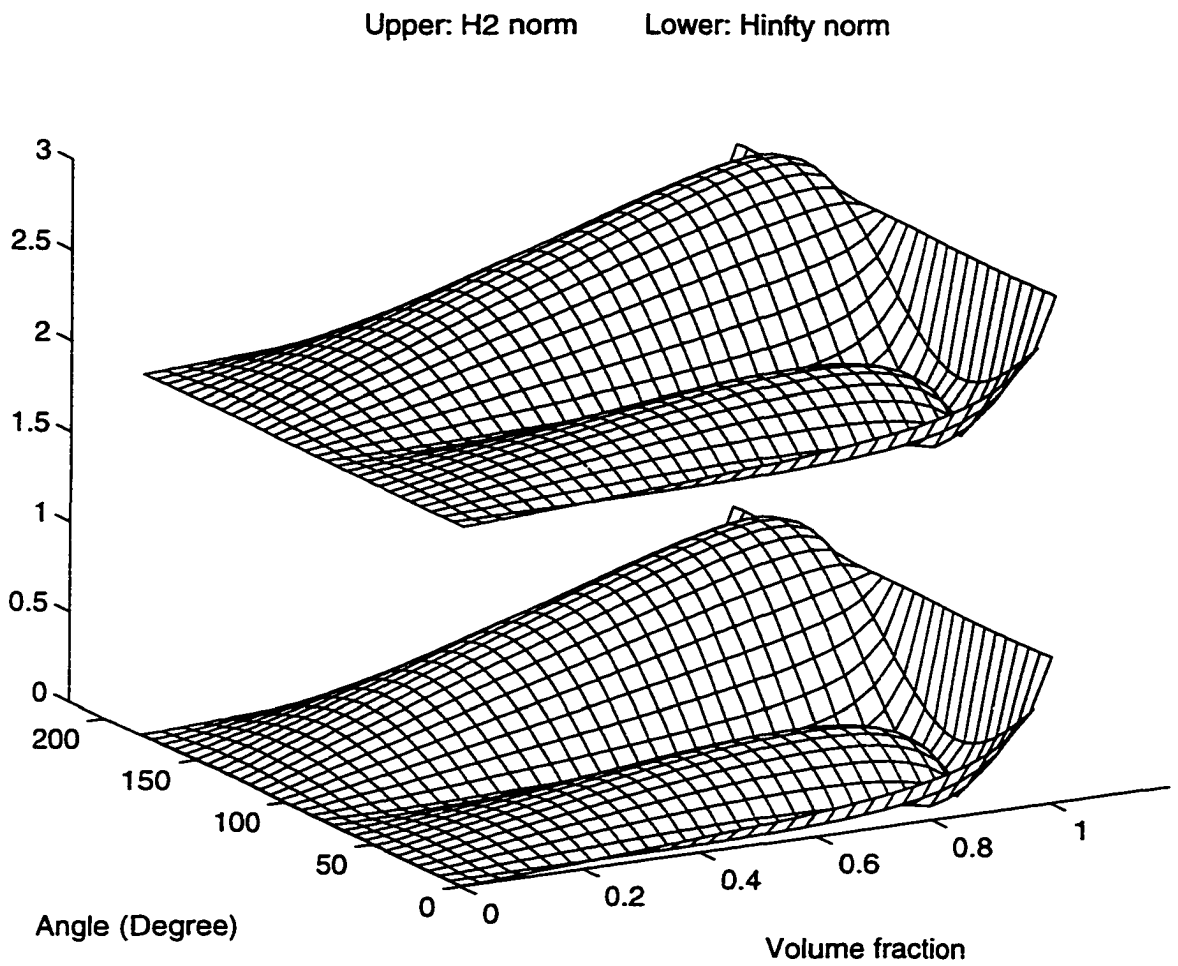

Figure 7.34 H_2 and H_∞ norms of the 5th mode versus volume fraction v_f and orientation of piezoelectric fiber θ

(Collocated sensor and actuator at (0.425m, 0.255m))

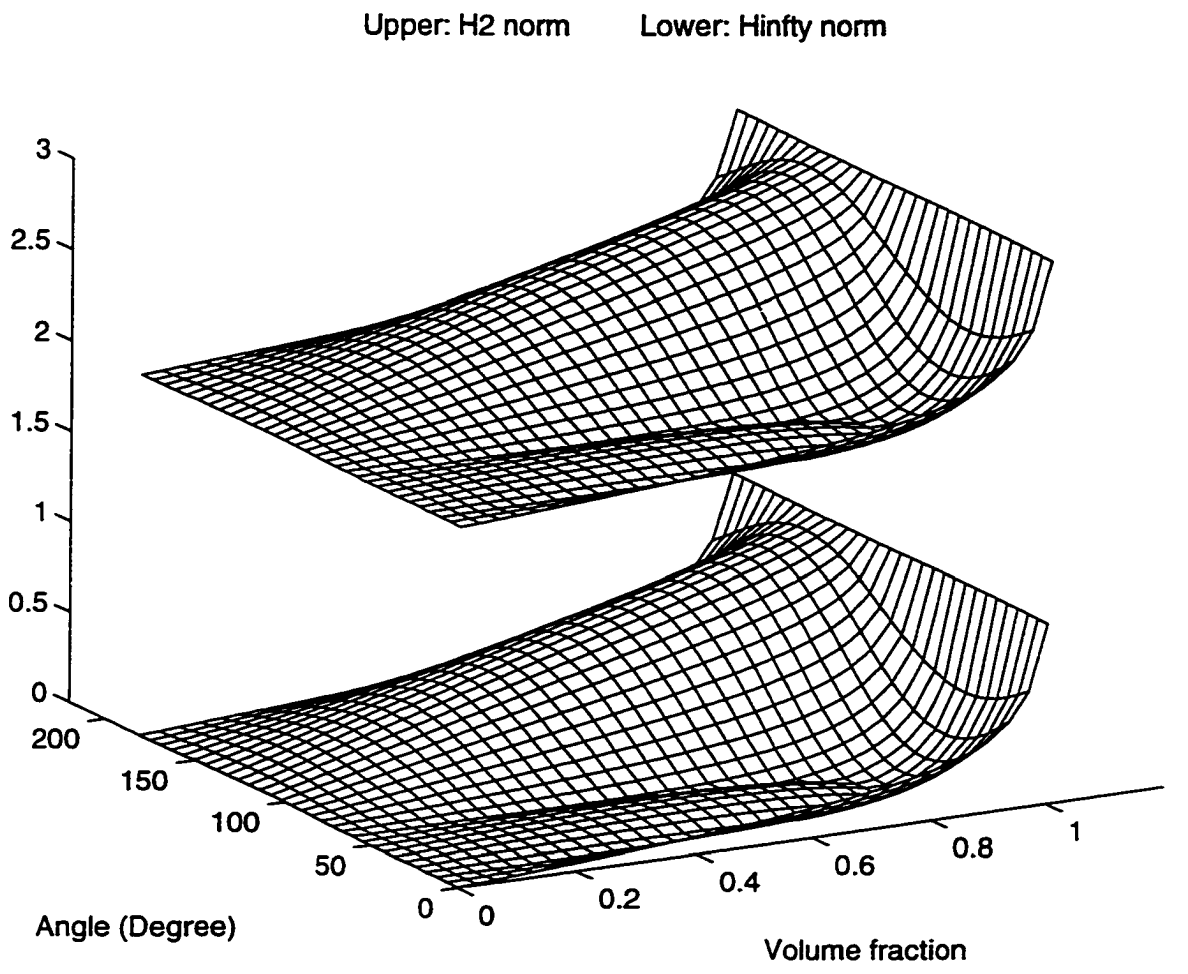

Figure 7.35 H_2 and H_∞ norms of the 5th mode versus volume fraction v_f and orientation of piezoelectric fiber θ

(Collocated sensor and actuator at $(0.4m, 0.24m)$)

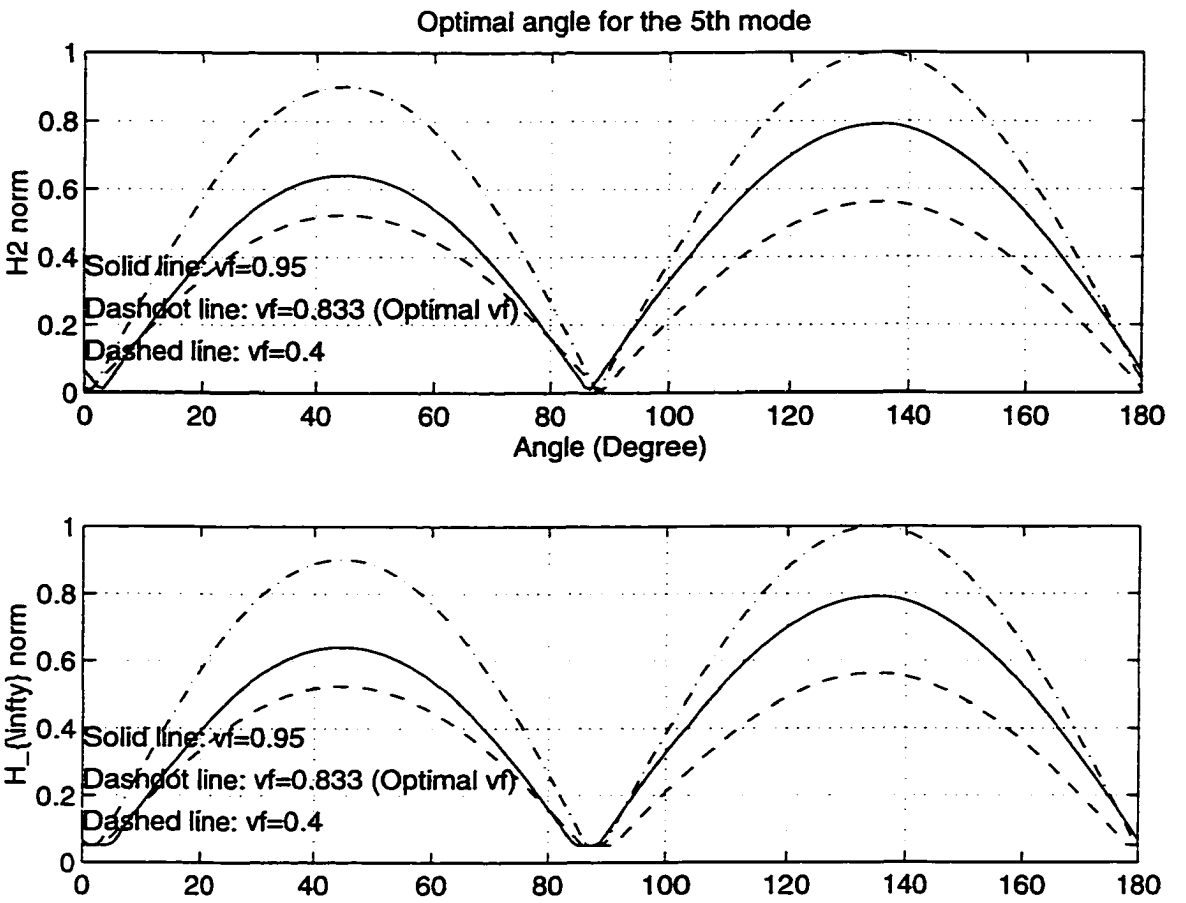

Figure 7.36 H_2 and H_∞ norms of the 5th mode versus orientation of piezoelectric fiber θ

(Collocated sensor and actuator at $(0.475m, 0.285m)$)

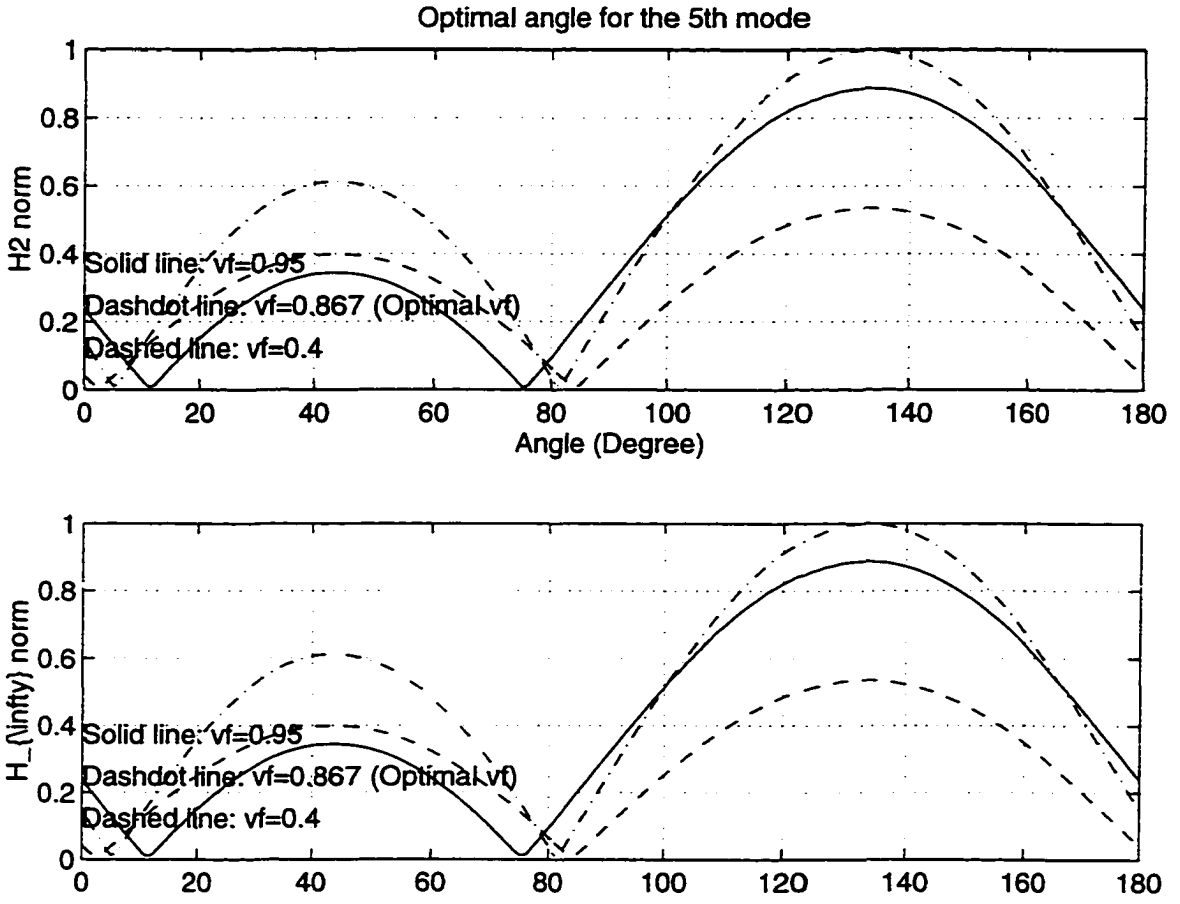

Figure 7.37 H_2 and H_∞ norms of the 5th mode versus orientation of piezoelectric fiber θ

(Collocated sensor and actuator at (0.45m, 0.27m))

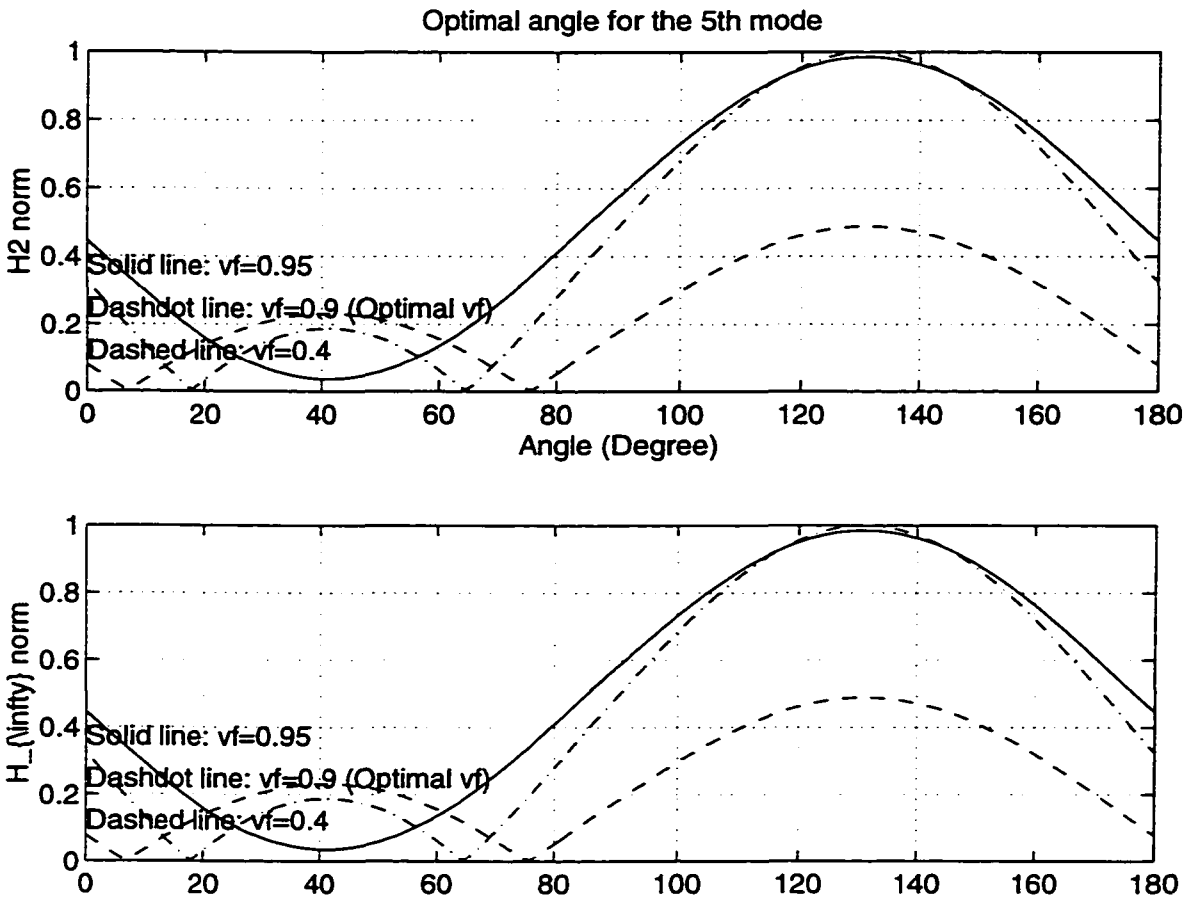

Figure 7.38 H_2 and H_∞ norms of the 5th mode versus orientation of piezoelectric fiber θ

(Collocated sensor and actuator at (0.425m, 0.255m))

CHAPTER VIII

PROPOSED INDEX FOR PLACEMENT OF PIEZOELECTRIC ACTUATOR

In the preceding chapter, the H_2 and H_∞ norms of a cantilevered beam and a simply supported plate were studied. For collocated sensor/actuator placement, comparison of the indices was made through single mode model, three mode model, and six mode model for beam and plate cases. In the case of non-collocated sensor/actuator, beam index was used to verify the agreement of both norms. For application of piezoelectric fiber actuator, a plate case study shows good agreement between H_2 and H_∞ norms versus volume fraction and orientation of the PZT fiber. These case studies uncover the similarity between the results of two popularly used norms, which implies the possibility of deriving a simple index based on one theory and with good agreement to both norms.

8.1 Proposed V Index

The definition of H_2 norm is in equation (7.3) which is for a MIMO system. For a SISO system, the equation can be simplified as:

$$\|H\|_2 = \left[\frac{1}{2\pi}\int_{-\infty}^{\infty} H(j\omega)H^*(j\omega)d\omega\right]^{1/2} \tag{8.1}$$

Note that:

$$H(j\omega)H^*(j\omega) = |H(j\omega)|^2 \tag{8.2}$$

In general, a transfer function can be written as [12]:

$$H(j\omega) = \sum_{i=1}^{\infty} \frac{\Phi_i^{(I)}(\mathbf{x}_I)\,\Phi_i^{(O)}(\mathbf{x}_O)}{-\omega^2 + j2\zeta_i\omega_i\omega + \omega_i^2} \tag{8.3}$$

where $\Phi_i^{(I)}(\mathbf{x}_I)$ and $\Phi_i^{(O)}(\mathbf{x}_O)$ are mode shape related functions. Institution of equations (8.2), (8.3) into equation (8.1) results in:

$$\|H\|_2 = \left[\frac{1}{2\pi}\int_{-\infty}^{\infty}\left|\sum_{i=1}^{\infty}\frac{\Phi_i^{(I)}(\mathbf{x}_I)\,\Phi_i^{(O)}(\mathbf{x}_O)}{-\omega^2 + j2\zeta_i\omega_i\omega + \omega_i^2}\right|^2 d\omega\right]^{1/2} \tag{8.4}$$

Note that function $\Phi_i^{(I)}(\mathbf{x}_I)$ and $\Phi_i^{(O)}(\mathbf{x}_O)$ are independent of frequency ω Thus each term of the summation will remain after the integration over frequency range. Approximately write equation (8.4) as:

$$\|H\|_2 \approx \left[\frac{1}{2\pi}\left|\sum_{i=1}^{\infty} K_i\Phi_i^{(I)}(\mathbf{x}_I)\,\Phi_i^{(O)}(\mathbf{x}_O)\right|^2\right]^{1/2}$$

$$= \frac{1}{\sqrt{2\pi}}\left|\sum_{i=1}^{\infty} K_i\Phi_i^{(I)}(\mathbf{x}_I)\,\Phi_i^{(O)}(\mathbf{x}_O)\right| \tag{8.5}$$

where K_i is a constant to be determined, and $\frac{1}{\sqrt{2\pi}}$ can combine with K_i. The parameter K_i is a constant which determines the contribution of each mode to the global index. In many control cases the lower order modes are dominant in the system if the system is excited by a broadband disturbance force. The H_2 and H_∞ norms for three and six mode model of beam and plate also show that first mode has the largest contribution. Therefore a simple expression for K_i is suggested as:

$$K_i = \frac{1}{\omega_i^2} \tag{8.6}$$

To ensure the contribution of each mode is accumulated, move the absolute operator into the summation operator and the proposed index for a n mode system is finally written as:

$$V = \sum_{i=1}^{\infty} \left| \frac{\Phi_i^{(I)}(\mathbf{x}_I)\Phi_i^{(O)}(\mathbf{x}_O)}{\omega_i^2} \right| \tag{8.7}$$

8.2 Index for a Cantilevered Beam

Equation (8.7) is used to predict the index for the beam described in the previous chapter. For the beam with a piezoelectric actuator:

$$\Phi_i^{(I)}(\mathbf{x}_I) = \frac{\partial^2 \phi_i(x_I)}{\partial x^2} \tag{8.8}$$

$$\Phi_i^{(O)}(\mathbf{x}_O) = \phi_i(x_O) \tag{8.9}$$

The V indices for single mode models appear to be identical with the H_2 and H_∞ norms. In figures 8.1 and 8.2, comparisons are made for three mode model and six mode model. For the same system with fixed sensor location, the V index is shown in figures 8.3 and 8.4. The overall agreement of the proposed index with H_2 and H_∞ norms can be found through all these cases.

8.3 Index for a Simply Supported Rectangular Plate

In the plate case with a piezoelectric actuator, as derived in equation (6.37), the $\Phi_i^{(I)}(\mathbf{x}_I)$ and $\Phi_i^{(O)}(\mathbf{x}_O)$ have the following forms:

$$\Phi_i^{(I)}(\mathbf{x}_I) = C_x \frac{\partial^2 \phi_i(x_I, y_I)}{\partial x^2} + 2C_{xy} \frac{\partial^2 \phi_i(x_I, y_I)}{\partial x \partial y} + C_y \frac{\partial^2 \phi_i(x_I, y_I)}{\partial y^2} \tag{8.10}$$

$$\Phi_i^{(O)}(\mathbf{x}_O) = \phi_i(x_O, y_O) \tag{8.11}$$

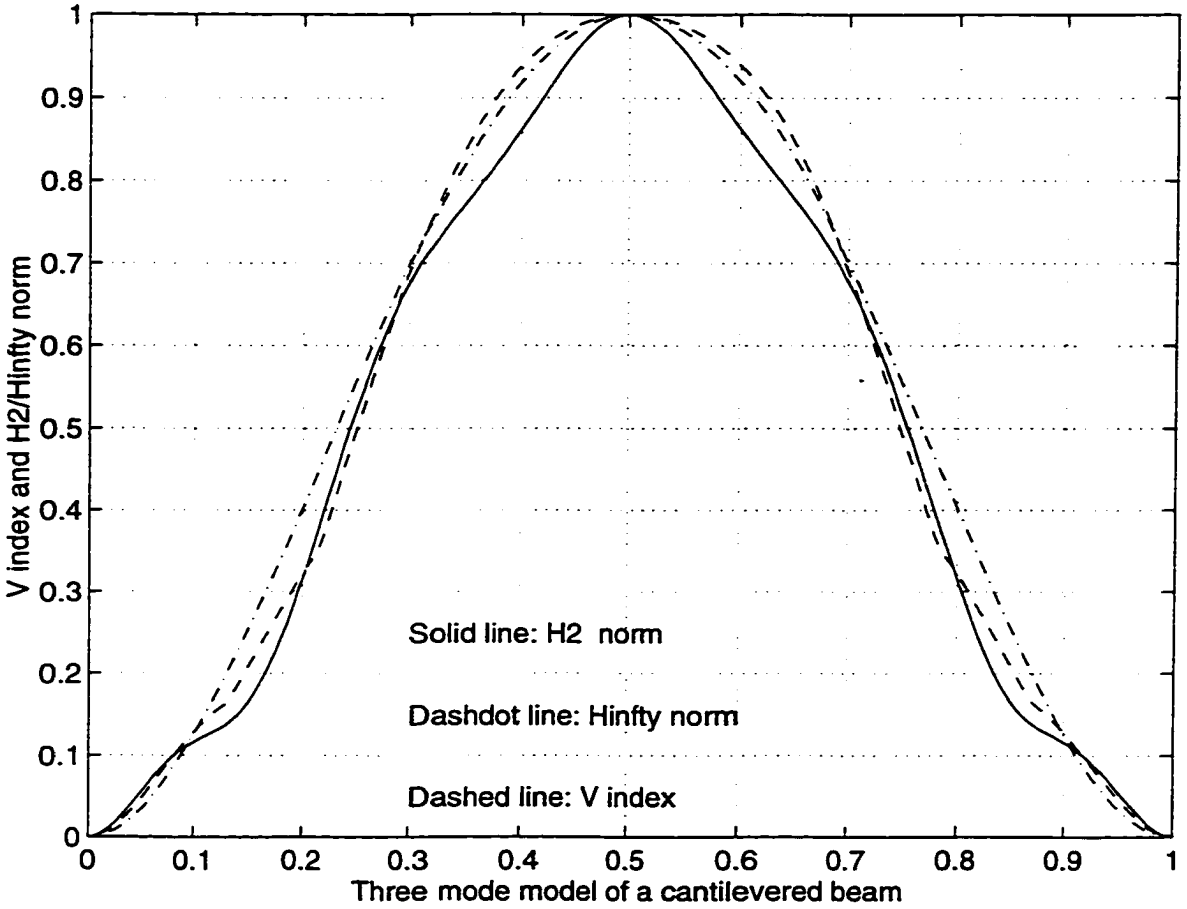

Figure 8.1 *V* index for three mode model of a cantilevered beam

(Collocated sensor and actuator)

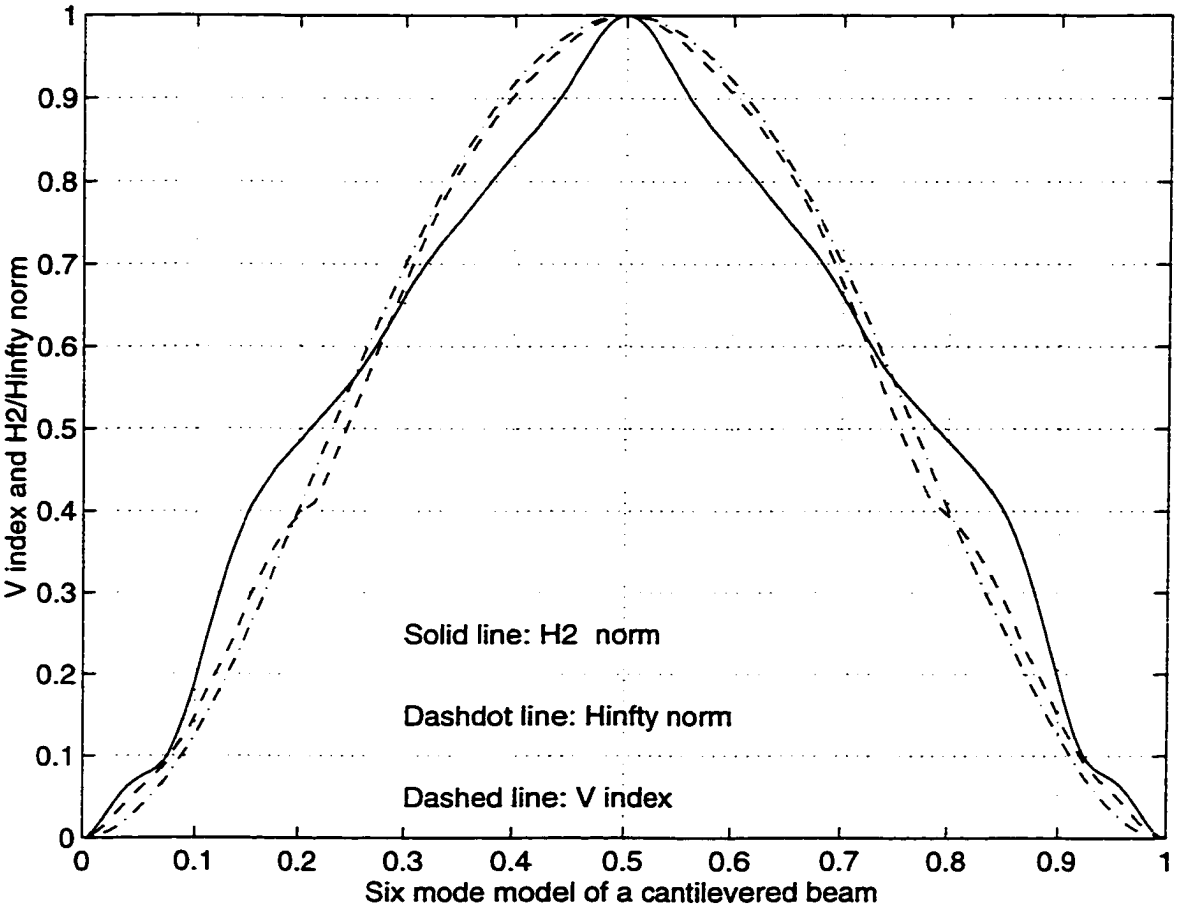

Figure 8.2 *V* index for six mode model of a cantilevered beam

(Collocated sensor and actuator)

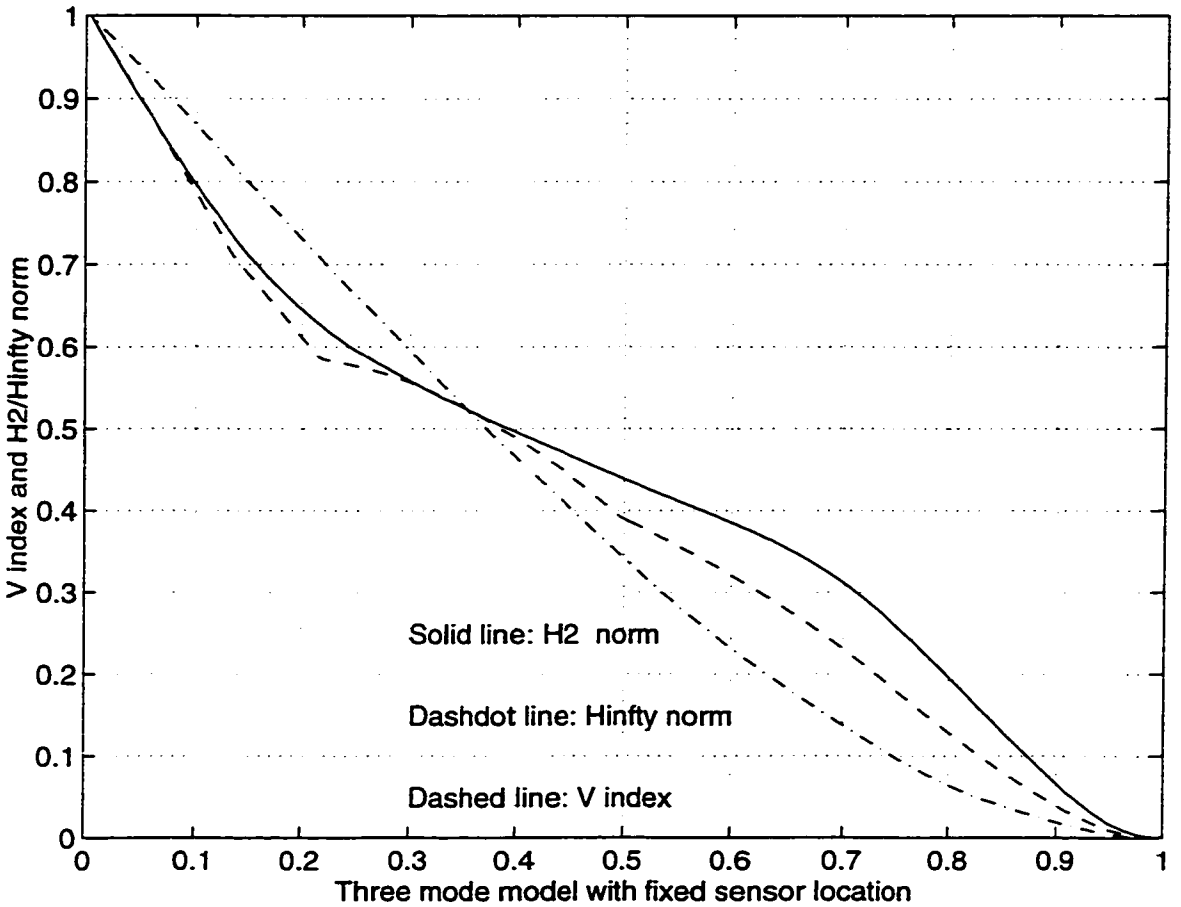

Figure 8.3 V index for three mode model of a cantilevered beam with fixed sensor location ($x = 0.6m$)

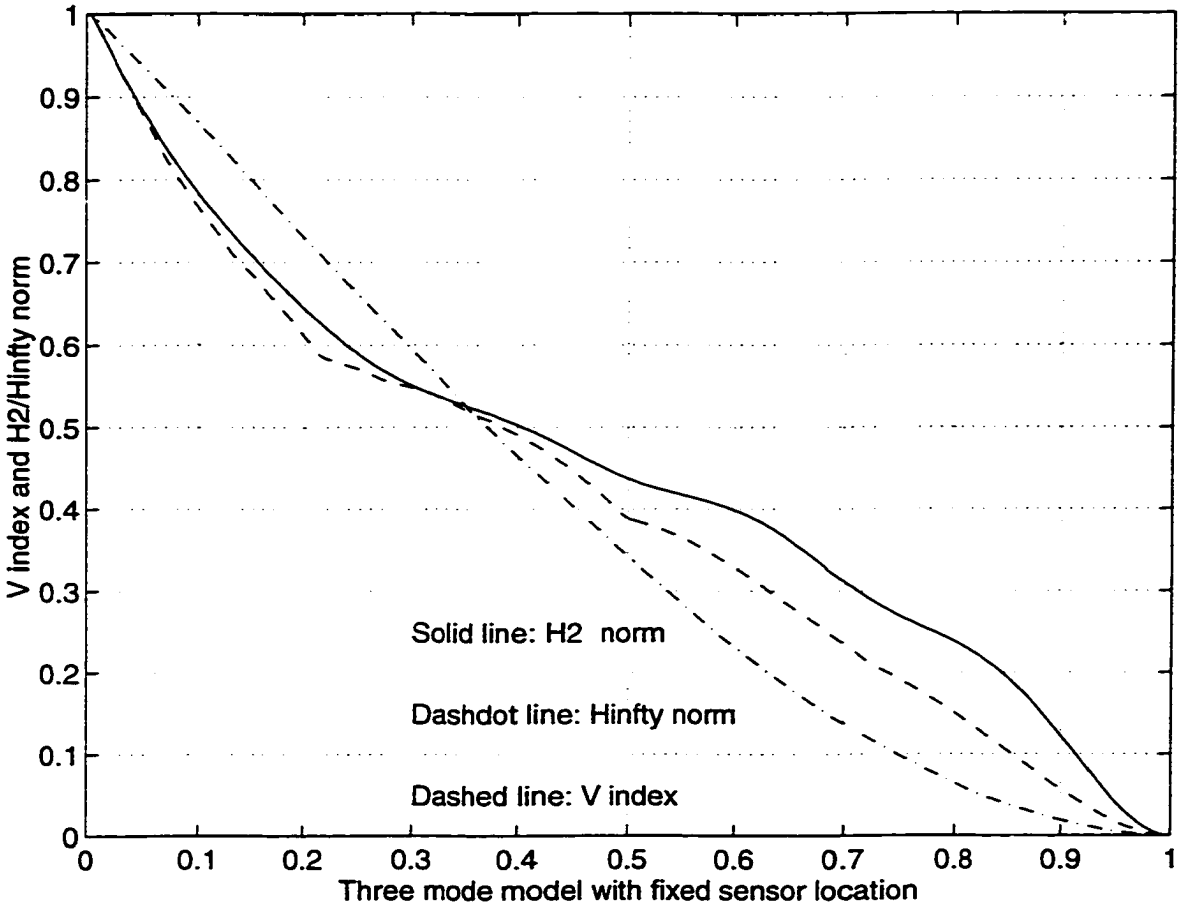

Figure 8.4 V index for six mode model of a cantilevered beam

with fixed sensor location ($x = 0.6m$)

In figures 8.5 and 8.6, comparisons are made for three mode model and six mode model. As shown in the proceeding chapter, H_2 norm and H_∞ norm agree with each other for all these cases. To indicate the results clearly, only H_2 norm is used as reference. The agreement between the proposed V index and H_2 norm are verified through all the figures.

For piezoelectric fiber actuators with collocated point sensors, the V index retains the property exhibited by H_2 and H_∞ norms, that the orientation of PZT fiber has an optimal value which is associated with different mode shape and independent to volume fraction of the fiber. The optimal angle of the fiber matches the values by H_2 and H_∞ norms exactly, as shown in figure 8.7 to figure 8.9.

8.4 Remarks on the Proposed V Index

A piezoelectric actuator is used to derive the equations. By using equation (6.22) with equations (6.23) and (6.24), it is assumed that the sensor is of the displacement type. In an actual application, the actuator could be a point force exciter and the sensor could be of piezoelectric type. Figure 8.10 shows a sequence from input (control voltage V_a) to output (sensed signal V_s) associated with equations (6.25) and (6.26).

The $\Phi_i^{(I)}(\mathbf{x_I})$ and $\Phi_i^{(O)}(\mathbf{x_O})$ in equation (8.7) are associated with **B** matrix and **C** matrix respectively. If the sensor is of the piezoelectric type, the output voltage signal is proportional to the curvature of the sensor location [1, 14, 37]. On the other hand, if the

actuator is a point force shaker, the effectiveness of the control force depends upon the mode shape instead of curvature. Thus the conclusion in table 8.1 can be made for choice of $\Phi_i^{(I)}(\mathbf{x}_I)$ and $\Phi_i^{(O)}(\mathbf{x}_O)$ functions:

		Point type	Piezoelectric type
Actuator: $\Phi_i^{(I)}(\mathbf{x}_I)$	Beam	$\phi_i(x_I)$	$\frac{\partial^2 \phi_i(x_I)}{\partial x^2}$
	Plate	$\phi_i(x_I, y_I)$	$C_x \frac{\partial^2 \phi_i(x_I, y_I)}{\partial x^2} + 2C_{xy} \frac{\partial^2 \phi_i(x_I, y_I)}{\partial x \partial y} + C_y \frac{\partial^2 \phi_i(x_I, y_I)}{\partial y^2}$
Sensor: $\Phi_i^{(O)}(\mathbf{x}_O)$	Beam	$\phi_i(x_O)$	$\frac{\partial^2 \phi_i(x_O)}{\partial x^2}$
	Plate	$\phi_i(x_O, y_O)$	$C_x \frac{\partial^2 \phi_i(x_O, y_O)}{\partial x^2} + 2C_{xy} \frac{\partial^2 \phi_i(x_O, y_O)}{\partial x \partial y} + C_y \frac{\partial^2 \phi_i(x_O, y_O)}{\partial y^2}$

Table 8.1 Choice of $\Phi_i^{(I)}(\mathbf{x}_I)$ and $\Phi_i^{(O)}(\mathbf{x}_O)$

If $\mathbf{x}_I = \mathbf{x}_O$, the result is given for a collocated sensor/actuator case. If either $\mathbf{x}_I$ or $\mathbf{x}_O$ is fixed, the index shows the effectiveness corresponding to choice of placement for sensor or actuator respectively.

The mode shapes and their derivatives can be calculated analytically for simple structures, or by Finite Element Method for arbitrarily shaped structures [24, 25, 44].

Similar to the H_2 and H_∞ indices, the proposed V index takes care of the overall performance of the control systems. If the point sensor/actuator is used, and the control of some particular mode is desired, one should ensure the controllability and observability of the systems [15, 19].

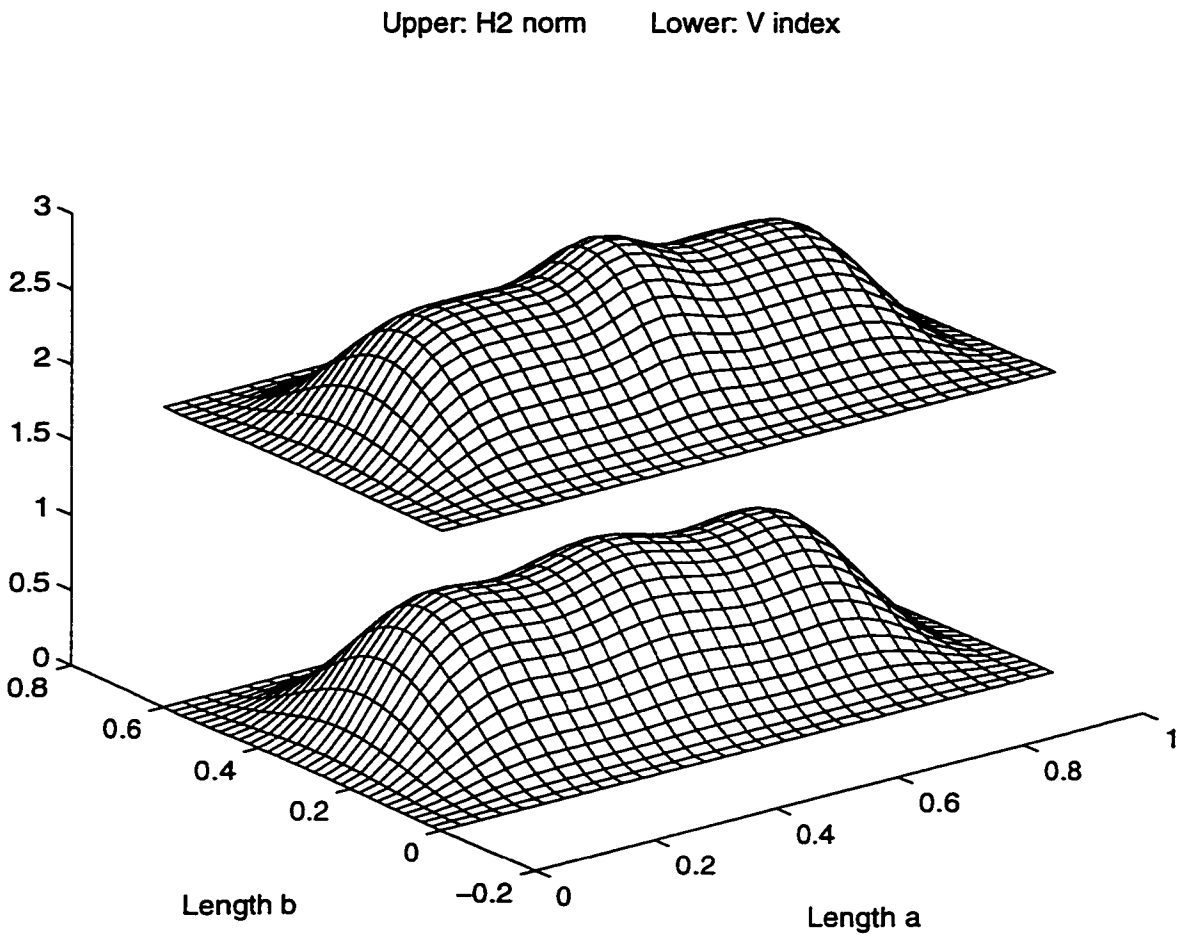

Figure 8.5 *V* index for three mode model of a simply supported plate

(Collocated sensor and actuator)

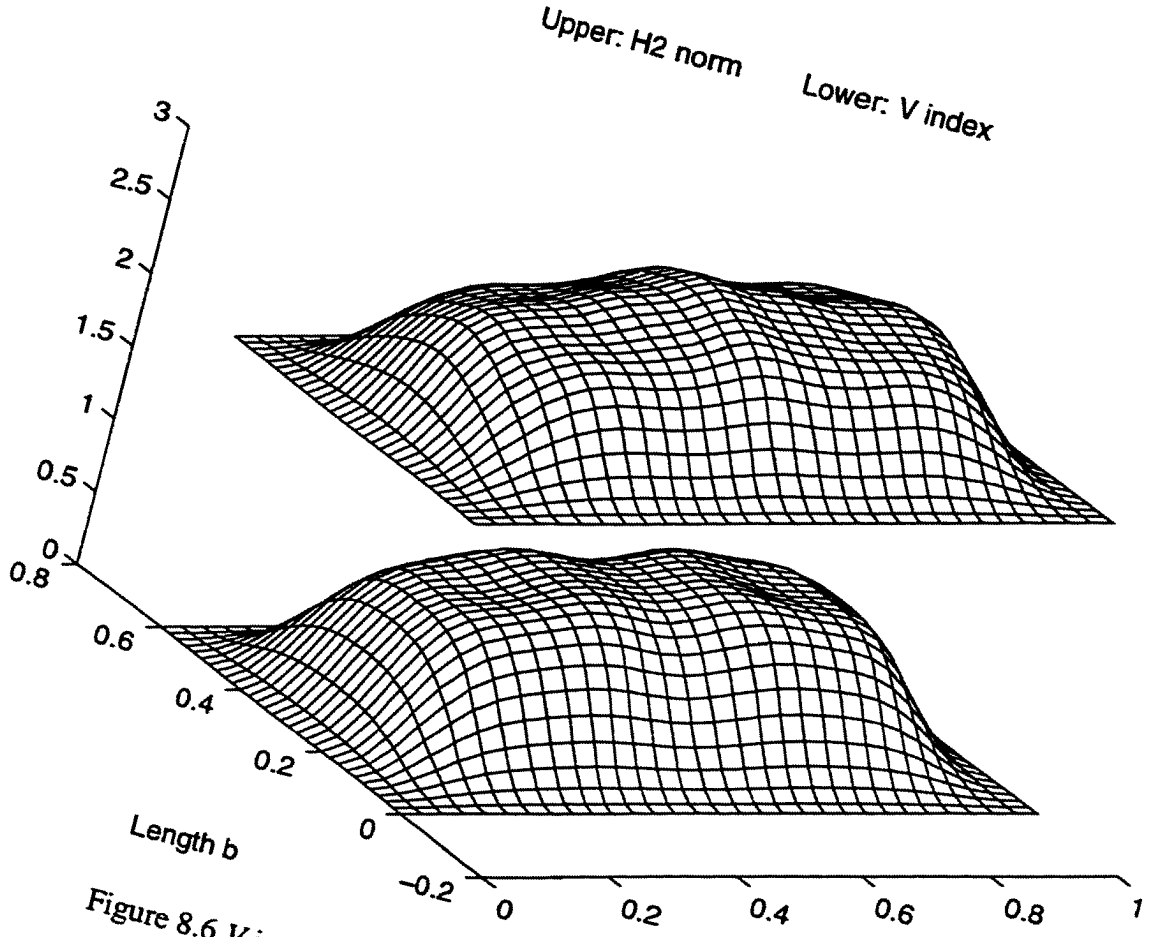

Figure 8.6 *V* index for six mode model of a simply supported plate (Collocated sensor and actuator)

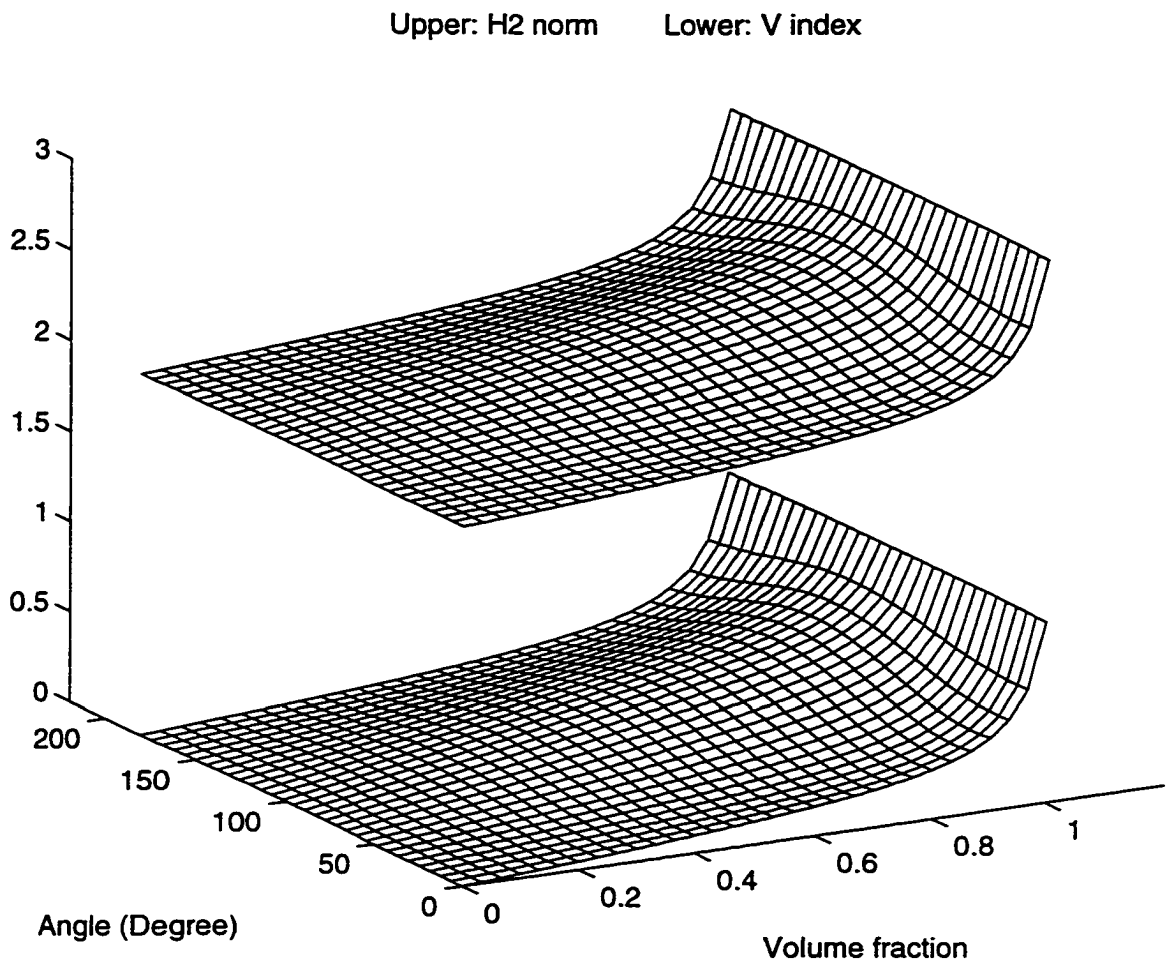

Figure 8.7 V index of the 1st mode versus volume fraction v_f

and orientation of piezoelectric fiber θ

(Collocated sensor and actuator at $(0.367m, 0.22m)$)

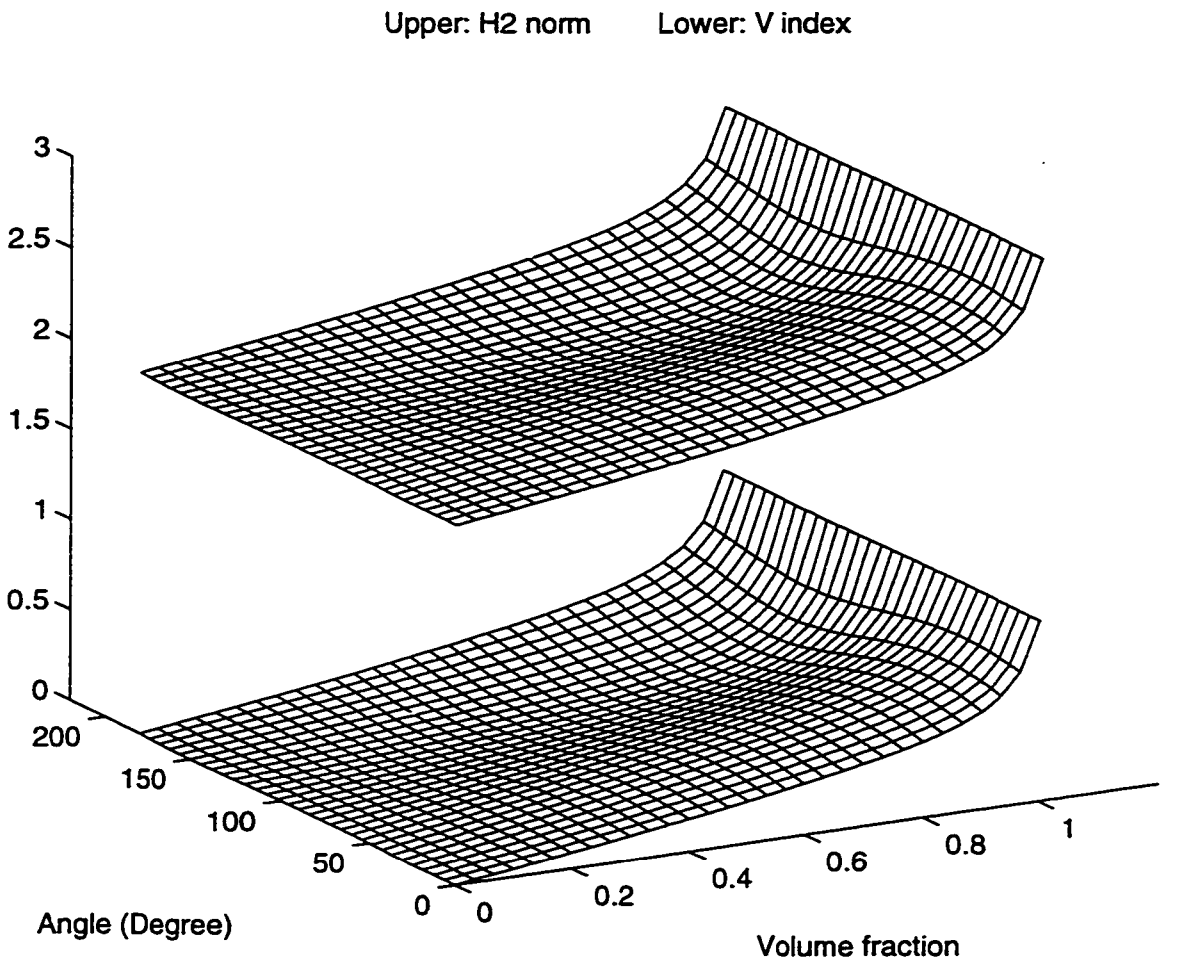

Figure 8.8 V index of the 2nd mode versus volume fraction v_f

and orientation of piezoelectric fiber θ

(Collocated sensor and actuator at $(0.367m, 0.22m)$)

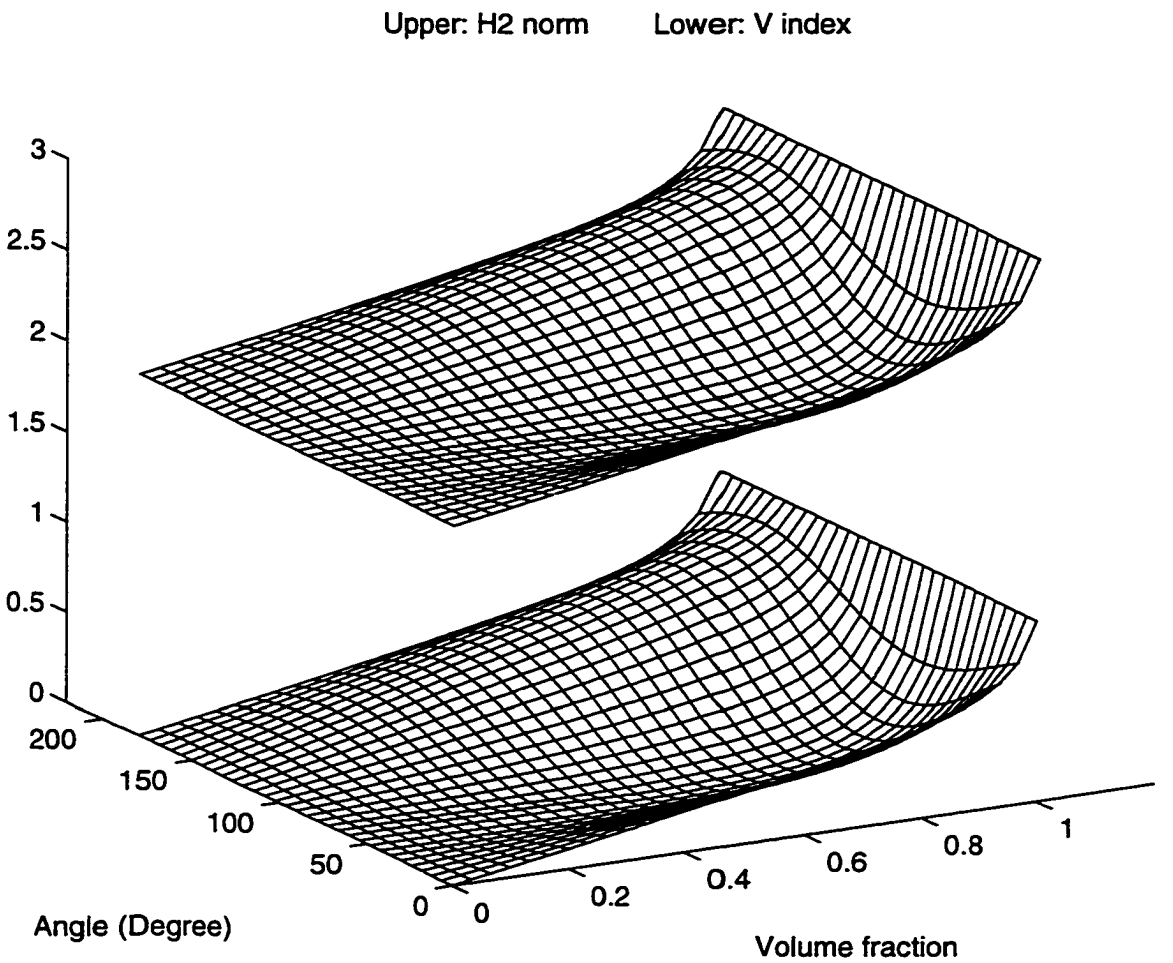

Figure 8.9 V index of the 3rd mode versus volume fraction v_f

and orientation of piezoelectric fiber θ

(Collocated sensor and actuator at $(0.367m, 0.22m)$)

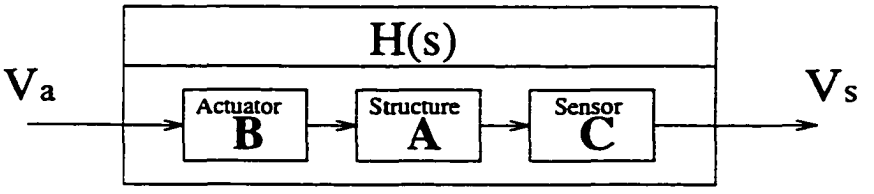

Figure 8.10 Control system sequence

CHAPTER IX

CONCLUSIONS

An equation is derived to model the piezoelectric actuators incorporation with flexible structures. This equation eliminates the discontinuity problems occurring in conventional calculation of the actuation force, which must be solved by incorporating the piezoelectric actuators into the structures using Finite Element Method. This equation also permits the comparison of the performance indices over the entire structure for a piezoelectric actuator with fixed area, which is unachievable if the Finite Elements Method is used for complicated structures.

An index has been developed for placement of the piezoelectric actuator for control of vibration of a flexible structure. This index is derived from the definition of H_2 norm. Both piezoelectric patch and piezoelectric fiber actuators are used to verify the effectiveness of the proposed index. A cantilevered beam and a simply supported rectangular plate are utilized as the dynamic structure with surface bonded piezoelectric actuator. Finally H_2 and H_∞ norms are taken as references to validate the proposed index.

The comparison of H_2 and H_∞ norms shows good agreement for beam and plate models with single, three, and six modes. The comparison of H_2 and H_∞ norms is also made for a cantilevered beam with fixed sensor location, and a simply supported plate

with a piezoelectric fiber actuator. Agreement between those two norms as well as the proposed index is demonstrated through all the cases.

The proposed index has a concise form, which requires only the natural frequencies and corresponding mode shapes to calculate the index. Since these modal parameters are available either by analytical method or via experiment, the proposed method has solved the problem in derivation of the equations for an arbitrarily shaped structure with incorporated piezoelectric actuator. The method also overcomes the difficulty in handling large structures because of the simplicity of the calculation.

The proposed index is valid for either point or distributed sensors or actuators. Application of the method for different combinations of sensors and actuators has been discussed.

The piezoelectric fiber actuator, which is able to supply anisotropic control actuation to the structure, has an optimal fiber orientation, which is related to different structures, but independent of the volume fraction of the PZT fibers. Piezoelectric fiber actuator with volume fraction $v_f < 1$ creates twisting moment, which has better performance than that of a monolithic piezoelectric patch actuator in control of twisting mode.

REFERENCES

1 Akishita, S.; Aoyama, S.; Yokoi, K.; Ma, C. H. 1995. "Simultaneous use of piezoelectric ceramics as sensor and actuator for through-plate transmission control", *1995 Design Engineering Technical Conferences*, vol.3, part C, p. 649-656

2 Alberts, T. E.; Colvin, J. A. 1991. "Observations on the natural of transfer functions for control of piezoelectric laminates", *J. of Intell. Mater. Syst. And Struct.*, Vol. 2, p. 528-541

3 Balas, G. J.; Doyle, J. C.; Glover, K.; Packard, A.; Smith, R. 1995 • - *Analysis and Synthesis Toolbox – For Use with MATLAB*, The MathWorks, Inc.

4 Baz, A.; Poh, S. 1988. "Performance of an active control system with piezoelectric actuators", *Journal of Sound and Vibration*, 126(2), p. 327-343

5 Bent, A. A.; Hagood, N. W.; Rodgers, J. P. 1995. "Anisotropic actuation with piezoelectric fiber composites", *Journal of Intelligent Material Systems and Structures*, vol.6, no.3, p. 338-49

6 Bent, A. A.; Hagood, N. W. 1995. "Improved performance in piezoelectric fiber composites using interdigitated electrodes", *Proceedings of the SPIE - The International Society for Optical Engineering*, vol.2441, p. 196-212

7 Burdisso, R. A.; Fuller, C. R. 1992. "Dynamic behavior of structural-acoustic systems in feedforward control of sound radiation", *J. Acoust. Soc. Am.*, vol.96, no.3, p. 1582-1591

8 Burdisso, R. A.; Fuller, C. R. 1994. "Design of active structural acoustic control systems by eigenproperty assignment", *J. Acoust. Soc. Am.*, vol.92, no.1, p. 277-286

9 Dimitriadis, E. K.; Fuller, C. R.; Rogers, C. A. 1991. "Piezoelectric actuators for distributed vibration excitation of thin plates", *Transactions of the ASME*, Vol. 113, p. 100-107

10 Doyle, J. C.; Glover, K.; Khargonekar, P. P.; Francis, B. A.; "State-Space Solutions to Standard H_2 and H_∞ Control Problems", *IEEE Transactions on Automatic Control*, Vol. 34, No. 8, August 1989, p. 831-847

11 Eckold, G. 1994. *Design and Manufacture of Composite Structures*, McGraw-Hill, Inc.

12 Ewins, D. J. 1984 *Modal Testing: Theory and Practice*, Research Studies Press Ltd., John Wiley & Sons Inc.

13 Gibson, R. F. 1994. *Principles of Composite Material Mechanics*, McGraw-Hill, Inc.

14 Gopinathan, M.; Pajunen, G. A.; Neelakanta, P. S.; Arockiasamy, M. 1995. "Estimation of distributed transverse displacement and velocity from distributed strain measurements in a cantilever beam", SPIE Vol. 2443, p.520-531

15 Hać, A; Liu, L. 1993. "Sensor and actuator location in motion control of flexible structures", *Journal of Sound and Vibration*, 167(2), p. 239-261

16 Hagood, N. W.; Bent, A. A. 1993. "Development of Piezoelectric Fiber Composites for Structural Actuation", *AIAA-93-1717-CP*, p. 3625-3638

17 Hong, J.; Bernstein, D. S. 1995. "Bode integral constraints and the zero spillover controller in active noise and vibration control", *1995 Design Engineering Technical Conferences*, vol.3, part C, p.325-332

18 Hong, J.; Akers, J. C.; Venugopal, R.; Lee, M. N.; Sparks, A. G.; Washabaugh, P. D.; Bernstein, D. S. 1996. "Modeling, identification, and feedback control of noise in an acoustic duct", *IEEE Transactions on Control Systems Technology*, Vol. 4, No. 3, p. 283-291

19 Hughes, P. C.; Skelton, R. E. 1980. "Controllability and observability of linear matrix-second-order system", *Journal of Applied Mechanics*, Vol. 47, p. 415-420

20 Kang, Y. K.; Park, H. C.; Hwang, W.; Han, K. S. 1996. "Optimum placement of piezoelectric sensor/actuator for vibration control of laminated beams", *AIAA Journal*, vol.34, no.9, p. 1921-6

21 Kondoh, S.; Yatomi, C.; Inoue, K. 1990. "The positioning of sensors and actuators in the vibration control of flexible systems", *JSME International Journal, Series III (Vibration, Control Engineering, Engineering for Industry)*, vol.33, no.2, p. 145-52

22 Lee, C. K. 1989. "Theory of laminated piezoelectric plates for the design of distributed sensors/actuators. Part I: Governing equations and reciprocal relationships", *J. Acoust. Soc. Am.* 87(3), p.1144-1158

23 Lee, A. C.; Chen, S. T. 1994. "Collocated sensor/actuator positioning and feedback design in the control of flexible structure system", *Transactions of the ASME. Journal of Vibration and Acoustics*, vol.116, no.2, p. 146-54

24 Lee, I. W.; Jung, G. H. 1997. "An efficient algebraic method for the computation of natural frequency and mode shape sensitivities—Part I. Distinct natural frequencies", *Computers & Structures*, Vol. 62, No. 3, p. 429-435

25 Lee, I. W.; Jung, G. H. 1997. "An efficient algebraic method for the computation of natural frequency and mode shape sensitivities—Part II. Multiple natural frequencies", *Computers & Structures*, Vol. 62, No. 3, p. 437-443

26 Lesieutre, G. A.; Yarlagadda, S.; Yoshikawa, S.; Kurtz, S. K.; Xu, Q.C. 1993. "Passively damped structural composite materials using resistively shunted piezoceramic fibers", *Journal of Materials Engineering and Performance*, vol.2, no.6, p. 887-92

27 Levine, W. S.; Athans, M. 1970. "On the determination of the optimal constant output feedback gains for linear multivariable systems", *IEEE Transaction on Automatic Control*, Vol. AC-15, No. 1, p. 44-48

28 Li, X. P.; Chang, B. C.; Banda, S. S.; Yeh, H. H. 1992. "Robust control systems design using H_∞ optimization theory", *Journal of Guidance, Control, and Dynamics*, Vol. 15, No. 4, p. 944-952

29 Liao, W. H.; Wang, K. W. 1995. "On the active-passive hybrid vibration control actions of structures with active constrained layer treatments", ASME 1995 Design Engineering Technical Conferences, Vol. 3, Part C, p. 125-141

30 Lindberg, R. E.; Longman, R. W. 1984. "On the number and placement of actuators for independent modal space control", *Journal of Guidance*, Vol. 7, No. 2, March-April 1984, p. 215-221

31 Lim, K. B.; Lake, R.; Heeg, J. 1996. "Effective piezoceramic actuator placement for an experimental flexible wing", *1996 GNC Conference AIAA paper*, no.96-3758

32 Main, J. A.; Garcia, E.; Howard, D. 1994. "Optimal placement and sizing of paired piezoactuators in beams and plates", p. 373-381

33 Masters, A. R.; Jones, J. D. 1993. "Basic design guidelines for embedded piezo-actuators in a layered composite structure", *Smart Structures and Intelligent Systems*, vol.1917, p. 329-340

34 Meyer, R., Jr.; Yoshikawa, S.; Shrout, T. 1996. "Sol-gel derived PZT fibers-development and limitations", *Proceedings of the SPIE - The International Society for Optical Engineering*, vol.2716, p. 69-79

35 Morgan Matroc, Inc.; *Guide to Modern Piezoelectric Ceramics*

36 Papoulis, A. 1962. *The Fourier Integral and Its Applications*, McGraw-Hill Book Company, Inc.

37 Pota, H. R.; Alberts, T. E. 1995. "Multivariable transfer functions for a slewing piezoelectric laminate beam", *Transactions of the ASME*, Vol. 117, p. 352-359

38 Redmond, J.; Parker, G. 1996. "Actuator placement based on reachable set optimization for expected disturbance", *Journal of Optimization Theory and Applications*, vol.90, no.2, p. 279-300

39 Reismann, H. 1988. *Elastic Plates*, John Wiley & Sons, Inc.

40 Robbins, D. H.; Reddy, J. N. 1996. "An efficient computation model for the stress analysis of smart plate structures", p. 353-360

41 Rodriguez, H. M.; Burdisso, R. A. 1995. "Sensitivity analysis for feedforward control system design", *J. Acoust. Soc. Am.*, vol.98, no.6, p. 3352-3359

42 Seto, K.; Miyata, T.; Ren, M. Z.; Doi, F. 1995. "The modeling and active control of flexible plate structure for reducing noise radiation", *1995 Design Engineering Technical Conferences*, vol.3, part C, p. 359-368

43 Smith, G. C; Clark, R. L. 1997. "Optimal transducer placement for output feedback control of broadband structural acoustic radiation", *AIAA paper*, 97-1316, Apr. 1997

44 Sutter, T. R.; Camarda, C. J.; Walsh, J. L.; Adelman, H. M. 1988. "Comparison of several methods for calculating vibration mode shape derivatives", *AIAA Journal*, Vol. 26, No. 12, p. 1506-1511

45 Tanaka, M.; Matsumoto, T.; Huang L. 1995. "Computer simulation for active control of vibration in beam structures", *ASME 1995 Design Engineering Technical Conferences*, Vol. 84-3, Part C, p. 1095-1101

46 Ting, S. M.; Janas, V. E.; Safari, A. 1996. "Relic processing of fine-scale, large-area piezoelectric ceramic fiber/polymer composites", *Journal of the American Ceramic Society*, vol.79, no.6, p. 1689-92

47 Waller, D. J.; Safari, A. 1992. "Piezoelectric lead zirconate titanate ceramic fiber/polymer composites", *Journal of the American Ceramic Society*, vol.75, no.6, p. 1648-55

48 Wang, B. T.; Rogers, C. A. 1991. "Laminate plate theory for spatially distributed induced strain actuators", *Journal of Composite Materials*, Vol. 25, p. 433-451

49 Wetherhold, R. C.; Panthalingal, N. 1993. "Piezoelectric PZT/epoxy composites for sensing and actuaoting torsional motion", *SPIE*, vol.1916, p. 266-274

50 Xu, K.; Warnitchai, P.; Igusa, T. 1994. "Optimal placement and gains of sensor and actuators for feedback control", *Journal of Guidance, Control, and Dynamics*, Vol. 17, No. 5, p. 929-934

51 Yoshikawa, S.; Selvaraj, U.; Brooks, K. G.; Kurtz, S. K. 1992. "Piezoelectric PZT tubes and fibers for passive vibrational damping", *ISAF '92. Proceedings of the Eighth IEEE International Symposium on Applications of Ferroelectrics* (Cat. No.92CH3080-9), p. xii+644, 269-72

52 Zhou, S. W.; Liang, C. Rogers, C. A. 1996. "An impedance-based system modeling approach for induced strain actuator-driven structures", *Journal of Vibration and Acoustics*, Vol. 118, p. 323-331

VITA

Xuegeng Zhu obtained his B.S. degree from the Power Machinery Engineering Department at Shanghai Jiao Tong University, Shanghai, China, in July 1983. He obtained his M.S. from the Institute of Vibration, Shock and Noise Research at Shanghai Jiao Tong University in January 1989. He became a Ph. D. student in the Aerospace Engineering Department at Old Dominion University, Norfolk, Virginia in September 1995. He is currently a Senior Development Engineer with AP Automotive Systems, Inc. in Toledo, Ohio.

IMAGE EVALUATION TEST TARGET (QA-3)

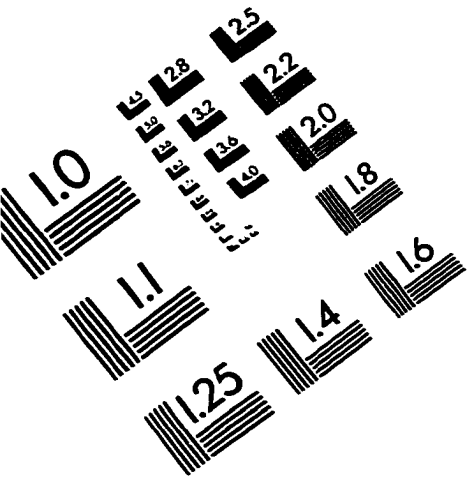

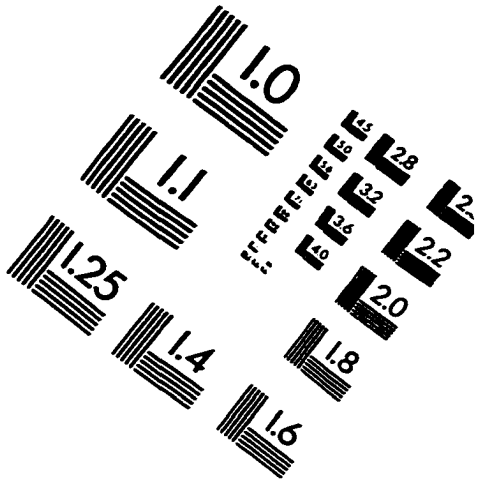

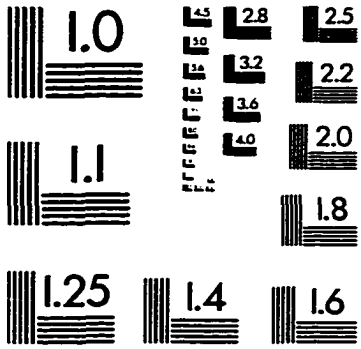

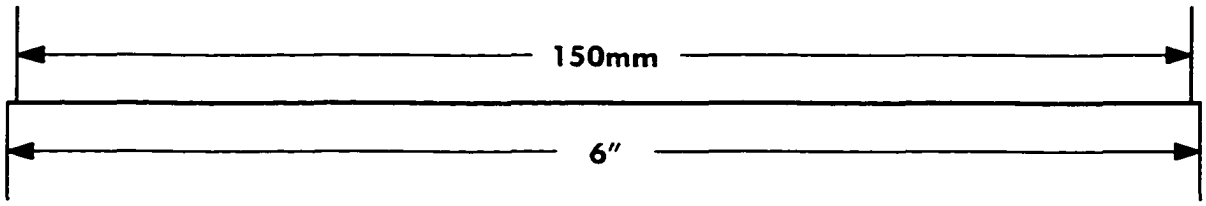

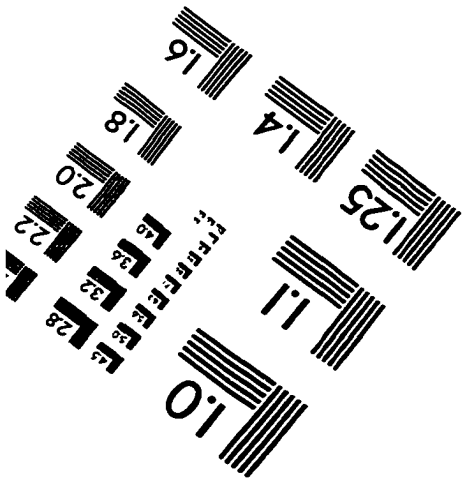

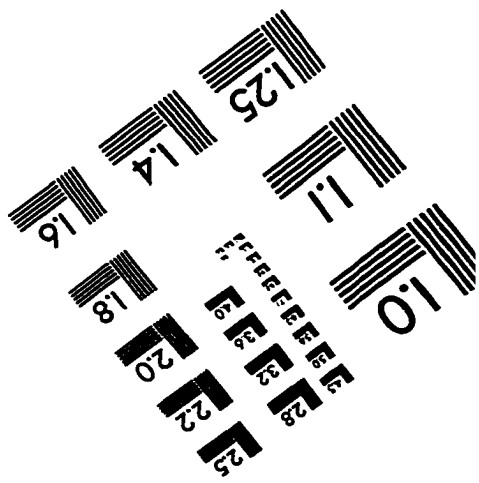

APPLIED IMAGE, Inc
1653 East Main Street
Rochester, NY 14609 USA
Phone: 716/482-0300
Fax: 716/288-5989